UNIVERSITY OF THE
WITWATERSRAND,
JOHANNESBURG

Photocatalytic production of hydrogen using TiO_2 based catalysts.

Prepared by:

Fahima Bhom

1842047

A dissertation submitted to the School of Chemical and Metallurgical Engineering, Faculty of Engineering and the Built Environment, University of the Witwatersrand, in fulfilment of the requirements for the degree of Master of Science in Engineering.

Supervisor: Prof. Yusuf Makarfi Isa

Co-Supervisor: Dr Atuman Samaila Joel

April 2025

PLAGIARISM DECLARATION

I Fahima Bhom (Student number: 1842047), am a student registered for MSc (Eng) chemical in the year 2025. I hereby declare the following:

- I am aware that plagiarism (the use of someone else's work without their permission and/or without acknowledging the original source) is wrong.
- I confirm that the work submitted for assessment for the above course is my own unaided work except where I have explicitly indicated otherwise.
- I have followed the required conventions in referencing the thoughts and ideas of others.
- I understand that the University of the Witwatersrand may take disciplinary action against me if there is a belief that this is not my own unaided work or that I have failed to acknowledge the source of the ideas or words in my writing.

Student Signature: fahima Date: 16/04/2025

ABSTRACT

Photocatalytic hydrogen production offers sustainable route to clean hydrogen production by utilizing water and sunlight. Although promising, this technology is still in its early stages, requiring advancements in materials efficiency and reactor design to achieve commercial viability. This study focused on evaluating the photocatalytic performance of TiO_2 catalyst through modifications with metals such as Cu, Ni, and Cu-Ni combinations. Metal-modified TiO_2 catalysts, synthesized via the incipient wetness impregnation method, were characterized to assess structural, morphological, and optical properties

The results demonstrated that metal modification progressively reduced the bandgap energy of TiO_2, enhancing visible light absorption and improving photocatalytic efficiency. It was also interesting to note that the bimetallic modified TiO_2 resulted in lower bandgap energy compared to the monometallic modified TiO_2. A further reduction in the bandgap energy was observed with increasing metal concentrations, indicating a correlation between metal loading and enhanced light absorption properties. Metal modified TiO_2 catalysts exhibited improved light absorption compared to unmodified TiO_2, indicating their potential for improved hydrogen production under solar irradiation.

Experimental investigations conducted under varying operational conditions, including different photoreactors, sacrificial reagents, and catalyst dosage indicated active surface reactions; however, hydrogen production was not detected. This could be attributed to the recombination of photogenerated charges or hydrogen levels being below the detection limit. To further analyse hydrogen generation, an Aspen plus model incorporating Langmuir-Hinshelwood kinetics was developed to simulate and analyse photocatalytic hydrogen production. The model demonstrated good agreement with literature results and allowed investigation of process parameters that affect the hydrogen production. It was found that hydrogen production rate is significantly affected by the type and concentration of the sacrificial reagent, catalyst type, catalyst dosage and light intensity.

Additionally, the study also conducted a preliminary techno-economic analysis of photocatalytic hydrogen production process using a Cu/TiO_2 photocatalyst in a pilot-scale compound parabolic concentrator (CPC) reactor. The analysis revealed a specific hydrogen production cost of R872,849.00/kg, driven by the low solar-to-hydrogen (STH) efficiency (<1%) and very limited hydrogen output. These findings emphasise the need for advanced

materials, improved reactor designs, and larger scale systems to make this technology economically viable. Future research should focus on achieving STH efficiencies exceeding 10% and optimizing operational parameters to enhance the economic feasibility of photocatalytic hydrogen production.

ACKNOWLEDGEMENTS

I would like to express my sincere gratitude to my Supervisor, Prof. Yusuf Isa, for his exceptional guidance, wisdom, and unwavering support throughout this research. His invaluable advice, constant encouragement, and profound knowledge have been a source of inspiration and have greatly contributed to the completion of this dissertation.

I am grateful to my Co-Supervisor, Dr Atuman Joel, for his dedicated mentorship and insightful feedback. His expertise and support have significantly shaped the direction and quality of this work.

I would like to extend my appreciation to the CHMT staff for their assistance with the laboratory equipment, setup, and technical support, which were crucial to the successful completion of this study. I am also grateful to the School of Chemistry staff for their contributions to the reactor setup and sample characterization.

I am deeply thankful to the members of the Sustainable Fuels and Petrochemical Research Group, as well as the Sustainable Process Engineering group, for their valuable discussions and constant support throughout this process.

My sincere appreciation goes to Wits University (PMA) for the financial support that made this research possible.

Finally, I would like to express my heartfelt gratitude to my family for their unending love, encouragement, and patience. Their belief in me has been a constant source of strength and motivation, and I could not have completed this journey without their unwavering support.

TABLE OF CONTENTS

LIST OF FIGURES

LIST OF TABLES

LIST OF PUBLICATION

F. Bhom, Y. M. Isa, Photocatalytic Hydrogen Production Using TiO_2-based Catalysts: A Review. *Global Challenges* 2024, 8, 2400134. https://doi.org/10.1002/gch2.202400134

CHAPTER 1
INTRODUCTION

1.1 Climate Change and Energy Demand

Energy is very essential for a country's socio-economic development and the well-being of its people [1]. Approximately, 85% of the world's energy is produced from fossil fuels such as coal, petroleum, and natural gas [2]. In South Africa, 85% of the energy comes from the combustion of coal, making the country one of the top greenhouse gas emitters in the world [3]. The use of non-renewable energy sources has caused great environmental degradation as the combustion of fossil fuels produces CO_2 which causes climate change [4]. The energy crisis has been caused by the diminishing fossil fuels, a consequence of population growth and the required industrialization [5]. Climate change and energy crises are the two biggest global challenges facing humanity today [6]. To address these challenges and achieve net zero CO_2 emissions by 2050, the International Governmental Panel on Climate Change (IPCC) recommended limiting warming to no more than 1.5 ºC. Overall, with an increasing population, global energy demand continues to increase, as shown in Figure 1.1, which illustrates the demand for different energy sources [7].

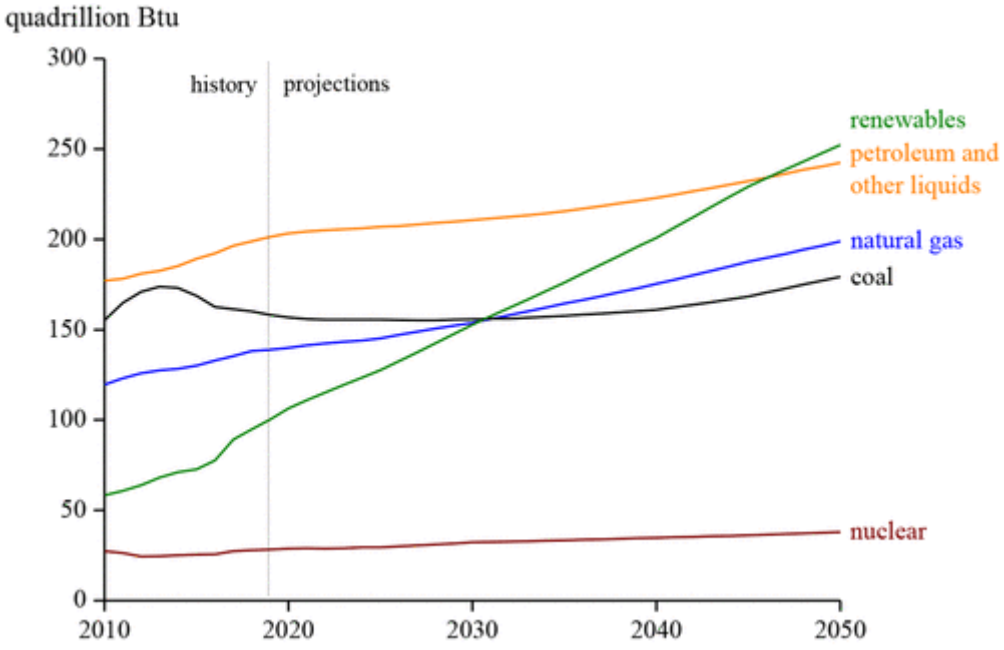

Figure 0.1: World energy consumption by energy source (2019) [7], [8]**.**

Over the last few years, there has been a lot of effort in finding renewable or alternative energy sources that are clean, sustainable and, reduce the energy crises [9]. In South Africa, only 8.8% of the energy is obtained from renewable sources [10]. Therefore, it is important to find sustainable alternative energy sources that minimize harmful emissions and reduce the excessive consumption of fossil fuels. Nonetheless, one of the challenges with renewable energy sources is the unpredictable availability of energy because of variability in location and time which may result in the energy not being available at the time of demand; therefore, an energy storage medium is required to store the energy [4].

Hydrogen (H_2) is one of the ideal energy storage carriers as it is a clean, most abundant element, exists in both water and biomass, has high calorific value, and can be stored either as a gas or liquid [4], [11]. However, hydrogen production is associated with high energy consumption, and storage and transportation of hydrogen are costly because of its extremely low volumetric density [11]. Therefore, researchers are investigating various aspects of hydrogen production, storage, safety, and its role in the energy transition [12]. Currently, hydrogen is mainly produced by industrial methods such as natural gas reforming, catalytic decomposition of natural gas, partial oxidation of heavy oils, coal gasification, and steam coal-iron gasification [13]. However, these methods are not favourable due to their reliance on non-renewable energy sources [14]. Hydrogen production (H_2) by photocatalytic water splitting (PWS) using abundant natural resources such as solar energy and water is considered to be one of the most promising technologies as it is environmentally friendly [15].

1.2 Hydrogen As Future Fuel

Previously, hydrogen was mainly used as a feedstock in petroleum and chemical industries [7]. However, hydrogen is also considered a possible energy vector because it is the most abundant element that exists in both water and biomass and has a high mass-energy density (122 kJ/g) [4]. The idea of using hydrogen as vehicle fuel was first proposed in the early 19^{th} century, but renewed interest in hydrogen emerged due to climate change and energy crises [16]. As a result, most research has shifted its focus towards its application as a fuel source in the transportation and energy sector [17]. Hydrogen is considered to be environmentally friendly because its combustion only releases heat and water vapor without producing greenhouse gases or harmful chemicals that affect the environment [18].

Many researchers have reported that hydrogen is the most promising and environmentally friendly energy source of the 21st century and can be utilized to decarbonize various sectors [19], [20]. Therefore, it is generally agreed that hydrogen is the promising solution to issues such as climate change and energy crises [21]. Hydrogen is a very advantageous fuel because of its excellent qualities such as overall storage capacity, efficiency, renewability, cleanliness, massive distribution, high conversion, zero emissions, and quick recovery [19]. However, the sustainability of hydrogen depends on the cleanliness of its production methods which is determined by the feedstock, energy used, and waste emissions [7]. According to Ji et al. [16], the whole life cycle of hydrogen will determine its sustainability. Hydrogen can be classified into five different types depending on the production pathway and feedstock used: Grey hydrogen, purple hydrogen, blue hydrogen, black hydrogen, and green hydrogen [19]. This is illustrated in Figure 1.2.

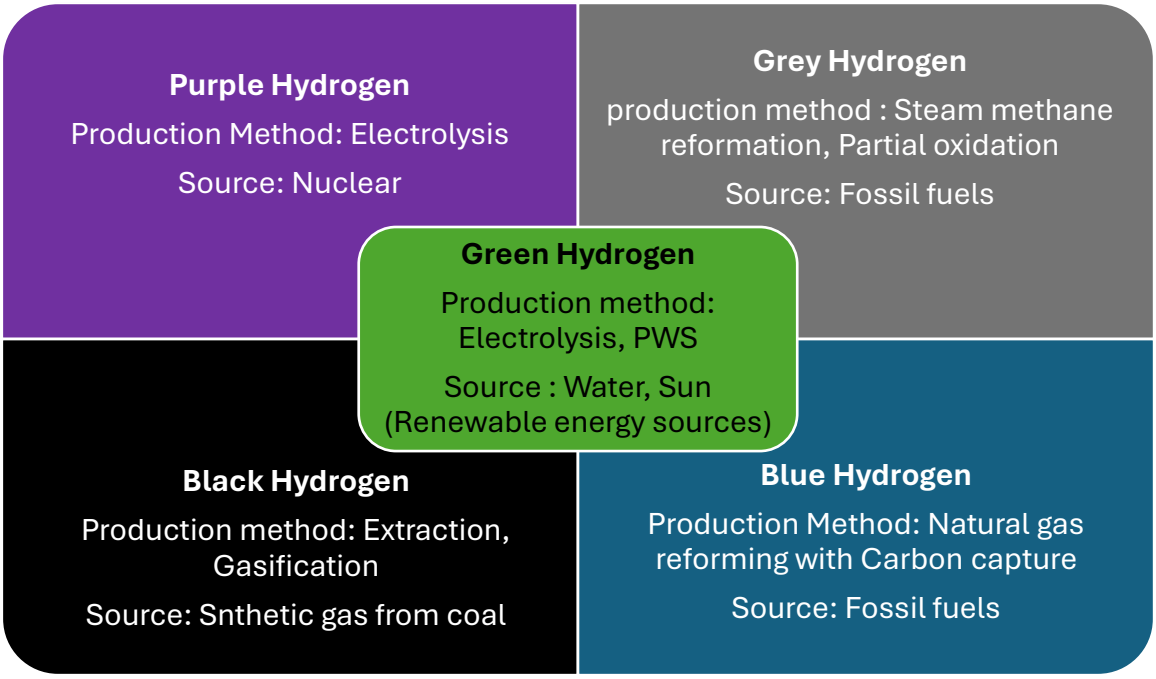

Figure 0.2: Hydrogen classification based on energy sources (adapted from [19]***)***

1.3 Research Motivation

In light of prior research, hydrogen production by photocatalytic water splitting (PWS) results in zero global warming and pollution [22] . However, almost all of the world's hydrogen is still produced from fossil fuels. Therefore, over the past years, numerous semiconductor photocatalysts have been researched and developed for PWS [23]. Titanium dioxide (TiO_2)

known as titania is one of the most effective photocatalysts used for H_2 production [24]. The advantages of using TiO_2 photocatalyst include its cost-effectiveness, chemical stability, abundance, and nontoxicity [9]. Although titania photocatalyst has excellent characteristics, it also has some drawbacks such as a large energy band gap, rapid recombination of photogenerated electron-hole pairs, and large overpotential for H_2 evolution on the TiO_2 surface [23]. To solve these problems, a lot of efforts have been made to improve the photocatalytic activity of TiO_2 in water-splitting reaction [25]. However, the development of more efficient and stable photocatalysts that result in enhanced hydrogen production is still necessary to achieve its industrial application [26]. The hydrogen evolution rate also depends on the details of the reacting system [9]. Therefore, it is important to determine the effect of various reaction conditions on the performance of photocatalysts and hydrogen production.

1.4 Problem Statement

Titanium dioxide (TiO_2) photocatalyst has a very wide energy bandgap and therefore, it can only absorb light in the ultraviolet range meaning it can only use a small fraction (about 3%) of the solar energy, leading to low photo-conversion efficiency [4], [9]. Therefore, improving the light absorption capacity and enhancing the overall photocatalytic activity of TiO_2 is crucial for advancing research in photocatalytic hydrogen production.

1.5 Aim and Objectives

Aim: To evaluate the photocatalytic production of hydrogen.

Objectives:

1) To investigate the performance of various metal-modified TiO_2 photocatalysts on the H_2 production rate.
2) To determine the influence of different sacrificial reagents on the H_2 production rate.
3) To evaluate the effect of catalyst dosage on the H_2 production rate.
4) To assess the impact of light intensity on H_2 the production rate.
5) To model and evaluate photocatalytic hydrogen production using Aspen Plus simulation software.

1.6 Scope of the project

This study focuses on a laboratory scale setup and a computer-based model designed to assess the photocatalytic production of hydrogen using TiO_2-based catalysts. The research

investigated three different types of metal-modified TiO_2 catalysts, examining the effects of various process variables, such as the type of sacrificial reagent, catalyst dosage and light intensity on the hydrogen production rate. All catalysts were synthesized using a consistent synthesis method, and the experimental work was conducted in a laboratory setup. Additionally, an Aspen Plus simulation was developed using a simplified kinetic model, which is most effective at moderate reactant concentrations. The study also includes a preliminary techno-economic analysis of the process.

1.7 Dissertation Layout

The structure of the dissertation is outlined below.

- ***Chapter 1****:* Introduction. The chapter highlights the challenges posed by climate change and energy crises, along with providing background information on hydrogen energy as a promising solution. It also provides research motivation, problem statement, aim and objectives, overall scope of the study and dissertation layout.
- ***Chapter 2***: Literature review. The chapter encompasses a brief overview of various hydrogen production, storage, transportation, and utilization technologies and provides an extensive review of Photocatalytic hydrogen production while discussing the various works that have been conducted by different researchers.
- ***Chapter 3***: Methodology. This chapter outlines the approach used to achieve the aim of the project. It provides an overview of the catalyst synthesis method, characterization techniques, photoreactor design, the process of photocatalytic hydrogen production, and the methodology used for developing Aspen Plus Simulation and conducting economic analysis.
- ***Chapter 4***: Results and discussion. This chapter presents research findings on metal-TiO_2 photocatalysts, including hydrogen production rates, experimental studies, and Aspen Plus simulation for photocatalytic hydrogen production. It also analyses the effects of various parameters on hydrogen production rates. Additionally, this chapter provides an economic analysis of the photocatalytic hydrogen production process.
- ***Chapter 5:*** Conclusion and Recommendation. This chapter provides a summary of the main findings and recommendations.

CHAPTER 2
LITERATURE REVIEW

2.1 Hydrogen Production Technologies

2.1.1 Overview of hydrogen production technologies

Hydrogen can be generated from variety of sources including fossil fuels, biomass, and water [28]. However, hydrogen sourced exclusively from renewable energy like water and solar power qualifies as a true eco-friendly energy carrier [29]. Nonetheless, several studies revealed that vast majority of the hydrogen is produced using non-renewable energy sources like petroleum and natural gas [28], [30], [31]. Amin et al. [31] highlighted that over 80% of hydrogen is derived from fossil fuels and pointed out a persistent rise in global hydrogen demand, with production reaching 95 million tons in 2022. Hydrogen production technologies encompass different methods or pathways employed to generate hydrogen from a range of resources [32]. This section focuses on various hydrogen production technologies, the resources or raw materials utilized, their efficiencies, relative production costs, technological maturity and research conducted in this field.

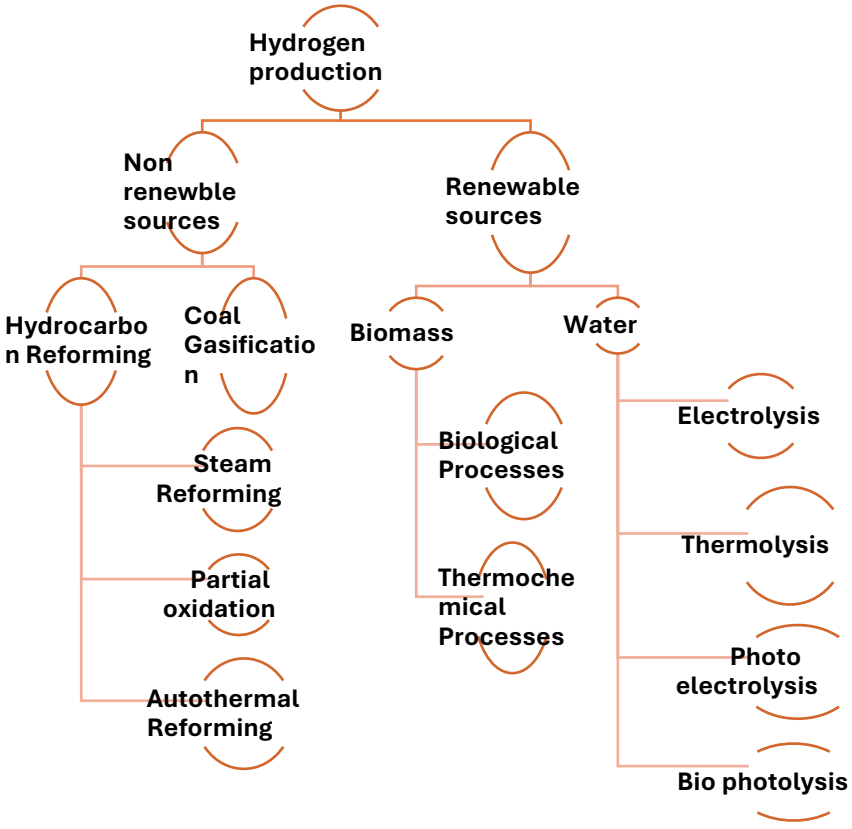

Figure 1.1:Hydrogen production technologies [33].

2.1.1.1 Hydrogen production from non-renewable energy sources

Hydrogen production from non-renewable energy sources refers to the hydrogen generated from fossil fuels such as coal, oil, and natural gas using different technologies. The major technologies are 1) Fossil hydrocarbon reforming technologies and 2) Coal gasification.

(1) Fossil Hydrocarbon reforming technologies

Hydrocarbon reforming technology is currently the most developed and mature technique used for generating hydrogen, it uses hydrocarbons along with either steam or oxygen as primary feedstocks [28]. The hydrocarbon reforming technologies are subdivided into steam reforming, partial oxidation, and autothermal reforming.

(a) Steam reforming

In steam reforming, hydrocarbons such as natural gas undergo a reaction with steam, facilitated by a catalyst at elevated temperatures, yielding hydrogen, carbon monoxide, and carbon dioxide [34]. Steam methane reforming (SMR) which utilizes the natural gas is the most commonly employed method for hydrogen production [35]. This view is supported by Pareek et al. [36] who reported that 96% of hydrogen production in the U.S. originates from SMR and by Ji et al. [37] who highlights that approximately, half of the world's hydrogen is produced using this technology. The overall SMR reaction is represented by Equation 2.1 [32].

$$CH_4 + 2H_2O \rightarrow CO_2 + 4H_2$$ ***Equation 2.1***

SMR requires temperatures ranging from 700-1000 ºC, indicating exceedingly high external energy demands [31]. Typically, SMR is mostly conducted using catalyst made from precious metal or nickel within reformer constructed from materials capable of ensuring thermal stress [28]. Ji et al. [37] suggested that reducing the energy demands can lead to decreased construction and operational cost of this process; similarly, they emphasized the importance of employing high-performance catalysts to enhance the hydrogen production capacity. This technique offers the advantage of enabling commercial hydrogen production that effectively meets the global demand at a low cost, however its main drawbacks include its dependence on the diminishing fossil fuel reserve and the generation of toxic emissions [31].

(b)Partial oxidation

Partial oxidation differs from steam reforming primarily in its use of oxygen rather than steam and its suitability for diverse feedstocks like methane, heavy fuel, and coal [33]. As an exothermic process, it avoids the high energy requirements needed in steam reforming [37]. Equation 2.2 can generally represent this reaction.

$C_nH_m + 1/2nO_2 \rightarrow nCO + ½mH_2$ ***Equation 2.2***

Partial oxidation can also be conducted with heterogeneous catalysts at lower temperatures, although some studies indicate it can occur without a catalyst [33], [38]. This technology offers several advantages, such as simpler operation, less need for desulfurization requirement, low methane slip and flexibility with different feedstocks [38]. However, its hydrogen yield is currently lower than that of steam methane reforming (SMR)[37]. Major challenges include shorter unit lifespans, low H_2/CO ratios, and issues like catalyst deactivation which limits its industrial viability [28], [37].

(c) Autothermal reforming (ATR)

Autothermal reforming (ATR) is an energy efficient method that combines elements of steam reforming and partial oxidation [32]. In this process, the heat generated from the exothermic partial oxidation supplies the energy needed for the endothermic steam reforming reaction [28], [38]. This process typically involves combining reactors in series to facilitate both reactions and like partial oxidation, it requires pure oxygen feed which adds to production costs [37]. ATR offers high thermal efficiency and is catalyst-dependent, yielding more hydrogen than partial oxidation, though less than steam reforming [28]. The disadvantage of this technology is its limited commercial experience; however, researchers are still focusing on improving catalysts for this technology [38].

(2) Coal gasification

Coal gasification is a thermochemical process that offers an alternative to direct coal combustion; in this process, coal and other feedstocks tar, biomass, solid, and plastic waste can be converted into gases like hydrogen and carbon monoxide [28]. This technology enables the production of power, liquid fuels, chemicals, and hydrogen [31]. During gasification, coal is reacted with gasifying agents such as hydrogen (H_2), oxygen or air, and steam under high temperatures and pressures to produce a mixture of hydrogen and carbon monoxide, known as synthesis gas [36]. Coal gasification methods are classified into two main types: (1) surface

coal gasification, a mature coal technology, and (2) underground gasification, a relatively newly developed technology [37].

The syngas can undergo further reactions to yield more hydrogen and carbon dioxide, this is represented by chemical Equations 2.3 and 2.4 [36]:

$3C+O_2+H_2 \rightarrow H_2+3CO$ ***Equation 2.3***

$CO+H_2O \rightarrow CO_2+H_2$ ***Equation 2.4***

A significant drawback of coal gasification is the high level of carbon dioxide emissions. Efforts to mitigate this environmental impact include integrating carbon capture and sequestration (CCS) with gasification, which has been shown to reduce emissions [35]. However, it requires substantial investments and incentives to make it viable [36]. Additionally, the quality and calorific value of the produced gas depend heavily on the grade and quality of coal [31]. Megia et al. [28] stated that from an economic standpoint, coal gasification benefits from relatively low feedstock cost compared to other fossil-fuel based technologies; however, the capital costs of the units remain high.

Hydrogen production is also possible using other non-renewable energy sources, such as nuclear power, which provides both electricity and heat that can be utilized for hydrogen extraction through various processes [35]. Table 2.1 presents cost estimates of different hydrogen production technologies.

Table 1.1:Cost estimates of various hydrogen production technologies [31].

Method	**Cost ($/Kg H_2)**
Natural Gas SMR	0.9-3.2
Coal Gasification	1.2-2.2
Nuclear energy	3.18- 3.63

2.1.1.2 Hydrogen production from renewable energy sources

As noted in Section 2.1.1, most hydrogen is currently produced from non-renewable sources. However, the growing demand for sustainable and clean energy sources has driven development of technologies to produce green hydrogen using renewable resources. Several processes used to produce hydrogen (H_2) from renewable sources, such as water, sunlight, wind, biomass, and geothermal energy are discussed below.

(1) Hydrogen production from water

Water is the most abundant source of hydrogen and can be split into hydrogen and oxygen with minimal environmental impact [28]. Four common technologies are used for water splitting, each differing in energy sources and operating conditions.

(a) Electrolysis

Electrolysis is the first-ever method used by humans to produce hydrogen [37]. It involves, applying an electric current to water which splits into hydrogen and oxygen [36]. Dincer et al. [38] reported that currently electrolysis contributed about 3.9% of global hydrogen production, primarily on a small scale. The main electrolysis technologies are alkaline electrolysis (AEL), solid oxide electrolysis (SOEL), proton-exchange membrane (PEM), and alkaline anion exchange membrane (AEM) [28]. Among these, AEL and PEM are regarded as the most cost-effective and scalable technologies; interestingly, these technologies can also be coupled with renewable sources [31].

Electrolysis driven by renewable sources like wind, solar, or ocean wave energy is sustainable and allows for scalability without CO_2 emissions [28]. Pareek et al. [36] suggests that the renewable-powered electrolysis could lower hydrogen production costs, particularly when using wind or nuclear energy. Conversely, Dincer et al. [38] reported that photovoltaic (PV) electrolysis is still significantly more expensive than fossil fuel-based hydrogen production technologies. Wind-powered electrolysis is already implemented in various countries, though challenges such as the variability of the wind energy supply still remain. Similarly, solar-powered electrolysis faces efficiency and consistency issues due to solar cell limitations and varying sunlight availability. Overall, electrolysis shows great potential to meet the demand for green hydrogen and researchers are focusing on improving the efficiency and reducing the cost of electrolysis.

(b) Thermolysis

Thermolysis is a thermochemical process that involves decomposition of water at extremely high temperatures, making it highly energy-intensive [38]. Key challenges include separation of the products and the availability of a material that can withstand high temperatures [28]. Alternatively, hydrogen can also be generated by thermochemical water splitting cycles, which operate at lower temperatures and higher efficiencies [33]. Pareek et al. [36] reported that the heat can be provided using nuclear or solar energy resulting in clean and pure hydrogen. However, hydrogen production via water thermolysis is costly such that its 12.5 times more

expensive than coal gasification and 3.3 times more than commercial electrolysis [39]. Another major issue is the hydrogen and oxygen tend to recombine back into water, limiting its commercial viability; however, the ongoing research aims to improve this technology, especially by integrating renewable energy sources [37].

(c) Photo electrolysis

Photo electrolysis is a sustainable, eco-friendly process that uses the two most abundant renewable resources like water and sunlight [36]. In photo electrolysis, hydrogen is produced directly from sunlight without using any expensive solid-state photovoltaic junction [40]. This process occurs in a photoelectrochemical cell (PEC), which contains anode and cathode electrodes, with a photocatalyst applied to one or both electrodes [38]. When the photoelectrode absorbs photons with energy extending its band gaps, it initiates water splitting to produce hydrogen [28]. The major disadvantages of photo electrolysis include low conversion efficiency and ineffective photocatalytic materials [33]. Another photo electrolysis technique is called photocatalytic water splitting which involves the use of semiconductor powder instead of photo electrodes to generate hydrogen [32]. Another method known as photocatalytic water splitting or photocatalytic hydrogen production, uses semiconductor powder instead of photoelectrodes to generate hydrogen. This technique, which is the focus of this study is discussed in detail in Section 2.2.

(d) Bio photolysis

Bio-photolysis is a biochemical process for hydrogen production that mimics the photosynthesis process found in plants [28]. Bio-photolysis occurs in a specially designed photoreactor, where light-sensitive microorganisms act as biological converters to split water and produce hydrogen [38]. There are two types of bio-photolysis: direct and indirect [36]. This process is an environmentally friendly since it only requires water. However, further technological advancements are needed to make bio-photolysis efficient and cost-effective enough for large scale hydrogen production [32], [37].

(2) Hydrogen production from biomass

Biomass is a renewable energy source that includes a wide variety of materials such as wood, grass, agricultural products, crop residues, plant and animal wastes, municipal solid wastes, food scraps and algae [33]. Over the past two decades, bio-hydrogen production has gained significant attention as a way to reduce waste by converting it into hydrogen [36]. Megia et al [28], reported that in developed countries, hydrogen production from biomass is both

technically and economically feasible due to the advanced technologies and favourable economic conditions. There are two pathways for producing hydrogen from biomass: 1) Biological processes and 2) Thermochemical processes [37]. The biological processes include dark fermentation and photo fermentation, while the thermochemical processes involve gasification, pyrolysis, and liquefaction [32], [38].

(a) Biological processes

In the dark fermentation process, anaerobic bacteria are used to convert carbohydrate-rich substrates into hydrogen, organic acids, and CO_2 without the need for light [37]. Megia et al. [28] highlighted that although this method is limited by metabolic factors that restrict hydrogen yield, there have been advancements to improve efficiency. A key advantage of dark fermentation is that it can produce hydrogen continuously, as it does not rely on the light; however, its main drawback is low energy conversion efficiency [33], [38]. In photo fermentation, photosynthetic bacteria use light as an energy source to convert biomass into hydrogen and carbon dioxide [32]. While this method can use a wide variety of substrates and waste streams, it faces challenges such as the need for large reactor volumes and significant surface area to capture enough sunlight [28]. Biological hydrogen production is still in the early stages of development and requires significant research and development to optimize and scale up [36].

(b) Thermochemical processes

Biomass thermochemical conversion process is similar to that of fossil fuels and uses similar processes discussed in section 2.1.1.1. Ji et al. [37] reported that hydrogen production from biomass gasification achieves only 50% efficiency. However, the challenge with biomass gasification is that large-scale cultivation of energy crops requires significant natural resources and land [35]. Additionally, biomass gasification is more complex than coal gasification, as it produces undesirable by-products that need additional processing to produce pure synthesis gas [36]. The drawback of all thermochemical processes is that the yield depends heavily on the feedstock used [28]. Despite these challenges, these processes have advantages such as CO_2 neutrality and availability of cheap, abundant feedstock [33]. Ji et al. [37] concluded that biomass gasification is cost-effective and environmentally friendly, but it still requires improvements in efficiency and product purity to become a more viable alternative.

2.1.2 Overall comparison

This section summarizes and compares the hydrogen production technologies discussed earlier. Currently, hydrogen is primarily produced from natural gas and fossil fuels through steam reforming, a well-established and cost-effective method suitable for large-scale production [36]. However, due to the environmental impact of fossil fuels, research is increasingly focusing on hydrogen production from renewable sources [31]. Efforts to reduce carbon dioxide emissions have led to technologies like carbon capture and sequestration combined with hydrogen production from non-renewable sources [32]. Nonetheless, transitioning to renewable energy sources for hydrogen production remains a promising option [37].

Significant progress has been made in hydrogen generation from renewable sources, such as biomass and water [28]. Biomass-based hydrogen production provides comparable yields to water-based methods but with lower operating costs and greater energy efficiency [31]. Electrolysis, when powered by renewable energy, offers a feasible method for hydrogen production, although it remains costly [36]. With ongoing improvements in efficiency and cost-effectiveness, electrolysis could potentially address environmental concerns [32]. Biological hydrogen production methods offer clean and pure hydrogen, but these technologies are still in the early stages of development and require further research to become commercially viable [36]. Comparing the cost of various hydrogen production technologies, fossil fuel reforming remains the most cost-effective method (\$0.75/kg H_2) due to its high energy efficiency. On the other hand, photoelectrochemical hydrogen production, which is still in the early stages of research, is the most expensive method (\$10.36/kg H_2) and suffers from low photo efficiency [38].

Photocatalytic water splitting is a promising pathway for renewable, clean hydrogen production. However, it is still in the early research phase and requires advancements in material science and reaction efficiency to become a significant contributor to sustainable hydrogen production in the future [38]. Therefore, this study aims to explore photocatalytic hydrogen production by examining various photocatalysts and identifying optimal conditions for hydrogen generation. A detailed literature review on this topic is provided in Section 2.2.

2.2 Photocatalytic Hydrogen Production

2.2.1 Photocatalytic water splitting (PWS)

Photocatalytic water splitting involves dissociation of water into stoichiometric hydrogen (H_2) and oxygen (O_2) by harnessing solar energy and converting it into chemical energy with the use of a photocatalyst [41]. Photocatalytic water splitting allows the production of hydrogen using the two most abundant renewable sources such as water and sunlight [42]. Photocatalysts are semiconductor materials that absorb photons and facilitate the reaction [43]. Water splitting is an endothermic process and is characterized by a significant positive change in the Gibbs free energy ($\Delta G^{\circ} = +\frac{237kJ}{mol}, 2.46\ eV\ per\ molecule$) [44].

2.2.1.1 Photocatalytic water splitting mechanism

The photocatalytic water-splitting process involves the following steps: light absorption, charge generation and separation, and redox reactions at the catalyst's surface [45]. Firstly, the photocatalyst absorbs light with energy greater than its band gap (E_g) energy [46]. The band gap of a photocatalyst refers to the difference in energy levels between its unoccupied conduction band (CB) and electron occupied valence band (VB) [41]. Upon irradiation, the electrons (e^-) from the valence band transition to a conduction band forming holes (h^+) in the VB [44]. Eidsvåg et al. [47] reported that based on the ΔG°, for a photocatalytic water splitting process a photocatalyst with a bandgap greater than 1.23 eV is essential. In the second step, the electron, and holes created move towards the catalyst's surface and react with water in an oxidation and reduction reaction [44]. The electron reduces H^+ , while the hole oxidizes H_2O to produce hydrogen and oxygen, respectively [48]. The photocatalytic water splitting mechanism is described by Equation 2.5-2.8 and the process is illustrated in Figure 2.2 [45].

Catalyst → Catalyst ($e^- + h^+$) ***Equation 2.5***

Catalyst ($e^- + h^+$) → Catalyst ***Equation 2.6***

$H_2O + h^+ \rightarrow 1/2O_2 + 2H^+$ ***Equation 2.7***

$2e^- + 2H^+ \rightarrow H_2$ ***Equation 2.8***

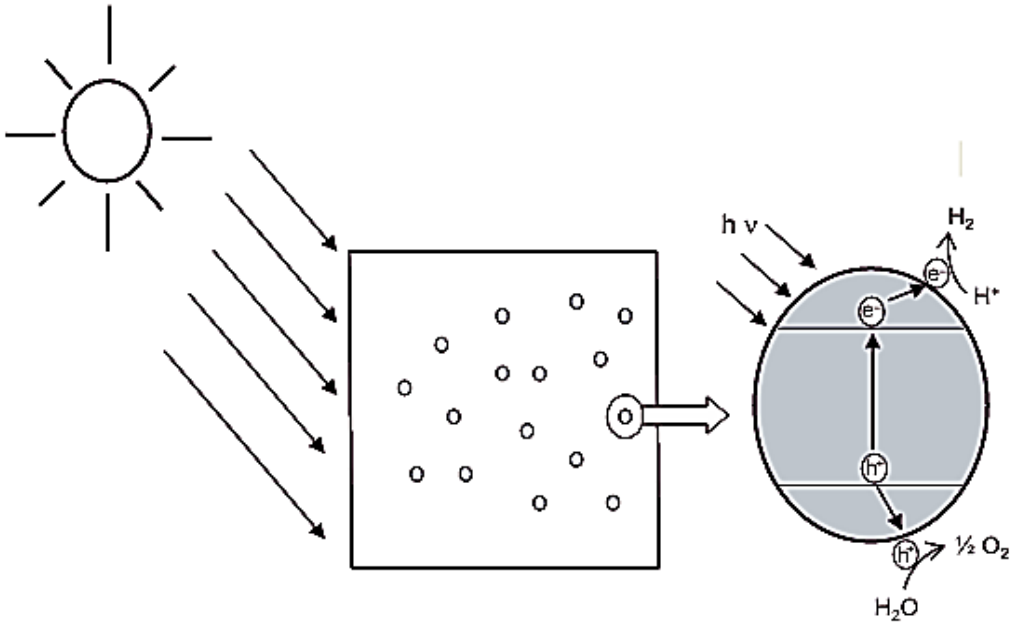

Figure 1.2: Photocatalytic water splitting mechanism [44].

The primary challenge in photocatalytic water splitting is the recombination of electron-hole pairs (charge) (e^- / h^+), as shown by Equation 2.6 [45]. The charge recombination results in no net chemical reaction and hydrogen cannot be produced [48]. Eidsvåg et al. [47] reported that the effectiveness of the photocatalyst is maximized in an ideal situation such as in the absence of electron-hole recombination.

2.2.1.2 Types of photocatalytic water splitting reactions

Photocatalytic water splitting is classified into two types of reactions: 1) Photochemical cell reactions and 2) Photo-electrochemical cell reactions.

(1) Photochemical-cell reactions

In photochemical cells, water splitting occurs by the direct use of solar energy [49]. The powdered photocatalyst is present as dispersed particles in an aqueous solution, this allows particles to function as micro photoelectrode that performs redox reactions to produce hydrogen and oxygen (Figure 2.3) [44]**.** According to Liao et al. [48], the benefit of photochemical cell is that the suspended photocatalyst particles maximizes the available surface area for efficient photocatalytic reactions.

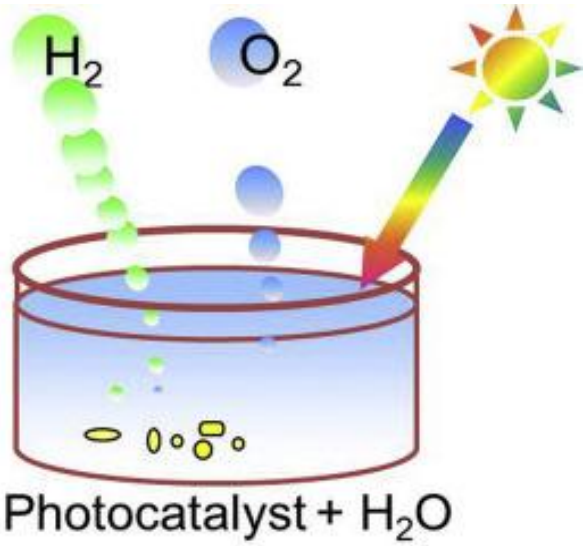

Figure 1.3: Schematic of a Photochemical cell [50].

(2) Photoelectrochemical-cell reactions

Fujishima and Honda in 1972 pioneered the production of hydrogen via photocatalytic water splitting in a photoelectrochemical cell [51]. In Photoelectrochemical cells (PEC), as opposed to photochemical cells, a thin layer of photocatalyst is applied on either one or two electrodes to form photoelectrodes which are submerged in an aqueous electrolyte [48].The photoelectrode is exposed to light to conduct the water-splitting reactions [44]. This process requires an additional source of power to electrolyze water before generating hydrogen [41]. As shown in Figure 2.4, the generated electrons are transferred from the photo-anode to a cathode, leading to the generation of hydrogen, this chemical reaction results in an electric current to flow through the external circuit [52]. Pareek et al. [42] reported that this technology is still not commercially viable and requires research on suitable +semiconductors and the design of the reactors. Jiang et al. [53] studied photoelectrochemical cell reactions and identified challenges in controlling various parameters, such as light absorbance by the photocatalyst, determining instantaneous substrate concentration, and maintaining pH of the reaction solution during the process. Ahmad et al. [52] reported that these factors significantly affect the kinetic behaviour which complicates the interpretation of the experimental findings.

Water splitting in a photochemical cell is a simple process as it does not require expensive equipment, and it is easy to use [48]. The disadvantage of a photochemical cell includes easy recombination of oxygen and hydrogen, whereas in photoelectrochemical cells, efficient separation of oxygen and hydrogen can be achieved enhancing the photocatalytic activity [44].

Additionally, Saddique et al. [41] reported that photochemical water splitting is a more viable option than photoelectrochemical water splitting due to its performance, cost-effectiveness, and environmental friendliness.

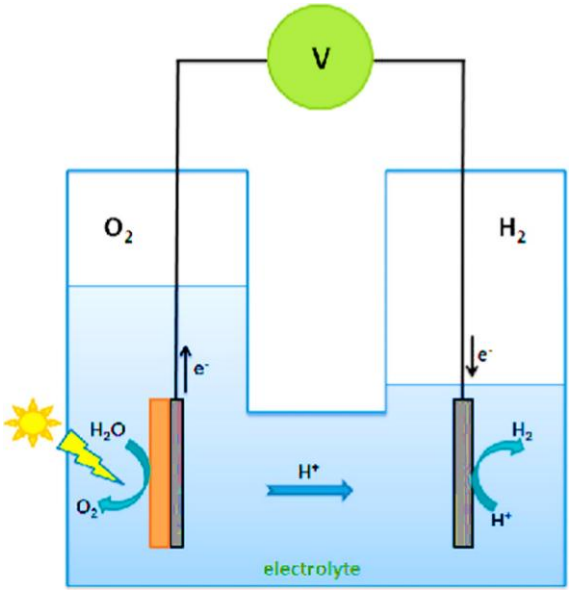

Figure 1.4: Schematic of a Photoelectrochemical cell [52]**.**

2.2.2 Photocatalysis

Photocatalysis refers to the chemical reaction that occurs as a result of photoirradiation in the presence of a photocatalyst [48]. The two types of photocatalysis processes are 1) homogeneous photocatalysis, in which the reactant and photocatalyst are in the same phase, and 2) heterogeneous photocatalysis, in which the reactant and photocatalyst are in different phases [43]. Sudhir et al. [54] reported that materials with semiconductor properties are commonly utilized as photocatalysts for light redox reactions driven by light. The working principle of a photocatalyst has been discussed in Section 2.1 of this work. Applications of photocatalysts include water purification, photocatalytic hydrogen production, controlling odour, deactivating cancer cells, and eliminating bacteria [55].

2.2.2.1 Types of photocatalysts

For effective photocatalytic water splitting, it is crucial to have a photocatalyst or semiconducting material with suitable properties such as conductivity, redox potential, band gap, non-toxicity, light absorption, cost-effectiveness, scalability, and fabrication versatility [54]. Numerous types of photocatalysts have been reported in the literature. These include photocatalysts like oxides such as TiO_2, Fe_2O_3, Ag_3PO_4, CuO, ZnO, MoO_3, and WO_3, sulfides such as CdS, $ZnInS_4$, nitrides such as g-C_3N_4 , and carbon-based materials such as Graphene,

nanotubes [45]. In recent years, numerous studies have focused on researching and developing various photocatalysts to enhance their efficiency in photocatalytic hydrogen production. According to Liao et al. [48], to obtain high photo conversion efficiency, it is crucial to ensure effective charge separation, prevent backward reactions of O_2 and H_2, and utilize both UV and visible light energy efficiently. An essential electrochemical property of the photocatalyst is its chemical stability against corrosion and photo-corrosion when exposed to an aqueous solution [41].

Titanium dioxide (TiO_2) is a widely recognized and highly promising photocatalysts, utilized for a range of applications including water dissociation, air and water purification, odor removal, antibacterial uses, and self-cleaning surfaces [51]. Its excellent properties, such as low cost, abundance, good chemical stability, nontoxicity, and capability to effectively oxidize and reduce water molecules, contribute to its enhanced photocatalytic performance [56]. TiO_2 exists in three different crystal polymorphs or phases such as anatase, rutile, and brookite; among these phases, rutile is the most stable phase [57]. The properties of the three phases are given in Table 2.2. However, due to the very high energy bandgap of TiO_2 (3.0-3.2 eV), it results in absorption of only UV light and hence low photo-conversion efficiency [58]. A summary of its various benefits and limitations can be found in Table 2.3. Nevertheless, several studies have revealed that TiO_2 has structural and chemical properties that allow the modification of bandgap and other properties [47]. Consequently, research has focused on improving the properties of TiO_2 photocatalyst to decrease its bandgap and enhance the photoconversion efficiency. A commercial TiO_2 known as TiO_2 P25 Degussa, comprising a mixture of anatase and rutile phase with an 80:20 ratio, is widely utilized and studied due to its high photocatalytic activity [59].

Table 1.2: Properties of TiO_2 polymorphs [57].

Property	**Anatase**	**Rutile**	**Brookite**
Crystal structure	Tetragonal	Tetragonal	Orthorhombic
Atoms per unit cell	4	2	8
Density, g cm^{-3}	3.83	4.24	4.17
Band gap, eV	3.26	3.05	N/A
Refractive index	2.57	2.95	2.81

Table 1.3: Advantages and Disadvantages of TiO_2 photocatalyst in water splitting [52].

Advantages	Disadvantages
▪ Enhanced photo-chemical stability ▪ Renewable hydrogen production through solar energy. ▪ Excellent resistance to photo-corrosion ▪ Abundant, cheap, and non-toxic ▪ Readily synthesized in nanocrystalline form through simple methods	▪ Rapid electron-hole pair recombination and potential backward reaction leading to formation of water. ▪ Wide band gap ▪ Significant over potential required for hydrogen production on the surface of TiO_2.

Many other oxide catalysts have been reported in the literature, but they have their limits contributing to low photocatalytic performance. For instance, ZnO, CuO, Fe_2O_3, and SnO, exhibit poor photochemical stability in solution, whereas other catalysts are comparatively expensive and challenging to acquire [60]. According to Ahmad et al. [52], most metal sulphide photocatalysts have a problem of photo corrosion but much of the recent literature suggests that a lot of modified sulfide photocatalysts tend to be good photocatalysts for hydrogen generation. Gandía et al. reported that the majority of the photocatalysts exhibit activity only under UV light, with very few catalysts developed to be active under visible light [44].

According to Villa et al., present photocatalytic solar to hydrogen (STH) efficiencies are reaching 1%, however, they are still lower than the efficiencies achieved by other well established hydrogen production methods based on fossil fuels [61]. Saddique et al. [41] reported that the overall performance of the photocatalytic hydrogen production process relies on the photocatalyst. Therefore, the advancements of effective photocatalyst systems are crucial to meet the requirements of solar to hydrogen efficiency and to advance photo-catalytic hydrogen production towards practical applications [41], [61]. A considerable amount of literature has been published on photocatalysts, however, the search for better photocatalysts continues to enhance the feasibility and sustainability of PWS as a method for hydrogen production. This review examines TiO_2-based photocatalysts with a focus on their application in photocatalytic water splitting. It combines existing knowledge on various aspects of photocatalytic water splitting using TiO_2-based photocatalysts.

2.2.2.2 Modification of TiO_2 photocatalyst

The research to date has focused on enhancing the photo-catalytic activity of TiO_2 catalysts under visible light conditions. The following modified TiO_2 photocatalysts have shown increased photoactivity as a result of the modification to their structural and chemical properties.

(1) Metal-modified TiO_2

One of the most widely used modification methods is metal doping. This process involves introducing elements, such as dopants, into the TiO_2 crystal structure. These dopants directly influence the surface electronic properties, physical characteristics, and light absorption capability of TiO_2, while preserving its original crystallinity [56][62]. Metal dopants generally used include transition metals, noble metals, and rare-earth metals.[63] Metal doping significantly impacts the photocatalytic activity of TiO_2 in several ways: i) prevention of rapid electron-hole recombination: This is achieved by an electron trap mechanism, where metal dopants capture electrons or holes within TiO_2, thereby extending the lifetime of the charge carrier and promoting more efficient charge separation. This process enhances the photocatalytic hydrogen production rate, ii) Creation of additional active sites: The electrons trapped by the metal provide extra active sites for photochemical reactions on the catalyst's surface. This not only improves the efficiency of these reactions but also lowers the over-potential required for water splitting, iii) Generation of new energy levels: metal doping introduces new energy levels within TiO_2, which facilitates improved charge transfer and reduces the bandgap of the material. This adjustment extends the light absorption range into visible spectrum, enhancing the photocatalytic activity [45], [56], [62], [64].

The enhanced photocatalytic activity of metal-modified TiO_2 can be attributed to two key phenomena: a) the formation of a Schottky junction under UV light irradiation, and b) the surface plasmon resonance (SPR) effect under visible light irradiation. Schottky junction is established under UV light by the arrangement of bands at the metal-semiconductor heterojunction, which creates an electronic barrier. This enables the transfer and capture of electrons into the metal, thereby reducing charge recombination and ultimately enhancing efficiency (Figure 2.5(a)) [45]. The photocatalytic efficiency of metal doped TiO_2 is determined by the metal's work function, representing the energy required to transition an electron from the Fermi level into the vacuum. A metal with a high work function improves its capacity to accept electrons, which, in turn, enhances charge separation [45]. The formation of

a large Schottky barrier result in enhanced hydrogen production as it enhances the differences in work function between the metal (s) and the semiconductor. The SPR effect is depicted in Figure 2.5(b). During exposure to visible light, photogenerated electrons in the localised surface plasmon resonance (LSPR) of noble metal/s can effectively move to the conduction band (CB) of TiO_2 which undergo reductions at the catalyst's surface, thereby increasing the photocatalytic activity [46].

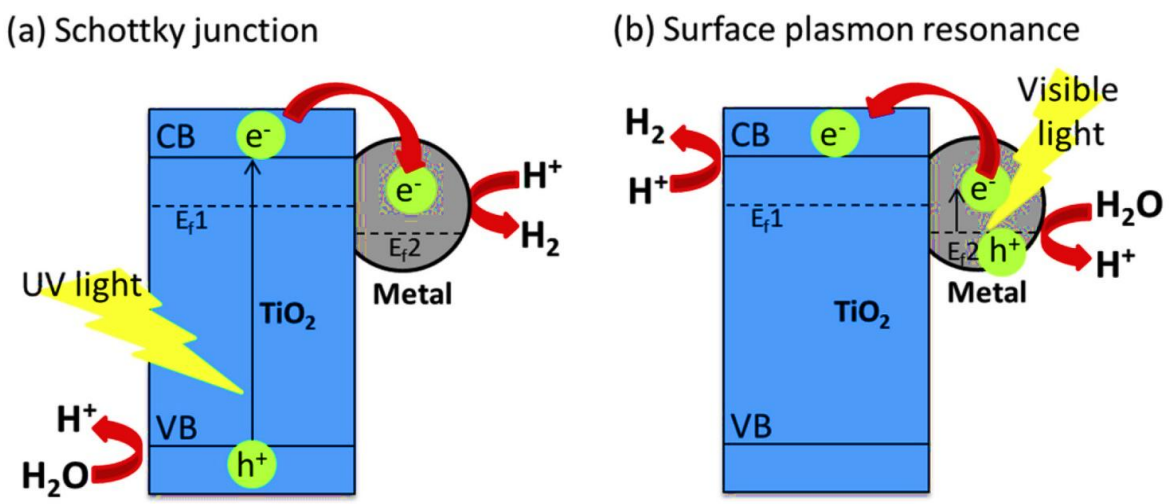

Figure 1.5: Photocatalytic water splitting on metal-doped TiO_2 [46].

Díaz et al. stated that the hydrogen production rate is influenced by the experimental configuration and cannot be utilized to compare the findings of various researchers [65]. Nevertheless, it is beneficial to contrast the experimental outcomes of a novel or modified photocatalyst with those attained using a widely recognized commercial catalyst like TiO_2 P25. Rusinque et al. [66] observed that the volume of hydrogen produced using Pd-doped TiO_2 is approximately three times higher than that produced with unmodified TiO_2. The introduction of metal dopants also causes a notable shift in absorption towards the visible light region [67]. This aligns with the findings of the study conducted by Díaz et al., which illustrated that under both UV and visible light irradiation, the hydrogen production rate obtained with Cu/TiO_2 was significantly greater than that with undoped TiO_2 [65]. The increased photocatalytic activity upon exposure to visible light irradiation indicates that the metal doping reduces the wide energy bandgap of the TiO_2 catalyst. Additionally, metal dopants create oxygen vacancies and result in the formation of Ti^{3+} within the TiO_2 lattice, which extends the lifespan of photogenerated electrons and holes [68]. Among various metals, noble-metal dopants are more effective for hydrogen production because they enhance photocatalytic performance in the

visible spectrum due to their pronounced SPR effect [69]. However , generally, doping with Ag and Au is thermodynamically more stable compared to doping with Pt, Pd, and Ru [47]. However, among all these metals, Platinum is the most extensively researched dopant due to its ability to yield a substantial rate of hydrogen production. However, the use of noble metal modified TiO_2 catalysts for large-scale hydrogen production is not economically feasible because of the expense and rarity of the noble metals [65]. This has motivated the search for alternative dopants and co-catalysts that are more cost-effective [70].

Based on the results collected by Sangpour et al. [71], Adamu et al. [57] noted that the photocatalytic performance of copper-doped TiO_2 is comparable to that of the platinum doped TiO_2. This aligns with the conclusion drawn by Díaz et al. [65] who suggested that copper is a promising substitute for platinum as it is a cost-effective, efficient co-catalyst and yields a comparable H_2 rate. This aligns with the results obtained by Chen et al. [72] who investigated Cu loaded TiO_2 nanorod photocatalyst and observed that a 0.1wt%-Cu/TiO_2 catalyst resulted in efficient hydrogen production (1023.8 $\mu mol.h^{-1}$), which is approximately 20 times higher than that resulted from pure TiO_2 (49.4 $\mu mol.h^{-1}$). Notably, this rate approached that of Pt/TiO_2 (1161.7 μmol.h-1) [72]. In a theoretical investigation conducted by Hussein et al. [73] to find the effects of copper doping on the photocatalytic performance of anatase TiO_2, it was noted that the improved H_2 rate using Cu/TiO_2 was due to the reduced bandgap and increased charge transfer rather than the surface chemistry of the adsorbed water. Various studies have shown that in Cu/TiO_2 catalysts, Cu exists in many different forms such as CuO (Cu(II)), Cu_2O (Cu(I)), and Cu (Cu(0)) [57]. Adamu et al. found that the distribution of Cu(II) and Cu(I) was influenced by the pH used during the synthesis process [57].

Numerous studies have extensively explored Cu-based TiO_2 catalyst and its application in photocatalytic water splitting. Hinojosa-Reyes et al. reported that hydrogen production through Cu-doped TiO_2 was four times greater than bare TiO_2 [74]. In a recent investigation by Quyen et al., [75] Cu-TiO_2 demonstrated excellent stability and resulted in a fairly constant hydrogen production rate even after being reused for five consecutive cycles. This indicates that the reusability and stability of the Cu/TiO_2 catalyst make it a suitable candidate for industrial photocatalytic water splitting. Another catalyst that has attracted significant attention due to its surface plasmonic resonance (SPR) effect is the Ni-based TiO_2 catalyst [76]. Chen et al. [77] reported that Nickel species such as metal nickel, nickel oxide, and nickel hydroxide are

more cost-effective compared to noble metals and have been proven to improve photocatalytic hydrogen production. Chen et al. [78] also reported that Nickel is one of the most suitable transition metals co-catalysts due to its affordability, abundance, and high work function (Ni Ø = 5.3 eV).

Díaz et al. investigated various metal-loaded TiO_2 (M/TiO_2) catalysts and found that the Cu and Ni loaded TiO_2 catalysts demonstrated notable photocatalytic activity under UV irradiation [65]. However, the H_2 rate obtained with Cu/TiO_2 photocatalyst was higher compared to that with Ni/TiO_2 photocatalyst. This observation is consistent with the findings of Montoya et al. [79], who observed that 1wt% Cu/TiO_2 resulted in 84.7 µmol/h of hydrogen as compared to 1wt% Ni-TiO_2 which resulted in 33.9 µmol/h of hydrogen under similar conditions. Notably, there is limited research available on the utilization of Ni/TiO_2 photocatalyst for the process of water splitting [78]. Various other effective non-noble metal dopants reported in the literature include Fe, Cr, Co , Rh, Ru, Nb, W, Ga, among others.

(2) Bimetallic TiO_2

Another interesting modification technique involves deposing bimetallic co-catalysts on TiO_2 and these types of catalysts have been extensively studied and widely utilized in industrial applications [67]. Naseri et al. [80] proposed that bimetallic deposited TiO_2 leads to an enhanced hydrogen production rate compared to monometallic deposited TiO_2. This corresponds with the findings of Tian et al. [81] who reported that the bimetallic cocatalyst has the potential to serve as an effective cocatalyst for TiO_2, enhancing its photocatalytic activity more efficiently. The literature contains numerous studies on bimetallic-deposited TiO_2 photocatalysts. Fuentes et al. [82] studied the performance of Pt-Ru, Pt-Ir, Pt-Ru-Ir, and Ir-Ru bi/tri metallic supported TiO_2 catalysts in an oxygen evolution reaction (OER). Bimetallic catalysts have also been used in thermo-catalytic processes such as methane reforming, carbon dioxide hydrogenation, and methane cracking [76].

Bimetallic co-catalysts composed of Cu and Ni, when doped on to various semiconductor materials, are known to enhance the efficiency of various valuable industrial reactions [83]. Tian et al. [81] investigated the Cu-Ni/TiO_2-based photocatalytic system in water splitting. It was found that the Cu-Ni bimetallic deposits function as active sites and result in high photocatalytic activity. In a recent investigation by Kotesh Kumar et al. [76] on Cu-Ni/TiO_2

for water splitting, it was observed that the Cu-Ni alloy nanoparticles exhibited substantial photo reactivity under solar light, leading to a H_2 rate of 35.4 $mmol.g^{-1}.h^{-1}$. The study concluded that this effect was attributed to surface plasmon resonance (SPR) and the synergistic effect between Cu and Ni metal species, ultimately enhancing the photocatalytic activity [76].

A highly dispersed and novel 1wt% Cu:Ni/TiO_2 catalyst synthesized by Ibrahim et al. resulted in maximum H_2 production rate of 8.5 $mmol.h^{-1}.g^{-1}$[84]. Majeed et al.[85] synthesized 0.8$Cu(OH)_2$-0.2 $Ni(OH)_2$/ TiO_2 nanorods and achieved a maximum H_2 production rate of 35 $mmol.h^{-1}.g^{-1}$. Nevertheless, these catalysts were only evaluated under a UV light source, and their activity under visible light was not assessed [84], [85]. Mohd Amin et al. [62] noted that the enhanced hydrogen production rate resulted from using a bimetallic catalyst was due to the reduced energy band gap of the catalyst. Other bimetallic catalysts that have been developed are given in Table 2.4. Various studies investigating bimetallic catalysts for PWS have examined the impact of different factors such as synthesis conditions, metal ratio and concentration, dosage of catalyst, and concentration of sacrificial reagent. However, there have been relatively few studies examining the impact of different sacrificial reagents or electron donors on the rate of hydrogen production using bimetallic catalysts.

Analysis of various literature sources indicates that the enhanced hydrogen production rates with bimetallic TiO_2 catalysts can be attributed to the synergetic effect of combining two metals. The photocatalytic efficiency of these bimetallic catalysts is improved through the following mechanisms: i) enhanced charge carrier separation: one metal traps an electron while the other traps holes, leading to better charge carrier separation and increased carrier lifetime. ii) Bandgap narrowing: The presence of two metals narrows the bandgap, which enhances light absorption and shifts the absorption edge into the visible region. iii) Increased active sites: the distribution of both metals on the catalyst surface provides more active sites for catalytic reactions. iv) Formation of heterojunctions: The combination of two materials with different work functions creates a heterojunction, resulting in a more appropriate Schottky barrier height and efficient charge transfer [56], [62], [69], [70].

Table 2.4 presents metal-, non-metal-, and bimetallic modified TiO_2 catalysts that have been researched in the past few years. From Table 2.4, it can be seen that most studies on metal/nonmetal/bimetallic doped TiO_2 catalysts were conducted using a well-known

commercial TiO_2 (P25 TiO_2) catalyst. According to Hanaor et al. [86], the metal dopants reduce the wide band gap of TiO_2 and can either facilitate or inhibit the phase transformation from anatase (A) to rutile (R), thereby affecting the photocatalytic activity and hydrogen production rate which are dependent on the structural configuration of TiO_2. Interestingly, in their study, Adamu et al. [57] examined the effects of various synthesis methods on the properties of Cu/TiO_2 catalyst for the reduction of carbon dioxide. The results indicated that doping P25 TiO_2 (80% anatase, 20% rutile) with Cu using the incipient wetness impregnation method resulted in a decrease in the anatase phase to 73% while the rutile phase remained unchanged. Conversely, copper doping using the sol-gel method prevented the transition of the anatase to the rutile phase and increased the anatase to rutile ratio (A/R) [57]. There are various studies conducted on metal-doped TiO_2 catalysts for photocatalytic water splitting. However, several studies reviewed did not account for the impact of doping on the A/R ratio and its subsequent effect on photocatalytic hydrogen production.

To summarise, modifying TiO_2 with metals effectively reduces the rate of charge recombination, improves response to visible light, and hence increases the activity of TiO_2 in photocatalytic hydrogen production. However, Yang et al. stated that the type and quantity of dopants are crucial parameters that influence the photocatalytic performance, such that if the amount of dopant surpasses a certain concentration, the lattice structure of TiO_2 becomes significantly distorted, consequently restricting improvements in photocatalytic performance [63]. Therefore, many researchers have studied the effects of metal concentration in the photocatalyst on its activity. For instance, Díaz et al. [65] studied the effect of Cu loading on TiO_2 on the rate of hydrogen production and found that as the concentration of Cu increased from 0.1 to 0.5 wt.%, the H_2 rate increased significantly; nevertheless, increasing Cu content above 3 wt.% led to a decrease in H_2 rate. Tian et al. found similar results and reported that the excessively elevated concentration of Cu/Ni alloy leads to reduced photocatalytic activity of Cu/Ni-TiO_2 [81]. The maximum hydrogen production rate was achieved when ratio of Cu to Ni was equimolar; furthermore, increasing the metal content beyond this ratio resulted in a decreased hydrogen production rate [81]. The findings of Kumaravel et al. [56], indicate that increased metal loading leads to the formation of a space charge layer, which enhances charge separation by increasing the surface barrier and reducing electron-hole recombination. However, beyond a certain metal concentration in TiO_2, photocatalytic activity diminishes significantly. Excessive metal loading can cause particle agglomeration, reduce surface area , decrease light penetration depth, increase scattering, and lower light absorption. It may also

create recombination canters [62], [69]. Overall, excessive dopant loading negatively impacts the photocatalytic efficiency of TiO_2 and results in decreased hydrogen production rates. Therefore, it is crucial to determine the optimal metal content in metal-modified TiO_2 catalysts that maximizes the rate of hydrogen production.

(3) Non-metal modified TiO_2

Previous research findings show that non-metal-modified TiO_2 photocatalysts also improve the photocatalytic activity of TiO_2. Various non-metals such as C, F, S, and N have been reported to increase the photocatalytic activity of TiO_2 [48] . Eidsvåg et al. [47] reported that the primary roles of the dopants are to increase the light absorption intensity and the ability to absorb visible light. The loading of non-metals on TiO_2 reduces the energy band gap which increases the visible light photocatalytic performance [45]. Among all these non-metals, nitrogen-doped TiO_2 is the most studied photocatalyst, and it also results in high hydrogen production rates [87]. Wang et al. [88] discovered that the N/TiO_2 films resulted in a hydrogen rate of 601 $\mu mol.g^{-1}.h^{-1}$, significantly surpassing the rates obtained with pure TiO_2 films and undoped P25 TiO_2. Wang et al. [89], in another study, found that the rate of hydrogen production was 760 $\mu molH_2.h^{-1}.m^{-2}$ when pure TiO_2 films were used, which increased to 4500 $\mu molH_2.h^{-1}.m^{-2}$ when N-doped TiO_2 films were used. This indicates that the non-metal dopant significantly enhanced the efficiency of TiO_2.

Literature reviews suggest that the improved photocatalytic activity of non-metal doped TiO_2 can be attributed to the following factors: 1) increased electron transfer efficiency resulting from higher charge carrier density and extended electron lifetime; 2) a reduction in the bandgap caused by the introduction of new energy levels above the valence band of TiO_2 [47], [69], [90]. Interestingly, Yang et al. [63] reported that non-metal doping is more effective than metal doping in improving the photocatalytic performance of TiO_2; this enhanced efficiency is attributed to the reduced formation of recombination centres in TiO_2 doped with non-metals. Nevertheless, a study focused on comparative analysis between metal and mom-metal doped TiO_2 catalysts for efficient hydrogen production was not found in the literature. Non-metal dopants lower the band gap energy, minimize the formation of recombined centres, and enhance TiO_2's sensitivity to visible light irradiation. Consequently, non-metal doping is a key strategy for improving photocatalytic hydrogen production [46].

(4) Semiconductor coupling TiO_2

A review of the literature shows that the performance of pure TiO_2 for photocatalytic hydrogen production is extremely low under visible light irradiation. Interestingly, Ahmad et al.[52] highlighted in a review that comparative studies have shown that heterojunction photocatalysts result in better photocatalytic activity as compared to single photo-catalysts. Many recent studies of modified TiO_2 catalysts coupled with binary composites (e.g., WO_3, SiO_2, Al_2O_3, SnO_2, CdS, PBS, Bi_2S_3) and transition metals oxides (e.g., Cu_2O, Fe_2O_3, ZnO, NiO) have demonstrated improvement in the performance of TiO_2 photocatalyst [45]. Combining TiO_2 with other materials enhances its surface area, light absorption capability, stability, and sensitivity to visible light [52].

The formation of heterojunction enhances photocatalytic activity by pairing a semiconductor with a larger band gap with one that has a smaller band gap, facilitating efficient electron transfer between the semiconductors. This improves functionality under visible light and enhances charge separation efficiency [52]. Formed heterojunction improves photocatalytic activity by preventing charge recombination and extending the range of photo-excitation [45]. This leads to charge separation, prolonged charge carrier's lifetime, and increased reactivity [91]. To achieve efficient water splitting using coupled semiconductor TiO_2 catalysts, the following conditions must be met: (i) the semiconductors should be resistant to photo corrosion, (ii) the small band gap semiconductor must be responsive to visible light, (iii) the conduction band (CB) of the small band gap semiconductor should be more negative than both that of the large band gap semiconductor and the reduction potential of H_2O/H_2, and (v) electron injection must be both rapid and efficient [92].

Lai et al. [93] investigated TiO_2 photocatalyst coupled with WO_3 and found that it results in enhanced electron-hole separation and visible light response. Similarly, the study by Georgieva et al. [94] demonstrated that the coupled TiO_2-WO_3 heterojunction increases photocatalytic activity because of the reduced electron-hole recombination. Several studies have revealed that other metal oxides, sulfides, and nitrides have been effective as co-catalysts with TiO_2 to improve its photocatalytic activity [45]. Various other heterojunction photocatalysts reported include CdS/TiO_2, $CoSe/TiO_2$, SnO_2/TiO_2, ZrO_2/TiO_2, Ag_2S/TiO_2, Fe_3O_4/TiO_2, Bi_2O_3/TiO_2 and SiO_2/TiO_2 etc.[63]. All these photocatalysts demonstrated a shift in absorption spectrum of the TiO_2 photocatalyst towards the visible light region resulting in increased photo conversion efficiency [63]. The heterojunction formed between non-oxide and oxide or other

non-oxide photocatalysts enhances the photocatalytic activity; however, many of the non-oxide composite photocatalysts encounter the issues of photo corrosion in aqueous solutions which limits their application in water splitting [48].

The coupling of non-oxide photocatalysts with oxide or other non-oxide photocatalysts forms a heterojunction. These heterojunctions can be categorized based on the type of semiconductors involved or characteristics of their band structure [95]. According to Zhao et al. [96], heterojunctions can be defined from different perspectives, with some overlaps among different types. They are classified according to several criteria: the nature of their component (such as Schottky junction, n-n , p-n, and p-p junction) , their energy band structure (Type I,II,III), the Z-scheme family, and the mechanism of carrier-movement (Type II, S-scheme)[96].

The main types of TiO_2- based heterojunctions are briefly discussed below:
i)Schottky heterojunction: A Schottky-like barrier forms at the interface between an n-type semiconductor and a metal when the work function of a metal exceeds that of the semiconductor [90]. The Schottky barrier aids in the spatial migration and separation of charge carriers, thereby reducing the electron hole recombination [96].

ii) p-n heterojunction : A P-n junction is created between a p-type and n-type semiconductors, generating an electric field at the interface due to the diffusion of electron and holes [90]. When exposed to light, the charge carriers move under the influence of this electric field and the difference of band potential, which enhances charge separation and improves photocatalytic activity [97].

iii) Type I : Type II: Type III heterojunctions: These heterojunctions are classified based on the band position of the involved semiconductors: i) Type I : in this configuration, the CB and VB of semiconductor I are both higher and lower, respectively, compared to Semiconductor II. This setup results in accumulation of electrons and holes in Semiconductor II but does not prevent their recombination, thereby reducing the photocatalytic activity. ii) Type II : This configuration is highly effective for charge carrier transfer, as CB and VB of semiconductor I are higher than the CB and VB of semiconductor II. This arrangement allows electrons to accumulate in semiconductor II while holes migrate to Semiconductor I upon irradiation, optimizing charge separation and enhancing photocatalytic performance. iii) Type III: Although similar to Type II, Type III heterojunction features a more significant band position

deference between the semiconductors such that the band gaps of the semiconductors do not intersect [95].

iv) Z-scheme: In Z-scheme heterojunction, electrons from the CB of semiconductor II transfer to the to the of VB of semiconductor I along a Z-shaped pathway and recombine with holes. Despite this recombination, the electrons in the CB of semiconductor I and the holes in the VB of semiconductor II maintain a high redox potential. This results in efficient charge separation and enhanced redox capabilities outperforming type-II and p-n heterojunctions [97].

v) S-scheme: This type of heterojunction consists of an oxidation-type semiconductor and a reduction-type semiconductor, with charge carriers flowing along a step-like, 'S'-shaped path that includes a charge recombination step. Similar to Z-Scheme, the S-scheme maintains the separation and high redox activity of photogenerated e- and h+ , enabling effective catalytic reactions. It addresses the limitations of Type II and p-n heterojunctions, which have oxidation potentials, and also overcomes the thermodynamic and practical issues associated with Z-scheme heterojunctions [97]. Figures 2.6 and 2.7 illustrate the band structure and charge carrier pathways for various types of heterojunctions.

(5) Ternary TiO_2

Ternary photocatalytic systems are composed of three different semiconductors. Xie et al. [98] investigated the ternary system of Pt/TiO_2-ZnO (Ti/Zn=10) for photocatalytic hydrogen production and the data obtained showed that the maximum H_2 rate was 2150 μmol h^{-1} g^{-1} and the stability of the photocatalyst also improved. Fajrina et al. [45] reported that according to most of the literature produced on ternary TiO_2 systems, most ternary composites contain heterojunctions of two semiconductors deposited with metal. For example, Spanu et al [99] investigated the ternary photocatalyst Pt/TiO_2-WO_3 and found a hydrogen production rate of 5.2 $\mu LH_2 . h^{-1} . cm^{-2}$. Toledo Camacho et al. [100] investigated Pd/TiO_2-WO_3 and observed that the H_2 rate was in the order Pd/TiO_2(nanotubes)/WO_3 >Pd/TiO_2(P25)/WO_3 > Pd/TiO_2(P25). Other ternary TiO_2-based photocatalysts reported by Fajrina et al. [45] include Cu/TiO_2/Ti_3C_2, Pt/WO_3/TiO_2, Cu-TiO_2/porphyrin, and Pt-RuO_2-TiO_2 etc. In ternary TiO_2 systems, such as Pt/TiO_2-ZnO, metal doping improves charge separation by trapping and accelerating the electron transfer, and coupling TiO_2 with narrow band gap semiconductors enhances its visible light activity [45].

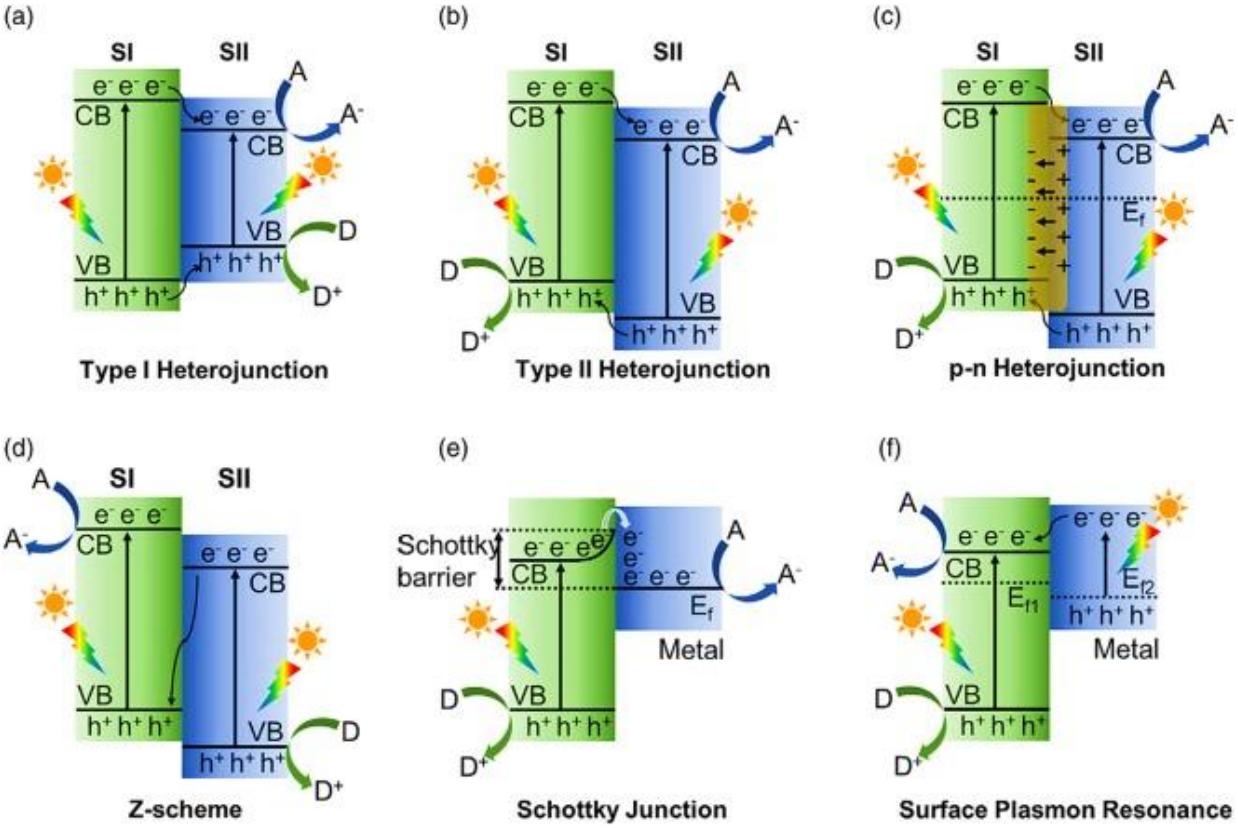

Figure 1.6: Different types of heterojunctions [90].

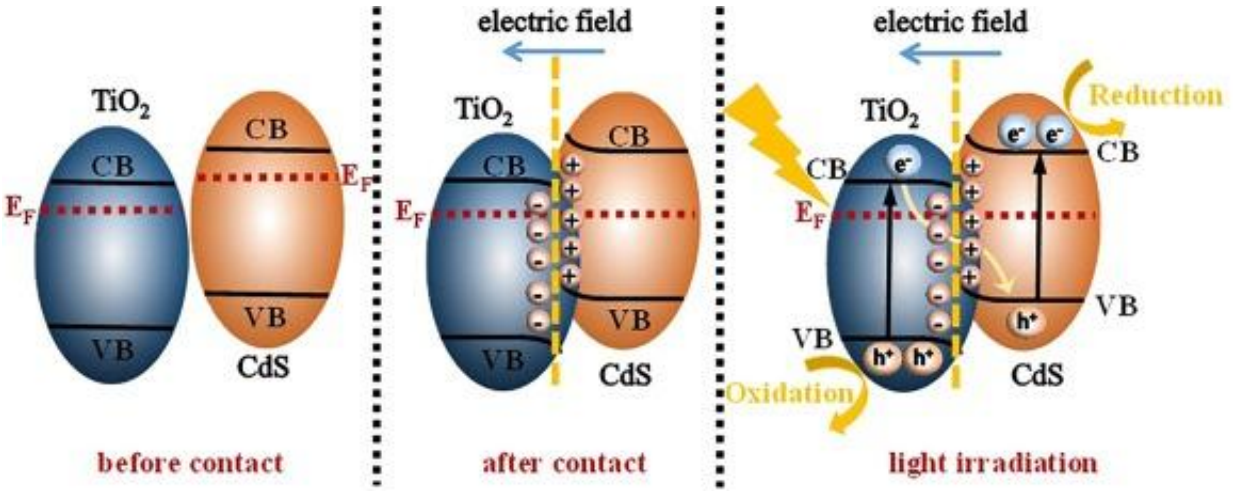

Figure 1.7: S-scheme heterojunction formation between TiO_2 and CdS photocatalysts [91].

(6) Photosensitizers TiO_2

The primary drawback of TiO_2 catalyst is its large band gap, which limits its ability to absorb visible light. Dye sensitization is one of the most effective methods for extending the absorption edge of TiO_2 into the visible light spectrum. This method involves sensitization of the TiO_2 semiconductor with the molecular dyes such as organic, inorganic, porphyrins, and ruthenium bipyridyl derivatives [90]. This process enables photoexcited electron from the dyes to be injected into the conduction band of TiO_2, initiating photochemical or redox reactions [92]. The dye sensitization enhances the efficiency of light-excitation process, broadens the excitation wavelength range into the visible spectrum, and thereby improves both photoelectric energy conversion efficiency and hydrogen production rates [63].

(7) Co-catalyst modified TiO_2

Another widely used method for modifying TiO_2 involves the use Co-catalysts, such as Pt, Rh, Au, Ag, Ni, Cu, and Co [101]. Co-catalysts enhance photocatalytic efficiency through several mechanisms: i) They reduce electron hole recombination rates because photo excited electrons from TIO_2 can be transferred to the metal particles, whose fermi are lower than that of TiO_2, facilitating efficient charge separation [92]. ii) Co-catalysts traps electrons, providing highly active reaction sites for the redox reactions on their surface. Additionally, co-catalyst can increase the stability of the photocatalysts by offering alternative reaction sites, which helps to minimize photocatalyst photo corrosion [90].

Table 2.4 presents various types of modified TiO_2 catalysts studied in recent years. However, the results obtained should not be compared with each other due to variations in experimental conditions.

Table 1.4: Modified TiO_2 catalysts for photocatalytic hydrogen production.

Photocatalyst	Metal concentration (wt.%)	Amount of catalyst	Light source	Sacrificial reagent (Vol. %)	H_2 production rate (mmol/ time/g Catalyst)	Quantum efficiency/ AQY	Ref	Year
Metal modified TiO_2								
Pt/TiO_2 (P25)	0.3%	50 mg	LED UV light	Methanol(20%)	58 mmol g^{-1} h^{-1}		[102]	2023
Pd/TiO_2	1%	0.0065 g/ 20ml	200W SB-1000P/F	1,2-ethanediol	44.5 mmol g^{-1} h^{-1}		[103]	2015
Au/TiO_2 (P25)	2%	6.5 mg	100W SB-100P/F	Glycerol (10%)	30.3 mmol g^{-1} h^{-1}		[104]	2018
Ag/TiO_2 (P25)	1.5%	-	254 nm UV light	-	23.5 mmol g^{-1} h^{-1}	>19%	[68]	2019
Fe/TiO_2 (P25)	2%	0.2 g/200ml	300 W Halogen Visible lamp	Methanol(25%)	< 10 mmol g^{-1} h^{-1}		[65]	2021
Cu/TiO_2 (P25)	1.5%	0.2 g/200ml	300 W Synergy UV lamp	Methanol(25%)	5100 μmol $g^{-1}h^{-1}$		[65]	2021
Cu/TiO_2	-	0.01g/1000 ml	300W Xenon lamp	methanol(10%)	45.6 mmol/h		[75]	2021
Ni/TiO_2 (P25)	5%	0.1g/100ml	300 W Xenon Lamp	methanol (30%)	600 μmol/h		[77]	2018
Ni/TiO_2 (P25)	1%	10 mg / 50 ml	450 W Hg lamp	Methanol (50%)	3390 μmol g^{-1} h^{-1}	2.8%	[79]	2018
Co-TiO_2	1%	10 mg / 50 ml	450 W Hg lamp	Methanol (50%)	24.8 μmol/h	2.1%	[79]	2018

Non-metal modified TiO_2								
N-TiO_2 films	-	-	Xenon Lamp	Methanol (10%)	4500 μmol h^{-1} m^{-2}		[105]	2013
S-TiO_2		100 mg/100 ml	AM 1.5 solar simulator	Methanol (20%)	163.9 μmol g^{-1} h^{-1}		[56]	2016
F-TiO_2			300W Xenon lamp	-	18270 μmol g^{-1} h^{-1}	21.6%	[56]	2018
Co-doped TiO_2 (Non-metallic, metal-metal, Non-metal, and metal co-doping)								
Pt-Pd/ Nb-TiO_2	3% NbPtPd (1:1)	0.5 g/L	500 W Hg-Xenon lamp	Methanol (30%)	0.8 mmol g^{-1} h^{-1} (visible) 4.5 mmol g^{-1} h^{-1} (UV)	3% UV, 0.8% Visible	[106]	2018
Fe/Ni-TiO_2	5% Fe, 4% Ni	0.4 g/600 ml	500W Xenon Lamp	Methanol (10%)	361.64 μmol g^{-1} h^{-1}		[107]	2012
Ni/N-TiO_2 (Nanotubes)	10% Ni	150 ml	Mercury lamp	Glycerol (10%)	30973 μmol/m^2		[108]	2020
Ni-NiO-TiO_2	1%	100 mg/347.8 mL	5W UV-LED solo P lamp	Methanol (50%)	1600 μmol/g		[109]	2023
Cu-Ni/TiO_2	1% (1:1)	80 mg/80 ml	300 W Xenon lamp	Methanol (37.5%)	13.5 mmol g^{-1} h^{-1}		[81]	2014
N-Ni/C/TiO_2	15%	50mg/100ml	2000W Mercury lamp	Methanol (25%)	0.383 mmol.sec^{-1}.g^{-1}		[110]	2017
Ni-Pd/TiO_2	1Ni1Pd10	50ml/5ml	400 W Mercury lamp	Methanol (50%)	210 μmol/h		[111]	2017
Semiconductor coupled TiO_2								
ZnO-TiO_2		100mg/100 ml	300W	Methanol (20%)	0.152 mmol g^{-1} h^{-1}		[112]	2017

(hollow spheres)			Xenon lamp					
WSe_2-TiO_2 (WSe_2 nanosheets)	20% $WASe_2$	10mg/30 ml	Xenon lamp	Methanol (17%)	2.28 mmol g^{-1} h^{-1}	AQY=43.8%	[113]	2022
SnO_2/TiO_2 (TiO_2 nanosheets)		20mg/100ml	300 W Xenon lamp	Methanol (20%)	16.7 mmol g^{-1} h^{-1}		[114]	2022
WO_3-TiO_2 (Nanofibers)	5%	30mg/60 ml	100 W Mercury lamp	Na_2S/Na_2SO_3	107.15 μmol g^{-1} h^{-1}		[115]	2020
Ternary TiO_2								
Pt/TiO_2-ZnO	0.5% Pt	0.5g/250 ml	400 W Mercury lamp (UV cut filter)	Methanol (10%)	2150 μmol g^{-1} h^{-1}		[98]	2016
Pd/TiO_2-WO_3 (TiO_2 nanotubes)	0.013 % Pd	500 ppm/0.6 L (Solar) and 500 ppm/0.25 L(UVA)	250 W/m^2-solar simulated light and 4 lamps of 15 W-UVA light	Methanol (50%)	Solar : 5.3x10^{-5} mol min^{-1} g^{-1} UVA : 5.3x10^{-5} mol min^{-1} g^{-1}	2.3% (solar) 7.7% (UVA)	[100]	2018
TiO_2/Ti_3C_2/g-C_3N_4		30 mg	300W Xenon lamp	Triethanolamine (10%)	1150 μmol g^{-1} h^{-1}		[116]	2021

2.2.2.3 Advantages and disadvantages of various modification methods

Various methods for modifying TiO_2 photocatalysts have been reported in the literature, each with its own set of advantages and limitations. The key benefits and drawbacks of these methods discussed above are highlighted in Table 2.5.

Table 1.5: Advantages and disadvantages of various TiO_2 modification methods [117], [118], [119], [120]

Method	Advantages	Disadvantages
Metal doped TiO_2	○ Improves electron-hole separation ○ Extends light absorption into visible range ○ Enhances photocatalytic activity ○ Allows for tunable electronic band structures and band gap narrowing ○ ImprovesTiO_2 conductivity	○ Can be expensive ○ May function as recombination centres ○ Poses the risk of metal leaching ○ Might introduce impurities ○ Certain metals can be toxic: e.g. Pb, Hg, Fe, Cd
Non-metal doped TiO_2	○ Enhances visible light absorption ○ Improves charge carrier separation and migration ○ Alters the band structure ○ It has minimal risk of impurities ○ Cost-effective	○ Provides limited enhancement in TiO_2 properties and overall photocatalytic activity, faces Challenges in precise doping control and achieving uniform doping ○ Can function as recombination centres
Semiconductor coupled TiO_2	○ Enhances electron-hole separation ○ Spatially separate reduction and oxidation site ○ Optimizes the reduction and oxidation potential of photogenerated electrons and holes ○ Improves product selectivity, pore structure and electronic properties of the catalyst.	○ Involves complex synthesis methods ○ May suffer from instability ○ There is ongoing debate regarding the actual charge migration pathways
Dye sensitization	○ Narrows band gap ○ Improves charge mobility	○ Dye aggregation on TiO_2 structure can hinder electron

	○ Reduces bulk recombination centres ○ Enhances charge separation and transfer	injection and reduce photocatalytic activity ○ The synthesis method can be complex
Co-catalyst loaded TiO_2	○ Increases surface area ○ Improves adsorption of reactants on catalytic surface ○ Enhances electron-hole separation	○ Exhibits low light utilization efficiency

2.2.3 Factors Affecting Photocatalytic Hydrogen Production

The efficiency of a photocatalyst and its ability to produce hydrogen during photocatalytic water splitting are influenced by several factors. By optimizing various parameters during the reaction, the photocatalyst's efficiency can be significantly improved. Hence, it is crucial to control these parameters to achieve high photoconversion efficiency and to enhance the total solar-to-hydrogen (STH) efficiency of the process. These factors include both the physical properties of the photocatalyst, such as its structure, morphology, band gap, corrosion resistance, as well as the experimental parameters like pH, temperature, the type and concentration of the sacrificial reagent, and the intensity of the light. Therefore, it is important to understand and control these parameters to advance the performance of the photocatalytic water splitting process.

2.2.3.1 Structure, Crystallinity, and Morphology

The synthesis methods used for catalyst preparation affect the structure and morphology of the photocatalyst. The different reaction conditions used during the catalyst formation result in different crystal sizes, shapes, and structures [52] Adamu et al. [57] stated that different crystal structures and orientations of the polymorphs of TiO_2 result in distinct photocatalytic properties. For instance, Park et al. [121] found that anatase phase exhibits higher photocatalytic activity compared to the rutile phase, this is due to the different structure of the two phases contributes to different energy band gaps. In general, anatase phase results in enhanced photocatalytic performance compared to other phases because of its appropriate band gap and higher kinetic stability [46]. Interestingly, Eddy et al [59] reported that the combination of TiO_2 polymorphs in a binary mixture exhibited a notable enhancement in photocatalytic activity, with the binary mixture of anatase and rutile being extensively studied. Similarly, Eidsvåg et al. [47] reported in a review that the optoelectronic properties and hence catalyst performance are influenced by its crystallinity, with highly crystalline catalysts outperforming

their amorphous counterparts. Liu et al. [122] investigated the crystalline TiO_2 nanotubes and amorphous TiO_2 nanotubes and concluded that the crystallite structure yielded better photocurrent properties due to the reduced charge recombination. This aligns with the findings of Fajrina et al. [45], who reported that the smaller sized crystalline photocatalysts facilitate rapid transfer of e^- and h^+ to the active sites, thereby reducing the charge recombination.

Anggoro et al. [60] stated that rate of hydrogen generation is significantly influenced by the morphology of TiO_2 nanoparticles, indicating that morphological modification is an efficient method to enhance the photocatalytic performance. In a review, Jagadeesh et al. [123] highlighted that semiconducting nanostructure in one-dimensional (1D: nanorods, nanowires, nanotubes) and two-dimensional (2D: nanosheets, nanolayers, nanofibers) forms exhibit enhanced photocatalytic activity due to increased charge separation and reduced recombination rate. Various 1D, 2D, and 3D TiO_2 structures investigated for photocatalytic water splitting are given in Table 2.6. Wang et al. [124] investigated the photocatalytic performance of the NiO-TiO_2 nanorod structure for hydrogen production using a methanol-water mixture and found that the hydrogen production rate was 1.3 times higher with the 2NiO-TiO_2 catalyst compared to pure TiO_2.

Table 1.6: Different TiO_2-based nanostructures reported for hydrogen production.

Catalyst	**Structure**	**H_2 rate**	**Reference**
TiO_2	Nanosheets	270 μmol /h	[125]
0.18%-Pd/TiO_2	Nanosheets	3096 μmol/g/h	[126]
2NiO/TiO_2	Nanorods	701 μmol/g.cat	[124]
Pd0.22Pt0.78-TiO_2	Nanowires	11 mmol/g.cat	[127]
CoNi-TiO_2	Nanoflowers	6580.9 μmol/g/h	[128]

The properties of the catalyst, such as shape and composition, depend on the temperature utilized for catalyst preparation, which is determined by the synthesis method used [45]. Buraso et al. [129] studied how varying the calcination temperature affects the photocatalytic performance of the TiO_2 catalyst in the degradation of methyl orange. It was observed that as the calcination temperature increased, the particle size and degree of crystallinity of the TiO_2 catalyst also increased. It was also observed that with an increase in calcination temperature from 400 to 700 ^oC, the TiO_2 crystal system changed from anatase to rutile, and the direct band gap (Eg) decreased from 3.30 eV to 2.98 eV. In summary, it was determined that the improved

activity of the TiO_2 was attributed the purity of the anatase phase, reduced particle size, and increased surface area of nanoparticles [129]. This agrees with Eidsvåg et al. [47] who reported that the size of nanomaterials and cocatalysts can influence the photocatalytic activity, with smaller particles being more favourable to reduced electron-hole recombination probability.

Anggoro et al. [60] reported that the morphology and structure of mono or bimetallic catalysts can exist in different forms such as alloys, core-shell, and Janus type. Tian et al. [81] and Kotesh Kumar et al. [76] synthesized Cu/Ni-TiO_2 photocatalyst using a simple hydrothermal process and co-impregnation method, respectively. Both approaches led to the formation of Cu-Ni alloy on TiO_2 nanoparticles and the synergetic effect between the two metals resulted in decreased electron-hole recombination rates which in turn enhanced the hydrogen production rate. Ramírez et al. [130] investigated CuO/TiO_2 and NiO/TiO_2 core-shell catalysts for photocatalytic production of hydrogen and found that CuO/TiO_2 resulted in the maximum H_2 rate of 153.8 μmol/g/h, which was 3.2 and 11.2 times higher than that resulted from NiO/TiO_2 and TiO_2 P25, respectively. The core-shell structure resulted in the creation of a heterojunction between the TiO_2 shell and CuO core, which inhibited the recombination of electrons and holes and increased charge transfer, resulting in increased hydrogen production rates.

Overall, this indicates that the photocatalytic efficiency of TiO_2 is strongly determined by its particle size, crystallite size, shape, and morphology; hence, the selection of appropriate synthesis methods is vital for an enhanced hydrogen production rate. Various synthesis methods have been reviewed in Section 5.

2.2.3.2 Band gap

The bandgap is the most crucial characteristic of the photocatalysts, representing the energy required for an electron to transition from the valence band (VB) to the conduction band (CB) [47]. For a water splitting reaction, the semiconductor's conduction band must exhibit a greater negative potential than the redox potential of H^+/H_2, while its valence band must possess a more positive potential than the redox potential of O_2/H_2O; this necessitates that the acceptor's relative potential is thermodynamically lower than the conduction band of the semiconductor [45]. N. Ain et al. [62] reported that the band gap of TiO_2 is suitable for water splitting, as the top of the VB (+2.7 V vs NHE at pH 7) is more positive compared to O_2/H_2O redox couple (+1.23V vs NHE at pH 7) and the bottom of the CB (-0.5 V vs NHE at pH 7) is more negative

than the H^+/H_2 redox couple (0 V vs NHE at pH 7). Eidsvåg et al. [47] reported that for photocatalytic water splitting, a photocatalyst with a bandgap of at least 1.23 eV is necessary, as depicted in Figure 2.8.

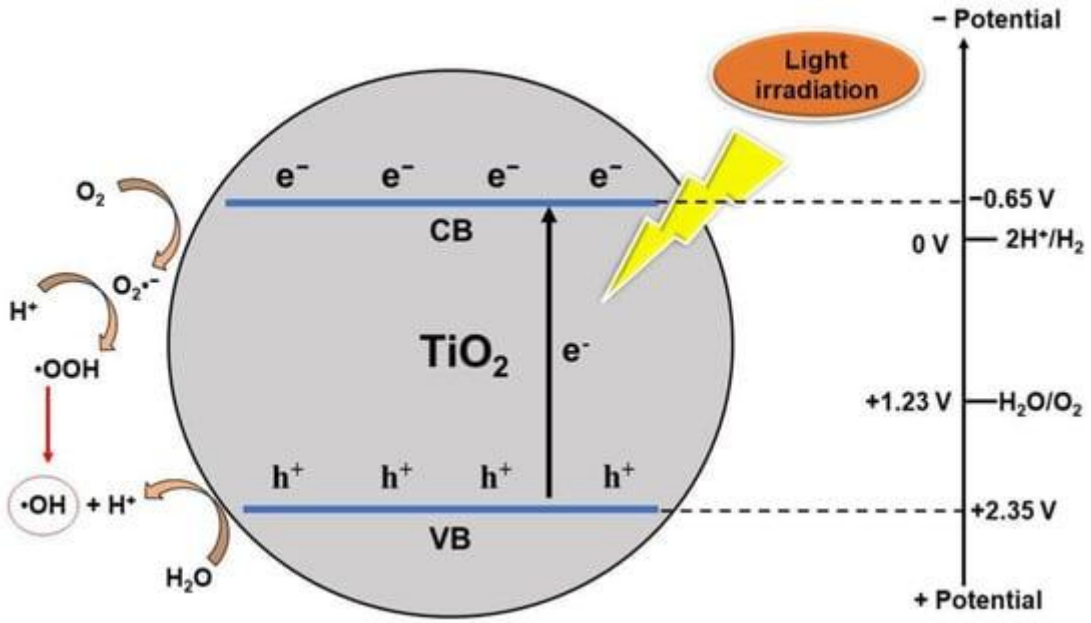

Figure 1.8: Schematic diagram of photocatalytic process and TiO_2 band gap [59]**.**

Notably, with a rise in the band gap of the photocatalyst, it absorbs light with shorter wavelengths, indicating that photocatalysts with bandgap exceeding 3.15 eV solely absorb UV light and not visible light [46]. However, the band energy gap of TiO_2 is 3.2 eV, which prevents it from effectively catalysing the water-splitting reaction in the presence of visible light irradiation [52]. Hence, to enable the visible light absorption, it is essential to use effective strategies discussed in Section 3.2 to further reduce its band gap [45]. Díaz et al. [65] demonstrated that 0.5 wt.% Cu/TiO_2 resulted in a bang gap value of 3.03 eV. The results obtained by Kumar et al. [76] for single and dual metal-doped TiO_2 photocatalysts are given in Table 2.7.

Table 2.7 shows how doping with different metals affects the energy band gap of TiO_2, the results obtained for Cu/TiO_2 agree with that by Diaz et al. [65]. It can be seen that dual metal doped TiO_2 ($3Cu\text{-}5Ni/TiO_2$) decreases the band gap from 3.2 eV to 2.63 eV. It is notable that the quantity of metal loading also impacts the band gap of the photocatalyst, hence its ability to absorb visible light irradiation.

Table 1.7: Band gap and H_2 rate of mono($Cu\text{-}TiO_2$, $Ni\text{-}TiO_2$) and Bimetallic ($Cu\text{-}Ni/TiO_2$) photocatalysts [76]**.**

Photocatalyst	**Band gap (eV)**	**H_2 Uptake (µmol/gcat)**
TiO_2	3.20	nd
$2Cu/TiO_2$	2.92	180.9
$5Ni/TiO_2$	2.78	253.0
$0.5Cu\text{-}5Ni/TiO_2$	2.83	nd
$1Cu\text{-}5Ni/TiO_2$	2.78	nd
$2Cu\text{-}5Ni/TiO_2$	2.70	634.5
$3Cu\text{-}5Ni/TiO_2$	2.64	nd

2.2.3.3 Sacrificial reagent/electron donor in water solution

Sacrificial agents are organic species that function as scavengers of holes and increase photocatalytic activity as compared to pure water [46]. Sacrificial reagents are added to the water solution to prevent the rapid reverse reaction of hydrogen (H_2) and oxygen (O_2) to form water, and they function as reducing agents increasing the hydrogen production rates [52]. In the literature, photocatalytic water splitting, due to the use of sacrificial reagents that enhance the photocatalytic process, is often referred to as photocatalytic hydrogen production. In some cases, the presence of a sacrificial reagent prevents the production of oxygen, leading instead to the formation of other byproducts. The most widely used sacrificial reagents include alcohols such as methanol, phenol, and glycerol; adding alcohols to improve the photocatalytic activity and hydrogen production rates is known as photo reforming [45]. Chen et al. [131] demonstrated that hydrogen production using different sacrificial reagents decreases in the following sequence: glycerol > ethylene glycol > methanol > ethanol**(**Figure 2.9**)**.

Based on these results Fajrina et al. [45] indicated that the sacrificial reagent should contain an α-H to OH groups as these α-H are liberated into H^+ ions which are converted into H_2 using electrons during the photo-reforming reactions. This aligns with the findings of Qanugo et al. [46] which stated that Glycerol contains the most α-H hydrogen atoms compared to other alcohols thereby resulting in the highest H_2 production rate. However, López et al.[132] examined the impact of various sacrificial reagents on the hydrogen production rate using a Pt/TiO_2 catalyst. They observed that the hydrogen production rate decreased in the sequence:

methanol > ethanol > ethylene glycol > glycerol. This result contrasts with the findings of Chen et al. [131], likely due to differences in reaction conditions, such as variations in sacrificial reagent concentration and the use of different photocatalysts. Chen et al. [104] observed that hydrogen production rates were significantly affected by alcohol concentration, with higher alcohol concentrations leading to a decrease in H_2 rates in the order ethanol > methanol > ethylene glycol > glycerol. Conversely, opposite results were observed at lower alcohol concentrations. This indicates that the concentration of a sacrificial reagent is a critical factor affecting hydrogen production rates. Therefore, variations in the results could be due to differences in alcohol concentration and the varying stability of the photocatalysts used. Kumaravel et al. [51] investigated how different sacrificial reagents influences the performance of oxide photocatalysts and proposed that glucose and glycerol are the most efficient sacrificial reagents due to their accessibility, low toxicity, affordability, and easy dehydrogenation compared to other alcohols.

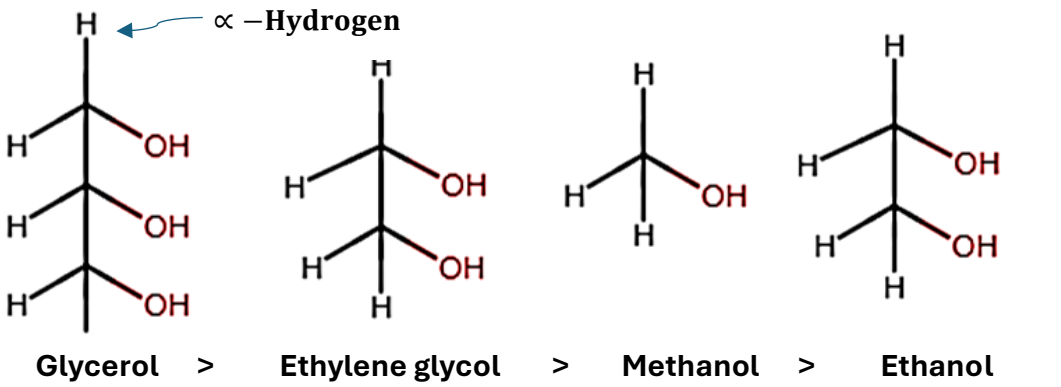

Figure 1.9: Structures of commonly used sacrificial reagents [45]**.**

Research findings of Lalitha et al. [133] showed that hydrogen production increased up to five times with increased methanol concentration over a 1wt% Ag_2O/TiO_2 photocatalyst. Tian et al. [81] investigated the impact of methanol concentration on the rate of H_2 production over TiO_2-1%Cu/Ni (1:1) photocatalyst and observed that photocatalytic performance is notably reduced when the methanol concentration deviates from 37.5 vol%. This indicates that achieving enhanced hydrogen rates requires an appropriate concentration of electron donors. Jiang et al. studied the impacts of mixed sacrificial reagents (single, binary, and ternary systems) on hydrogen production rate over a TiO_2 catalyst and discovered that the mixing of suitable sacrificial reagents in appropriate concentrations results in enhanced photocatalytic activity and hydrogen production rate [134]. However, as observed in Table 2.4, the most frequently used

sacrificial reagent is methanol; this choice is likely influenced by its cost-effectiveness and ready accessibility.

2.2.3.4 Intensity of Light

One approach to enhancing the photocatalytic hydrogen generation rate is to increase the intensity of light by using higher energy sources [46]. Regarding UV photon flux, two regimes are identified for photocatalytic water splitting [54]. These consist of a first-order regime for fluxes at approximately 25 mW/cm^2 , typically used for laboratory research, and a half-order regime at higher light intensities [52]. In the first-order regime, chemical reactions deplete the charges at a faster rate compared to recombination reactions, whereas in the half-order regime, the recombination reaction usually controls the overall rate [45]. Reim et al. [135] examined the impact of varying light intensity on the rate of photocatalytic hydrogen production, and the findings indicated that higher light intensity or photon flux led to an increase in the amount of hydrogen produced. Similar results were reported by Fajrina et al.[45] in a review. Wavelength and irradiation distribution across the reactors are two factors associated with the energy source that influence the photocatalytic efficiency. The light distribution across the reactor is determined by the position of the light source [136]. Kumaravel et al. [56] in a review, reported that the maximum hydrogen yield was obtained in a reactor featuring an internal light irradiation source (Type I) as compared to a reactor with a light source placed outside at a particular distance (Type II) from the reactor; Type II allows the photocatalyst to directly absorb more photons in this configuration. The schematic of the two types of photoreactors is shown in Figure 2.10.

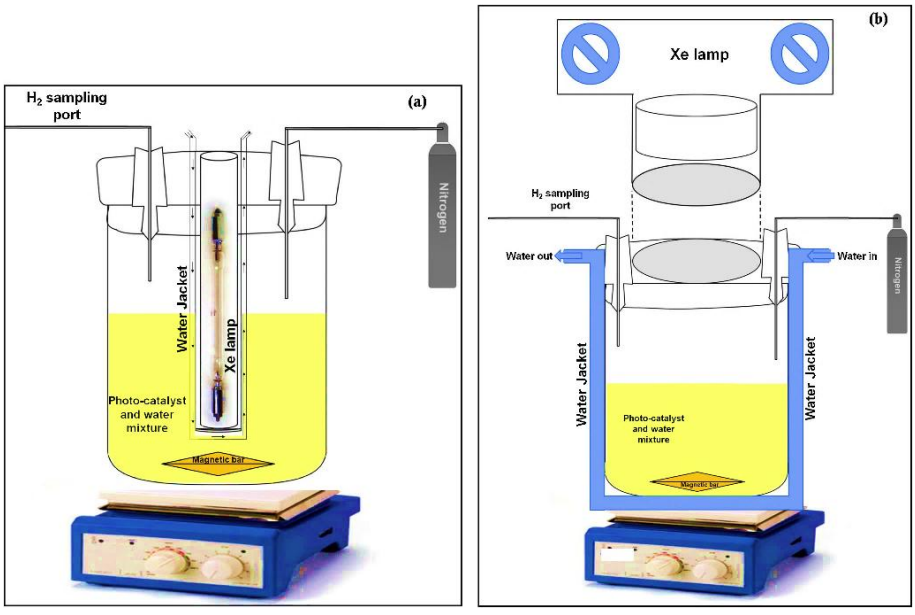

Figure 1.10 : Type I and Type II photoreactors [56].

2.2.3.5 Temperature

According to Fajrina et al. [45], thermodynamically, temperature cannot stimulate photocatalytic activity as it is not involved in the generation of e^- and h^+; however, temperature indirectly increases the photocatalytic activity by enhancing the desorption of the formed product from the surface of the photocatalyst and hence increases the rate of the reaction. Both Ahmad et al. [52] and Fajrina et al.[45] stated that the operating temperature varies for different materials. Although photocatalytic reactions are conducted at room temperature, increasing the temperature positively influences the activity of certain photocatalysts [137]. Zhang et al. [138] found that the ideal temperature range for the photocatalytic performance of crystalline TiO_2 is 60-80 ºC. Qanugo et al. [46] reported that the higher temperature also results in higher electron transfers from the valence band to higher energy levels, forming electron-hole pairs that can initiate the oxidation and reduction reactions, hence allowing reactions to complete more efficiently.

Boudjemaa et al. [139] observed that as the temperature increased from 30 to 50 ºC, the H_2 production rate increased from 59 mol/g.s to 370 mol/g.s. Muscetta et al. [140] studied the impact of temperature on the rate of hydrogen production with 1wt% Cu_2O/TiO_2 nanocomposite catalyst and observed that as the temperature rose from 20 ºC to 80 ºC, the hydrogen rate increased by 4.5 times. Velázquez et al. [141] similarly stated that the rate of hydrogen production is significantly influenced by the reaction temperature. Interestingly, Kumaravel et al. [56] emphasized the importance of maintaining the reaction temperature constant throughout the reaction because increased temperatures decrease the H_2 production efficiency through decreased trapping of charge carriers and reduced adsorption of reactants on the catalyst surface. Notably, Lakhera et al. [142] highlighted that the effect of temperature on catalytic activity varies with different catalyst and lower temperatures can decrease hydrogen production because the desorption of products slows down more than the adsorption of reactant. Overall, the literature suggests that temperature is crucial for optimizing photocatalytic efficiency. Therefore, it is essential to carefully regulate and adjust the temperature to maximize the effectiveness of the process.

2.2.3.6 pH

Production of hydrogen from water is directly proportional to the concentration of protons which is determined by the pH of the solution [46]. The pH of the solution also affects the stability and lifetime of a catalyst [58]. Fajrina et al. [45] reported that altering pH represent a

method to shift the band gap energy of a photocatalyst. Ali Ghasemi [55] reported that the efficiency of hydrogen production is higher in a weak basic solution than in an acidic or stronger basic solution (pH>10). Wu et al. [143] also noted that $CuOx/TiO_2$ photocatalyst resulted in a maximum H_2 rate in a mild basic solution. The findings of many other studies, including the review conducted by Qanugo et al. [46] indicated that TiO_2 is unstable in strong acidic or basic solutions. However, Nada et al. [144] found that greater amount of H_2 was generated in an acidic medium compared to a basic medium, indicating that at acidic pH levels, photocatalyst exhibit greater adsorption of H^+ ions, thereby enhancing the probability of reduction to produce H_2. However, in a review, Zhang et al. [145] concluded that according to prior studies, photocatalytic reactions in basic solutions generally offer more benefits for improving H_2 generation.

Notably, Lakhera et al.[142] reported that the pH of hydrogen production systems using sacrificial reagents is significantly affected by the adsorption of these reagents on the semiconductor. Consequently, it is essential to operate at a pH close to the pKa of the sacrificial reagent or electron donor to optimize hydrogen production activity [142]. Hence, the variations in the effects of pH on photocatalytic activity reported by different authors may be attributed to the use of different sacrificial reagents in their studies. Karimi Estahbanati et al. [146] performed a kinetic analysis to assess the impact of pH on the rate of photocatalytic H_2 production and observed that the highest rate was achieved at a pH~8 for all the substrates or sacrificial reagents investigated.

Several studies also pointed out the effects of other factors on photocatalytic activity and hydrogen production rates. These factors include corrosion resistance, oxygen vacancies, and operating pressure, and the stirring rate of the reactor solution.

2.2.4 Photocatalyst Synthesis Methods

As discussed in section 4.1, photocatalytic H_2 production also depends on the composition, morphology, and surface properties of the photocatalysts, and these properties are influenced by the methods used to synthesize or modify the catalysts. For example, Chakhtouna et al. [147] found that the photocatalytic activity of Ag doped TiO_2 nanoparticles is notably impacted by the synthesis parameters and the methods used. Adamu et al. [57] reported that various forms (e.g. crystals, nanoparticles, powder) of single- or mixed-phase TiO_2 can be obtained based on the synthesis method utilized.

Yang et al. categorized TiO_2 synthesis methods into three types: 1) solid phase, 2)liquid phase and 3) gas phase [63]. Solid phase involves the preparation of raw materials, intermediates, and solid particles. It is straightforward and well-suited for large scale production. However, it requires substantial energy and tends to produce large particles. Gas phase methods involve utilizing gaseous raw materials or converting raw materials into their gaseous forms through various techniques. Solid nanoparticles are then produced by processes such as condensation and deposition, using either physical or chemical methods. 3) Liquid phase methods are often preferred due to their advantages: they are easy to operate, require simple equipment, involve lower reaction temperatures, and consume less energy compared to other methods [63].

The primary liquid phase methods for synthesizing TiO_2 include : i) Sol-Gel Method: This wet chemical process involves dissolving metal precursors in a solvent to form a gel through hydrolysis. The gel formation occurs under heating, continuous stirring, and the addition of templating agents, (ii) Hydrothermal/Solvothermal method: This technique heats an aqueous solution of TiO_2 precursor in an autoclave at elevated temperatures and pressure to facilitate the synthesis, (iii) Microemulsion method: This method uses emulsifiers such as surfactants, weakly polar organics, and alcohols, to create an immiscible emulsion. The resulting homogenous latex reacts to form amorphous TiO_2, which is then converted into nanoparticles through calcination, iv) Precipitation method: This approach involves reacting inorganic titanium salt solution with a precipitating agent to form a precipitate. The precipitate is then calcined at high temperatures to yield TiO_2 powder [63], [148]. In addition to these methods, other TiO_2 synthesis techniques include combustion, Sono chemical, chemical vapor deposition, and physical vapor deposition. The advantages and disadvantages of various methods are summarised in Table 2.9.

According to Eidsvåg et al., the choice of method for doping or modifying TiO_2 with metals affects its performance [47]. Saleh et al. [102] studied the influence of co-catalyst loading method on the rate of hydrogen generation; the results obtained are presented in Table 2.8. From Table 2.8 it can be seen that for Cu, the photo deposition and for Ni, the impregnation methods resulted in the maximum H_2 production rates. The hydrogen production rate is influenced by both the loading method and the type of co-catalyst used [102].

Table 1.8: Effect of metal loading methods on hydrogen production rate [102].

Photocatalyst	**Method**	**H_2 rate ($mmol.g^{-1}.h^{-1}$)**

Cu-TiO_2	Impregnation	17.3
	Photo deposition	24
	Hydrothermal	7
Pt/TiO_2	Impregnation	58
	Photo deposition	36
	Hydrothermal	53

2.2.5 Photoreactors

The type of reactor is a key factor that affects the process of photocatalytic hydrogen production [136]. Photoreactor refers to the vessel in which a photocatalyst reacts with the reactant under light irradiation to produce products [46]. The efficiency of the photocatalyst is influenced by the design and setup of the photocatalyst and light distribution within the reactor [45]. Various types of photoreactors have been developed based on factors such as the phase of the photocatalyst, the nature of the reaction solution, and operational requirements [149]. Photocatalytic water splitting occurs in two fundamental reactor configurations based on the form of the photocatalysts: 1) Powder form suspended in liquid and 2) Photocatalysts immobilized onto continuous inert carriers [45]. For optimal photocatalytic activity, an ideal photoreactor should ensure a consistent distribution of light throughout the photoreactor [46]. The different positions of the light source that are reported are discussed in Section 4.4. The batch reactor is the most extensively studied photoreactor utilizing a powdered photocatalyst [136]. The summary of different types of reactors is given in Table 2.10. The schematic diagram of an innovative twin-reactor system facilitating the separate production of hydrogen and oxygen is presented in Figure 2.11.

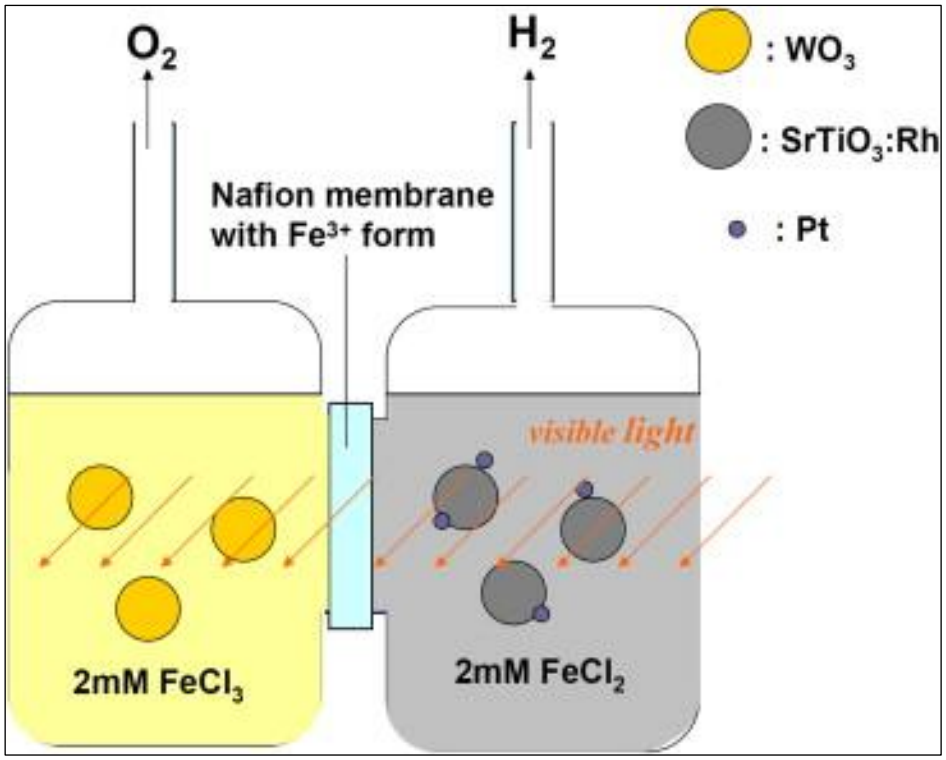

Figure 1.11: Schematic diagram of a twin reactor system [150].

Table 1.9: Advantages and disadvantages of different synthesis methods.

Method	Phases		Advantages	Disadvantages	References
	Anatase	Rutile			
Precipitation	✓	✓	• Low temperature • Simple process • Large scale production	• Difficult to control the particle size • Easy agglomeration of the particles • Low purity and large and uneven particle size.	[57] [63]
Solvothermal/ Hydrothermal	✓	✓	• Easy control of surface and particle properties (size and shape). • High purity, Homogeneity, High crystallinity Good dispersion • Easy modification of the size of the doped photocatalyst.	• Extended synthesis rime • Requires expensive equipment • Difficulties in mass production	[147] [151]
Sol-gel	✓	✓	• Doping flexibility • Uniform chemical composition • Controllable microstructure and homogeneity	• Calcination stage leads to reduced surface area • Long Process time • Formation of agglomerates	[147] [63] [57] [151]
Micro-emulsion	**Amorphous**		• Simple equipment • Controllable particles	• Uncontrolled aggregation and flocculation. • Difficulties in mass production	[63]
Chemical vapor deposition	✓	✓	• High surface area particles • Easy to scale up	• Capital and energy-intensive	[63]
Impregnation			• High homogeneity • Low operation cost	• Agglomeration of particles	[147]

Table 1.10: Different types of photoreactors [45], [117], [136], [149], [150], [152].

Reactor	**Description**	**Advantages**	**Disadvantages**
Batch reactor	Batch configuration	• Possible to use an external light source • Excellent irradiation distribution • Effective mass transport • Provides large surface area for effective photocatalysis	• Challenges in separating the powdered catalyst from the reaction mixture • Undesired back reaction
Slurry reactor	It comprises catalyst in particulate form. Employed when reactants are present in both gas and liquid phases.	• Utilization of uniform external surface illumination throughout the reaction • Can operate in either fixed bed mode or continuous flow pattern	• Separating of catalyst particles from a mixture can be challenging • Continuous stirring causes additional cost
Fluidized reactor	It is a fusion of a stirred tank and packed bed continuous flow reactors.	• Significant photocatalytic efficacy • Enhanced heat and mass transfer efficiency	• Difficult Separation • Abrasion and attrition of the particles may cause reactor erosion
Optical fibre reactor	Optical Fibers are utilized to evenly distribute light within a photoreactor by applying a coating of a	• Increased surface area • High efficiency in light utilization • Effective catalyst processing capabilities • Economical operation	• Catalyst deactivation at elevated temperatures • Complexity in uniformly coating Fibers

	photocatalyst onto the Fibers		
Monolith reactor	It uses monolith support comprising homogenous blocks with parallel channels, which can be extruded into various shapes and sizes.	• Increased surface-to-volume ratio • Minimal pressure drops • Enhanced flow rate	• Reduced light efficiency • Limited catalyst adhesion to the wall
Fixed bed reactor	It comprises solid catalyst particles loaded and packed into the bed.	• Provides large surface area • Accelerated reaction time • High conversion efficiency per catalyst mass • Economical operation	• Limited exposure of the catalyst to light • Low conversion and yield rate
Twin reactor system and H-Type		• Hydrogen and oxygen can be produced separately • Reduced risk of backward reaction • reduced cost of hydrogen separation before usage • Reduced risk of explosion hence it is safe for commercial operation and scalability.	• Increased cost

2.2.6 Quantum yield

Comparing the reaction rates of different photocatalysts reported by various research groups is challenging due to variations in experimental conditions. To effectively evaluate the photocatalytic hydrogen production from water splitting, it is essential to measure the quantum yield. This metric, which reflects the overall quantum efficiency of the photocatalyst system, enables a quantifiable comparison between different photocatalysts [153]. Quantum yield is a measure of energy efficiency used to assess the effectiveness of photon utilization in photochemical processes [154]. For photocatalytic hydrogen production, quantum yield is defined as the ratio of the hydrogen radical formation to the rate of absorbed photons (Equation 2.9 and 2.10) [155]. However, due to practical challenges like light scattering and reflection that complicate measuring absorbed photons or reacted electrons, IUPAC recommends using the term "Apparent quantum yield " [142].

Quantum yield can be calculated as follows [155].

$$QY_{H^{\cdot}} = \left[\frac{moles\ of \frac{H^{\cdot}}{s}}{moles\ of\ photons\ absorbed\ by\ the \frac{photocatalyst}{s}}\right]100 \qquad \textbf{\textit{Equation 2.9}}$$

The apparent quantum yield (AQY) can be calculated using Equation 2.10. [68]

$$AQY = \frac{Number\ of\ reacted\ electrons}{Number\ of\ incident\ photons} \times 100\%$$

$$= \frac{2 \times Number\ of\ H_2\ molecules\ evolved\ per\ hour}{Number\ of\ incident\ photons\ per\ hour} \times 100\% \qquad \textbf{\textit{Equation 2.10}}$$

Table 2.4 provides the apparent quantum yield (AQY) or quantum yield data for various photocatalysts reported in the literature. Notably, WSe_2-TiO_2 emerged as an effective photocatalyst, achieving an AQY of 43.8% [156]. Lakhera et al. [142] and Kumaravel et al.[56], summarised the photocatalytic activity of several photocatalysts, highlighting that TiO_2- based catalysts, including 1wt%Pt /N-TiNT, TiO_2 nanofiber, 0.5Wt% Ni/P25 TiO_2, and F-TiO_2, exhibit moderate quantum efficiency. Rusinque et al. [156] investigated how catalyst concentration and metal loading affect quantum yields, finding that these factors significantly influence the quantum yield. This finding aligns with results from Rusinque et al. [156] who reported that the quantum yield of 0.25 wt.% Pd-TiO2 photocatalyst varied with conditions: it was 17.4% near-UV irradiation at a photocatalyst concentration of 1g/L, decreased to 6.9% at a lower concentration of 0.15 g/l, and fell to 4.4% under visible light [155]. A recent study on TiO_2 based photocatalysts, revealed that incorporating single Cu atoms into TiO_2 achieved an

apparent quantum efficiency (AQE) of 56% at 365nm irradiation [157]. This performance surpasses all other state-of-the-art TiO_2- based photocatalysts, whose AQE ranges from 4.3-45.5% [157]. This indicates that the various factors discussed impact the photocatalytic activity of TiO_2-based catalysts, affecting hydrogen production rates and ultimately influencing the apparent quantum yield of the process.

2.2.7 Challenges And Future Perspectives Of Photocatalytic Hydrogen Production

Villa et al. highlighted both the advantages and challenges associated with photocatalytic water splitting. The benefits include its environmental friendliness, simple setup, and sustainability [61]. However, significant challenges remain, such as difficulties in separating products, low quantum efficiencies, and issues with reproducibility and scalability. Specifically, the simultaneous production of hydrogen and oxygen in the same reactor can lead to its rapid recombination and decreased photocatalytic efficiency, which undermines its practical and commercial feasibility.

To address these issues, various Z-scheme photocatalysts, which enable product separation, have been extensively researched and developed [61]. Despite these advances, achieving solar-to-hydrogen efficiencies greater than 10% remains a major challenge. Another approach involves using advanced photoreactor systems such as, H-type and twin reactor setups, which facilitate product separation but result in increased costs, impacting the economic viability of the process [48]. Thus, there is a pressing need to develop new materials, such as single-atom catalysts or innovative composites, which achieve high apparent quantum efficiencies (AQE) and significantly enhance photocatalytic performance.

A significant challenge in photocatalytic water splitting is the low quantum efficiency of many photocatalysts, primarily due to the rapid recombination of charge carriers, which affects the overall photocatalytic performance. As discussed in Section 2.2.3, several factors influence photocatalytic efficiency. Strategies to mitigate recombination rates and enhance hydrogen production rates include using co-catalysts and catalysts with smaller particle size [48]. Eidsvåg et al. [47] found that the size of the nanomaterials and co-catalysts can significantly impact photocatalytic activity by reducing recombination rates. Similarly, Jagadeesh Babu et al. reported that the 1D nanostructures offer rapid charge transfer and efficient charge separation, while 2D nanostructures also exhibit improved photocatalytic activity and hydrogen production.[123] Recent advancements have enabled the development of ultra-thin films and

nanoparticles in various forms-such as nanowires, nanorods, nanobelts, nanosheets, further enhancing photocatalytic performance [47].

Another challenge in PWS is the inconsistency in reported hydrogen production rate across various studies. These rates are significantly influenced by the specific experimental conditions and methods, which can vary widely [41]. This variability makes it difficult to compare different photocatalysts. To address this, establishing a global standard for testing and evaluating photocatalysts can help identify and optimize the most effective materials[142]. Eidsvåg et al. [47] also highlighted the need for standard experimental setups and suggested reporting apparent quantum yield (AQY) instead of hydrogen generation rate because AQY is less dependent on the experimental details.

Most research is conducted on a small laboratory scale, which often does not translate well to large-scale applications. The use of powdered photocatalysts in small particle sizes poses significant challenges in separating them from large volumes of water. To overcome this, developing scalable reactor designs that can handle larger quantities of photocatalysts while maintaining high efficiency is essential. Current laboratory reactors, which typically involve stirring photocatalysts in water, may not be practical for large-scale use due to the additional energy required [142]. A promising solution to this is the use of immobilized or fixed photocatalyst systems, which could enhance efficiency and operational simplicity [61]. However, the lack of scalable PWS systems for hydrogen production remains a significant challenge. Notably, the existing large-scale facilities achieve only a 1.5% solar-to-hydrogen efficiency, which indicates the necessity for further research advancements [48]. To advance photocatalytic water splitting towards industrial applications, continued efforts are necessary to develop photocatalysts and reactor designs that can achieve higher solar-to-hydrogen efficiencies.

2.3 Hydrogen Transportation And Storage

Hydrogen transportation technologies encompass the methods and processes for distributing and delivering hydrogen from production sites to end users or storage facilities [32]. Hydrogen can be transported by compressing it into gaseous form or by converting it into liquid form under high pressure [158]. Generally, gaseous hydrogen is transported via tube trailers or pipelines, while liquid hydrogen is delivered using road tankers [159]. Gaseous hydrogen transport is well-established and relatively low-cost, but it faces challenges such as high energy demands and low energy density [32]. According to Nikolaidis et al. [33], innovative solutions

are needed because transport losses for methane and electricity over long distances ranges from 5-7% , whereas losses for hydrogen through the same pipelines could reach to 20%. Liquid hydrogen transportation, while offering higher energy density requires substantial energy to liquefy the hydrogen, making it costly [32]. Additionally, Kanoglu et al. [160] reported that gaseous hydrogen transport via pipeline presents a more environmentally favourable option with a low energy footprint compared to other transportation methods.

Hydrogen storage is achieved through several methods, with traditional approaches including high pressure compression, cryogenic liquefaction, and underground storage, while advanced techniques involve storage in solid materials [159]. Gaseous hydrogen storage, such as compressed hydrogen and underground hydrogen storage, offers benefits like low energy demands, high purity hydrogen, and suitability for large-scale applications. However, it faces challenges remain including energy density, the requirements for high pressure, and the need for sizable storage facilities [32]. Alternatively, according to Abdalla et al.[161] , hydrogen liquefaction increases storage efficiency through high-density liquid hydrogen , but the process is energy-intensive, time-consuming, and results in approximately 10% . Solid state storage, a more recent innovation, incorporates hydrogen into solid materials via chemical or physical bonding [32]. This method provides high volumetric and gravimetric energy density, safer storage and more compact storage and the potential to store substantial quantities of hydrogen [32], [33]. Despite advancements in hydrogen storage technologies, further research is essential to enhance volumetric and gravimetric densities for more efficient storage [33]. In addition to storage improvements, the transportation of hydrogen fuel requires specialized expertise and technological advancements to overcome infrastructure challenges, lower costs, and ensure the safe and efficient distribution [32].

2.4 Hydrogen Applications

Hydrogen utilization technologies refer to the technologies that use hydrogen as a fuel or energy carrier across a variety of sectors, including transportation, electricity generation, heating, and industry [32]. Currently, hydrogen is predominantly used as a reactant in the petroleum industry and for producing ammonia in fertilizers [161]. It also plays a vital role in petroleum refining, methanol production, ore reduction, glass manufacturing, hydrochloric acid production, cooling systems , and aerospace applications [162]. Beyond its extensive use in the chemical and oil sectors, hydrogen can power internal combustion engines, fuel cells, turbines, cooking appliances, and gas boilers [33]. Fuel cell vehicles powered by hydrogen are viewed as a promising carbon- free alternative to fossil fuel based internal combustion engines

[159]. Hydrogen combustion offers a clean and adaptable energy source with benefits like reduced emissions; however, it does faces challenges such as, lower efficiency compared to fuel cells [32]. Key factors influencing the adoption of hydrogen as an alternative fuel in the transportation sector include capital costs and operational costs, infrastructure demands, refuelling range and facilities, refuelling time, the safety, emissions, space restrictions, and overall safety consideration [162].

CHAPTER 3
MATERIALS AND METHODS

This chapter outlines the materials, methods and experimental procedures used to prepare and characterize TiO_2 based catalysts, as well as their evaluation for photocatalytic hydrogen production. It includes the synthesis of monometallic and bimetallic catalysts, the characterisation techniques used, and the experimental setups for hydrogen production. Furthermore, the chapter describes the methodologies for gas collection and analysis to assess the photocatalytic efficiency. Additionally, it outlines the approach used to develop the Aspen Plus simulation and conduct an economic analysis of the photocatalytic hydrogen production process.

3.1 Materials

Titanium(IV) oxide (TiO_2) nanoparticles, consisting of a mixture of 65% rutile and 35% anatase with a particle size range of 25-65 nm, as well as Cu(II) nitrate hemi (penta-hydrate) and Nickel (II) nitrate hexahydrate were purchased from Sigma-Aldrich. All chemicals were used without further purification.

3.2 Preparation of Modified TiO_2 Catalysts

The monometallic Cu, Ni ,and bimetallic Cu-Ni doped TiO_2 catalysts were prepared using the incipient wetness impregnation and co-impregnation methods, respectively. To obtain monometallic doped TiO_2 catalysts, appropriate amount of metal precursors ($Cu(NO_3)_2.3H_2O$ or $Ni(NO_3)_2.6H_2O$) were dissolved in ethanol and the solution was well mixed with the TiO_2 catalyst. The formed paste was dried in an oven and calcined in a muffle furnace. To prepare bimetallic Cu-Ni/TiO_2, both metal precursors dissolved in ethanol solution were mixed with the TiO_2 catalyst. The amount (wt.%) of metal loaded on TiO_2 catalyst was varied and bimetallic catalysts (Cu-Ni/TiO_2) with different Cu: Ni ratios were prepared.

3.3 Catalyst Characterization

The catalyst samples were analysed using various characterisation techniques. The X-ray diffraction (XRD) patterns were obtained using a Bruker D2 phaser X-ray diffractometer (Cu source). Scanning electron microscopy (SEM) and energy dispersive spectroscopy (EDS) were used for morphological and elemental analysis. UV-vis spectra were measured using an ultraviolet-visible (UV-vis) spectrophotometer. The catalyst samples were evaluated for their photocatalytic activity in hydrogen production.

3.4 Photocatalytic Hydrogen Production

3.4.1 Reactor configurations

Two types of photoreactors were used to assess photocatalytic hydrogen production, each with distinct configurations in terms of reactor material, light source arrangement, and reaction scale, all of which influence light penetration temperature control and overall reaction efficiency.

A. Type I Photo-Reactor:

- **Design:** A closed box containing a 250 mL borosilicate Schott bottle, equipped with an inlet, outlet, and thermocouple. Two UV light bulbs were positioned 7 cm away from the reactor.
- **Light Delivery:** UV light was applied externally, with the UV bulbs placed outside the reaction vessel, resulting in indirect illumination.
- **Cooling System:** An air conditioner and internal fans were used to prevent overheating of the light sources.
- **Gas Collection:** The reactor was connected to a gas bag located outside the box.
- **Scale:** This configuration was compact and suitable for small volume experimental screening.

The Type I photoreactor is illustrated in Figure 3.1.

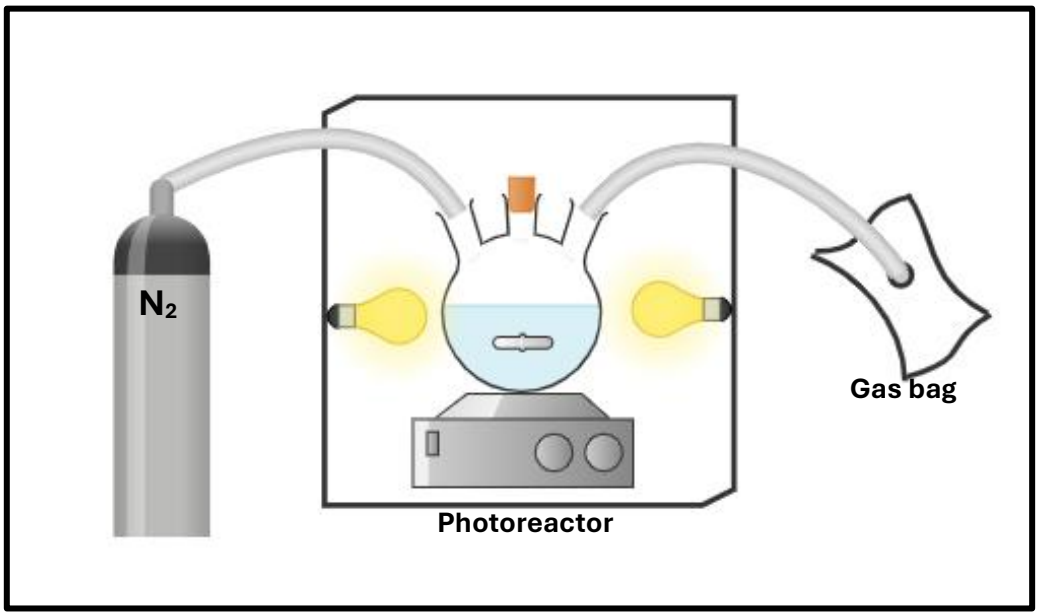

Figure 2.1: Schematic diagram of a Type I photocatalytic reactor.

B. Type II Photo-Reactor:

- **Design:** A larger setup featuring a 1L double jacketed quartz immersion well photo-reactor, housed within a closed box. It included an external cooling tank and a gas bag for product collection.
- **Light Source:** A 450 W medium-pressure mercury lamp (UV light) was inserted directly into a double-jacketed quartz immersion well, ensuring uniform and direct illumination within the reaction medium.
- **Temperature Control:** Both Type I and Type II maintained a temperature of 25 ± 3 °C but Type II offered enhanced temperature regulation through its immersion well and water cooled jacket.
- **Stirring Mechanism:** In both setups, the reactor was placed on a magnetic stirrer.
- **Scale & efficiency :** The Type II setup allowed for a larger reaction volume and more direct delivery, enhancing photon absorption and potential reaction efficiency.

The Type II reaction configurations used in this study is shown in Figure 3.2.

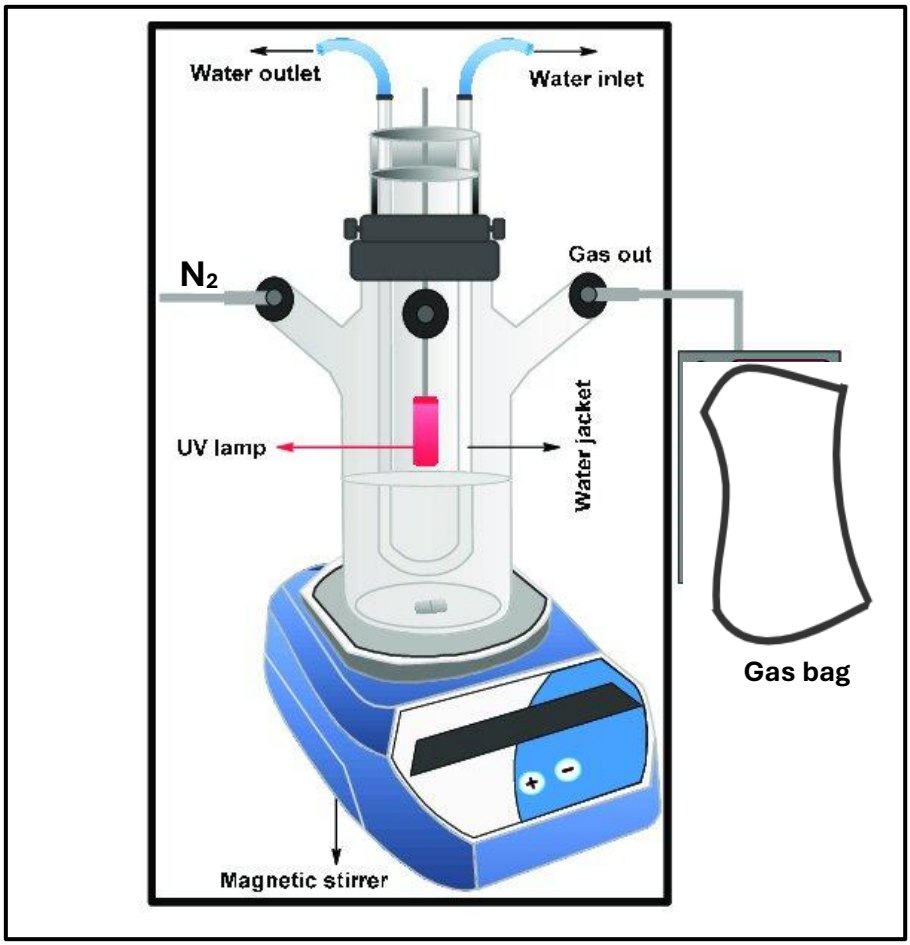

Figure 2.2: Schematic diagram of a Type-II photocatalytic reactor (Adapted from [163]***).***

3.4.2 Methodology

Photocatalytic hydrogen production was conducted following an established procedure from the literature. Firstly, the powdered photocatalyst (1.25 mg/mL), distilled water, and sacrificial reagent (20%) were added to the photo-reactor. The mixture was stirred in the dark for 30 minutes to ensure homogeneity. To remove dissolved oxygen, the solution was purged with N_2 gas for 30 minutes. Nitrogen also served as the carrier gas, directing the produced gases to the gas collection system. Once oxygen removal was complete, the light source was turned on, and the reaction proceeded for 4 hours with continuous stirring to prevent settling of the photocatalyst.

3.4.3 Gas collection methods

Two different methods for gas collection were evaluated:

Method One:

- Gas was collected using a gas bag.
- The collected gas was transferred into a syringe and manually injected into a gas chromatograph for analysis.

Method Two:

- Direct gas collection from the reactor headspace was performed using a gas-tight syringe every hour.
- In this case, the gas bag was disconnected, and the reactor remained closed at the outlet without using carrier gas.

Analysis: The collected gas from both methods was analysed at regular intervals using gas chromatograph (Bruker, 430-GC) equipped with a thermal conductivity detector (TCD) and nitrogen (N_2) as the carrier gas

3.5 Aspen Plus Modelling and Simulation

The Aspen Plus simulation of photocatalytic hydrogen production involved selecting chemical components, defining the Langmuir-Hinshelwood-Hougen-Watson (LHHW) kinetic model, and setting up a batch reactor for the process. Kinetic parameters were derived from literature experimental data and were used in the simulation model, which was validated by comparing simulated results with experimental results. The effect of process parameters, including sacrificial regent type, catalyst dosage, and light intensity, was analysed by adjusting these factors within the simulation.

3.6 Techno-economic analysis

Techno-economic analysis (TEA) of the photocatalytic hydrogen production process was conducted based on data from a pilot-scale photocatalytic reactor setup, consisting of a 25 L compound parabolic concentrator (CPC) reactor. The analysis evaluated both fixed and operating costs using the methodology outlined in the literature. Fixed costs included direct costs such as equipment purchase, installation, and land costs, updated using Chemical Engineering Plant cost index (CEPCI). The plant lifetime was assumed to be 10 years for annualized capital cost calculations. Operating costs accounted for expenses related to chemicals, power, and annual maintenance, with the photocatalyst assumed to be replaced annually. Hydrogen production was modelled using pilot scale data, with a solar to hydrogen efficiency of 0.9% and an annual operating time of 2500 sunlight hours. The specific hydrogen cost was determined by dividing the total costs by the hydrogen output rate, and the Gross economic potential (GEP) was evaluated by comparing the value of the product to the feed costs to assess the economic feasibility.

CHAPTER 4
RESULTS AND DISCUSSION

4.1 Experimental Study on Photocatalytic Hydrogen Production

The experimental study investigated the photocatalytic hydrogen production performance of various modified TiO_2 catalysts. It includes detailed analysis of the catalysts' properties using techniques such as X-ray diffraction (XRD), Scanning Electron Microscopy (SEM), Energy Dispersive Spectroscopy (EDS), and Diffuse Reflectance UV-Visible spectroscopy (UV-Vis DRS). These characterisation methods were used to explore the structural, morphological, and optical properties of the catalysts. The study also evaluated the photocatalytic hydrogen production under different reaction conditions. Additionally, different reactor configurations used in the laboratory setup for assessing the catalysts were compared to assess their efficiency. The results and observations from these experiments are discussed in detail in this section.

4.1.1 Characterizations of Photocatalysts

4.1.1.1 X-Ray diffraction (XRD) Analysis

The XRD patterns of TiO_2 modified with metal(s) (copper and nickel) were analysed to assess their structural characteristics and crystalline phases. The patterns for 1wt.% Cu/TiO_2 and 1wt.% $Ni\text{-}Cu/TiO_2$ are illustrated in Figure 4.1. and 4.2, respectively. Both patterns exhibited prominent peaks corresponding to the crystalline phases of TiO_2, specifically Anatase and Rutile. Notable diffraction peaks were observed at 2 theta values of 25.2, 37, 37.9, 48, 53.9, 55.1, 62.7, 68.8, 70.3 and 75 aligning with Miller indices (101), (103), (004), (200), (105), (211), (204), (116), (220) and (215) respectively, as reported by Saleh et al. [164]. These peaks are characteristics of the Anatase phase of TiO_2, consistent with (JCPDS No. 21-1272). Additionally, peaks at 2θ values of 27.4, 36.1, 41.2 correspond to the (110), (101) and (111) faces of the Rutile phase, confirming that the TiO_2 is a mixture of both phases.

The XRD patterns for both 1wt.% Cu/TiO_2, and 1wt.% $Ni\text{-}Cu /TiO_2$ primarily showed the peaks of TiO_2, without any distinct reflections corresponding to copper, nickel, or their respective oxides (CuO, NiO and CuO-NiO alloy). This finding aligns with previous studies by Tian et al [2] and Kumar et al. [165], [166] which indicated that the XRD detection limit is of 5 wt.% for modified TiO_2. The absence of these metal peaks indicates that metal loading is very low (1 wt.%) and that the metal particles are uniformly dispersed on the TiO_2 surface.

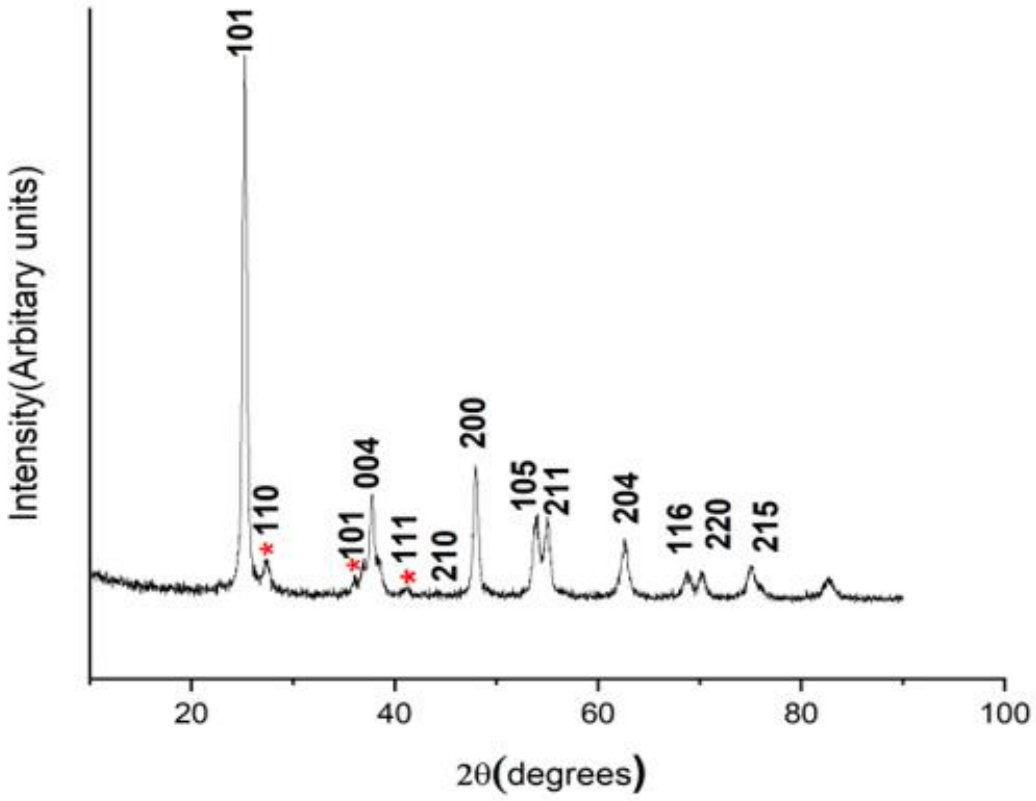

Figure 3.1 : X-ray diffraction pattern of 1wt.% Cu/TiO_2.

The XRD patterns were used to calculate the Anatase to Rutile (A/R) ratio using the Spurr equation (Equation 4.1) as reported by Jacob et al. [167].

$$\mathcal{X} = \frac{1}{[1+0.8\left(\frac{I_A}{I_R}\right)]} \qquad \textit{Equation 4.1}$$

Here, $\mathcal{X}$ represents the percentage of the Rutile phase, while I_A and I_R are the relative intensities of anatase (101) and rutile (110) peaks, respectively. The anatase to rutile composition of commercially obtained TiO_2 was 65:35 which shifted to 88.4:11.6 and 87.2:12.8 after modification with Cu and Cu-Ni, respectively. This indicates that the modification of TiO_2 with metal(s) alters its phase composition, impacting the anatase/rutile ratio. This observation supports findings from the literature that the Copper loading on TiO_2 inhibits the transition from the anatase phase to the rutile phase, thereby increasing the A/R [168].

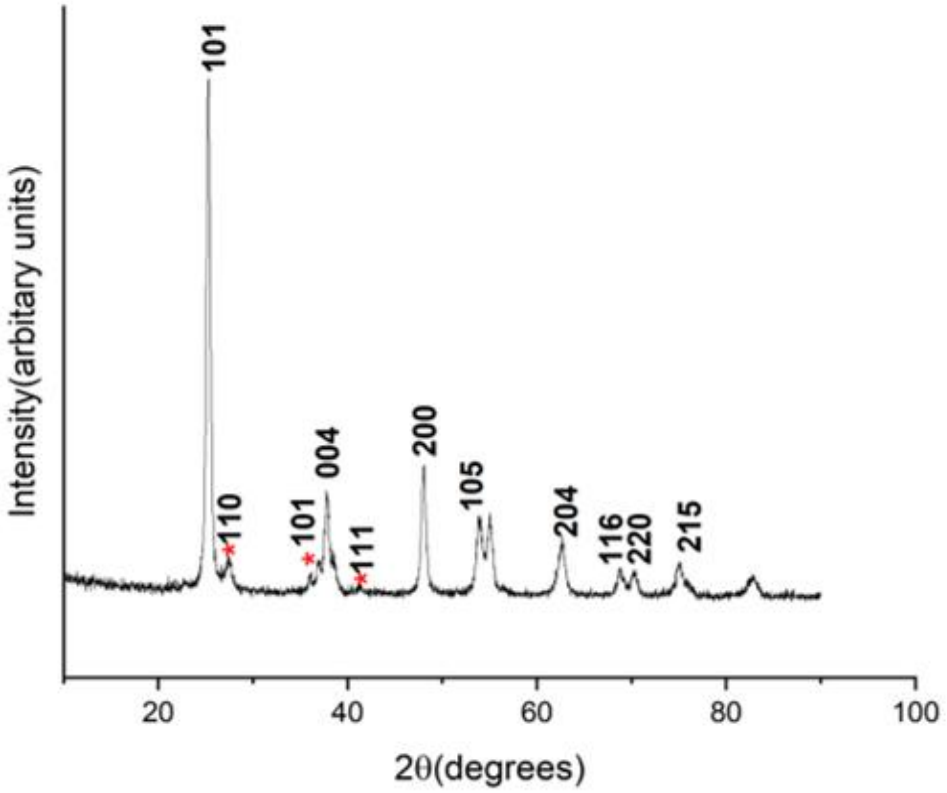

Figure 3.2: X-ray diffraction pattern of 1 wt.%-1Cu:1Ni/TiO_2.

The crystallite size of the samples was estimated using the Scherrer equation (Equation 4.2) [167]. In this equation, D is the crystallite size in nanometres, K is the Scherrer's constant (0.9),

$$\boldsymbol{D = \frac{K\lambda}{\beta cos\theta}} \qquad \textbf{Equation 4.2}$$

λ is the wavelength of the X-ray radiation (0.15406 nm), and β is the full width at half maximum (FWHM) of the peak being analysed. The crystallite size for Cu/TiO_2 ranged from 6 to 16 nm, averaging 10 nm, which closely aligns with the value reported by Adamu et al. [168] for Cu/TiO_2 with 100% Anatase composition (13.9 nm). Conversely, the average crystallite size for Cu-Ni/TiO_2 was found to be 8.5 nm, indicating a smaller size relative to Cu/TiO_2. This was further supported by the diffraction peak at 2θ = 25.2 for the plane (101), which exhibited a higher intensity for Cu/TiO_2 compared to Cu-Ni/TiO_2, suggesting greater crystallinity in Cu/TiO_2 . These findings are in line with the results reported by Salazar-Villanueva et al. [169] who observed similar trends in their study.

4.1.1.2 Scanning Electron Microscopy (SEM) and Energy dispersive Spectroscopy (EDS) Analysis

The scanning electron micrographs of Ni/TiO_2 obtained are presented in Figure 4.3. The SEM images reveal that the morphology of the catalyst particles appears slightly spherical, characterized by large agglomerates of smaller particles. According to the literature, pure TiO_2 typically exhibits spherical particles with a uniform size distribution [170]. The observed agglomeration in Ni-TiO_2 SEM images suggests that the introduction of nickel alters the particle shape compared to pure TiO_2. However, the images do not indicate any visible metal deposition, which may be attributed to the nickel's highly dispersed or well-incorporated nature within the TiO_2 support. Therefore, additional characterization techniques were used to provide further insight into the material's properties.

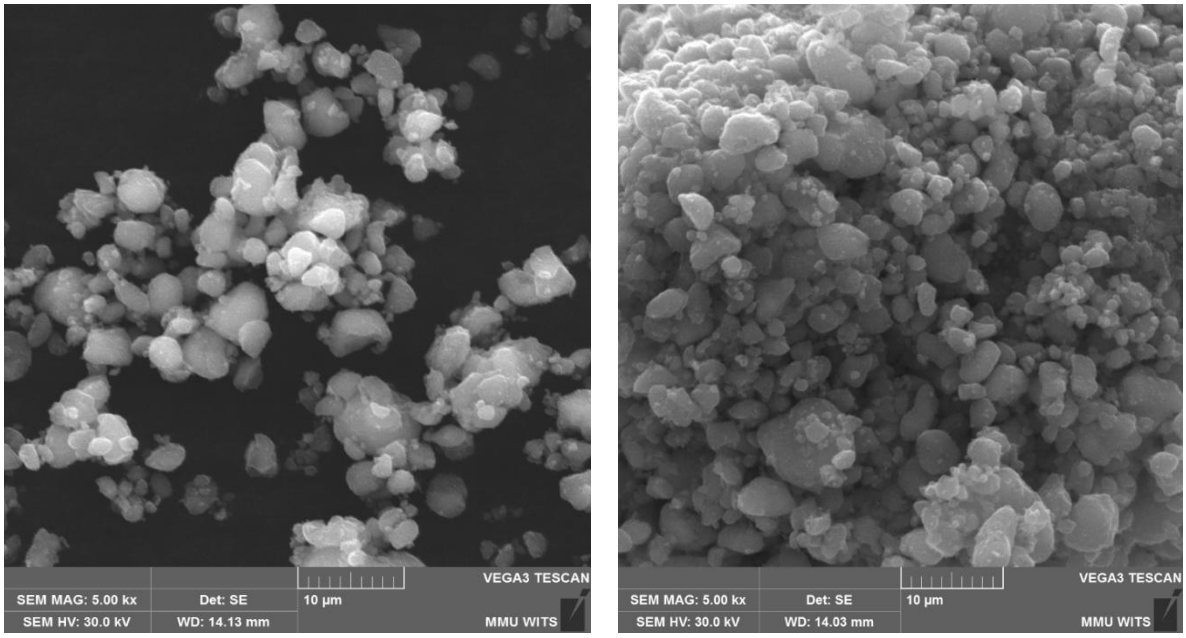

Figure 3.3: SEM images of Ni/TiO_2.

The elemental composition of the 1wt% Ni/TiO_2 was further assessed using Energy Dispersive Spectroscopy (EDS)(Figure 4.4). It provided an indication of the average elemental quantities, identifying the presence of elements such as Titanium (~50 wt.%), Oxygen (~48 wt.%), and Ni (~1.35 wt.%), along with trace amounts of impurities such as sulfur and carbon. The detection of carbon could be attributed to the use of carbon tape during sample preparation, while sulfur, which was not expected in the system, may have originated from impurities in the precursors. This confirms the successful incorporation of nickel onto the TiO_2 support. The

energy resolution peaks shown in Figure 4.4 for Titanium at 4.5 eV and Nickel at 7.5 eV align with findings reported in the literature [171]. The detection of nickel indicated the successful incorporation of nickel on to TiO_2 and confirmed the presence of nickel in amount closely matching that used during the synthesis of the Ni/TiO_2 catalyst.

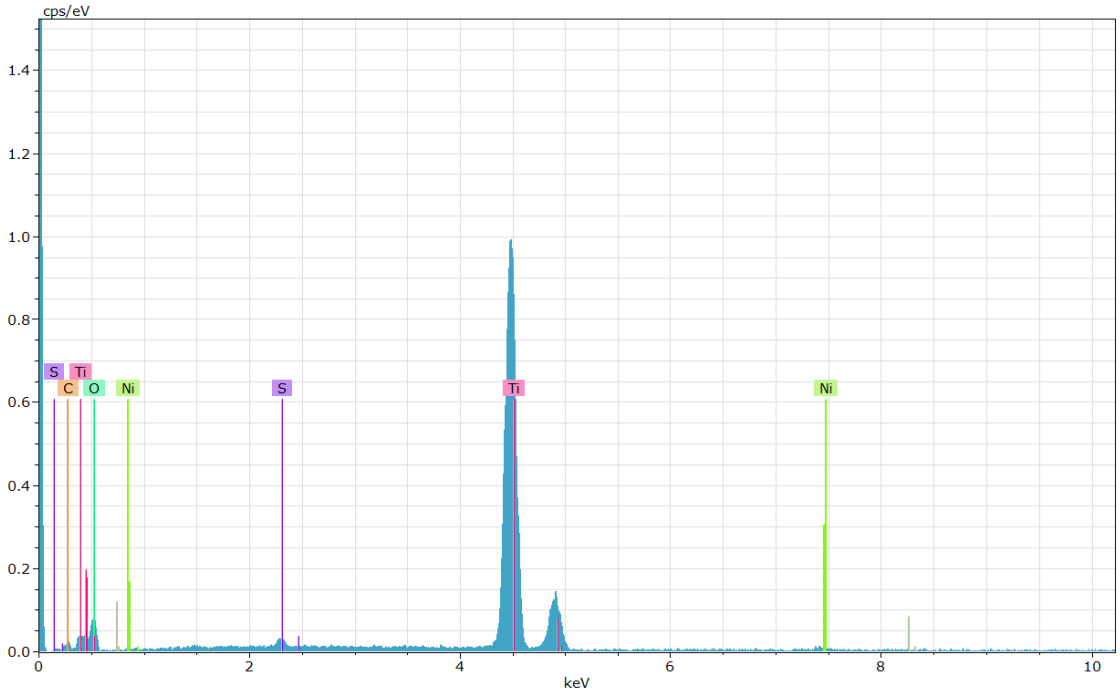

Figure 3.4: EDS spectrum of Ni/TiO_2.

4.1.1.3 Diffuse Reflectance UV-Visible Spectroscopy (UV-Vis DRS)

The optical properties of TiO_2, $Cu\text{-}TiO_2$, $Ni\text{-}TiO_2$ and $Cu\text{-}Ni/TiO_2$ were analysed using UV-Vis Diffuse Reflectance Spectroscopy (DRS). The absorption spectra for all four samples, shown in Figure 4.5, revealed that all four samples exhibited strong absorption in the wavelength range of 200-400 nm. Notably, all samples displayed a strong absorption band around 350 nm, which corresponds to the excitation of O 2p electrons to Ti 3d levels, indicating electron transfer from the valence band (VB) to the conduction band (CB). Furthermore, the spectra indicated a shift towards a longer wavelength for the metal-modified TiO_2, with absorption edges of Cu/TiO_2, Ni/TiO_2 and $Cu\text{-}Ni/TiO_2$ extending into the visible region (above 400 nm). This suggests that the band edge of modified TiO_2 has broadened into the visible spectrum, even though no distinct absorption peak was observed. According to Kumar et al. [166], this phenomenon may arise from additional energy levels introduced by the metal ions within the band gap of TiO_2.

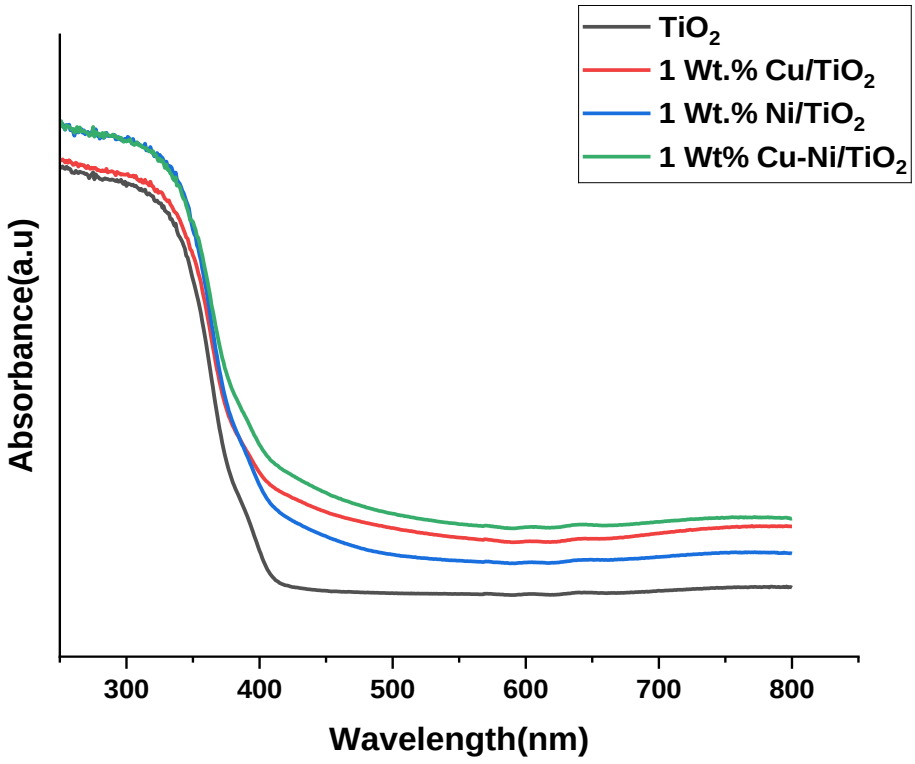

Figure 3.5: UV -VIS DR spectra of TiO_2 and metal(s)-modified TiO_2 catalysts.

As discussed in Chapter 2, this enhanced absorption and shift towards the visible spectrum could be attributed to the plasmon resonance effects of Cu and Ni [164]. The spectra also revealed that Cu-Ni/TiO_2 demonstrated higher absorption in visible region (400 – 800 nm) compared to Cu-TiO_2, Ni-TiO_2 and bare TiO_2. This enhanced absorption may be due to the synergetic effects of Cu-Ni alloy, as noted in the literature. Riaz et al. [171] suggest that the observed shift could be linked to the presence of impurity energy levels resulting from the metals well-dispersed on the surface of TiO_2 rather than incorporated into its framework. Interestingly, the 1 wt.% Ni-TiO_2 exhibited slightly higher absorption in the visible region than Cu/TiO_2, relatively aligning with findings from Nurlaela et al.[172], which indicated that 10 wt.% Ni/TiO_2 had higher absorption compared to 10 wt.% Cu/TiO_2.

Figure 4.6 presents the absorption spectra for TiO_2 and the 2-5 wt.% Cu/TiO_2 samples. As Cu concentration increased, the absorption edge shifted further into the visible region, with all samples displaying a broad absorption signal from 600- 800 nm. According to Chen et al. [173], this is consistent with the blue-green colour of Cu/TiO_2, which can be attributed to the d-d transition (Cu^{2+}/Ti^{4+}charge transfer transitions) in the CuO co-catalyst supported on TiO_2. This observation indicates that copper is loaded as CuO (Cu^{2+}) on TiO_2. This result agrees with that

reported by Kumar et al. [166] for Cu- and Ni- modified TiO_2. Additionally, light absorption properties improved with increased metal concentrations.

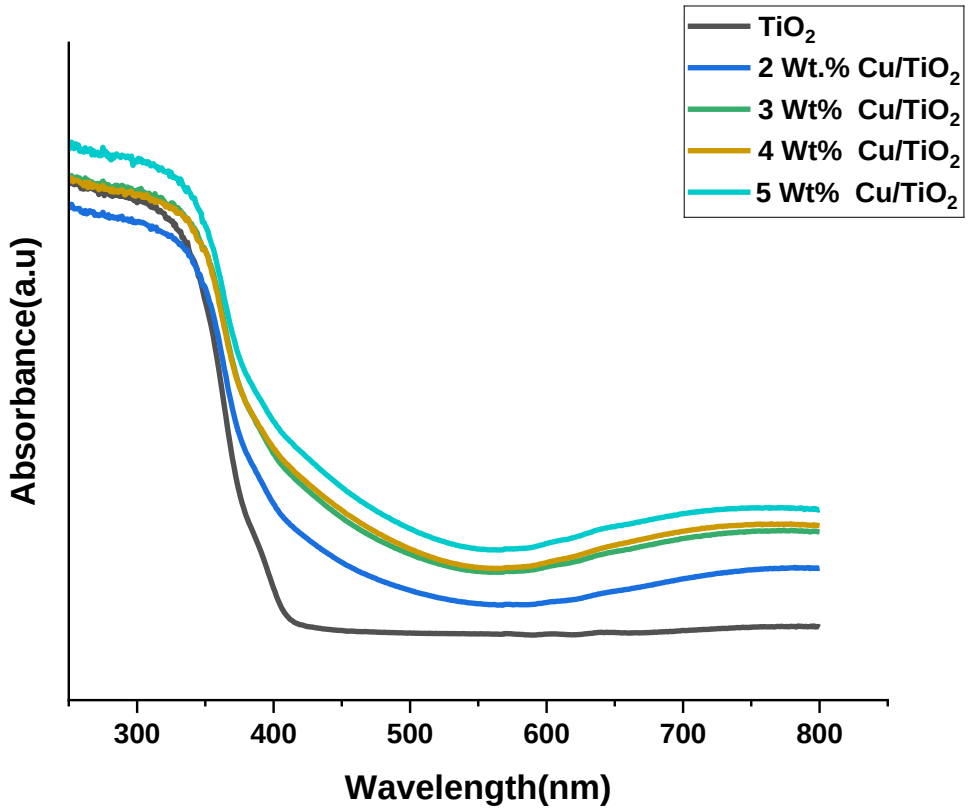

Figure 3.6: UV-Vis DR spectra showing absorbance profiles of various Cu-TiO_2 catalysts.

One of the most important parameters affecting photocatalytic activity is the characteristics band gap, which represents the energy required for an electron to transition from the valence band (VB) to the photocatalyst's conduction band (CB). The band gap energy was determined using the UV-Vis diffuse reflectance spectra and Tauc plot, which is the plot of $(F(R).hv)^{½}$ against hv, where F(R) is the Kubelka-Munk function derived from reflectance spectra: $F(R) = \frac{(1-R)^2}{2R}$ and hv is the photon energy [171]. The Tauc plots are illustrated in Figure 4.7, and the corresponding band gap energy values are presented in Table 4.1. As reported by Adamu et al. [168], the band gap energy values were determined by linear regression in the linear region of the plot, followed by extrapolation of the fitted lines to the points of intersection with the hv (x) axis.

From Table 4.1, it can be observed that the indirect band gap energy of TiO_2 is 3.12 eV, consistent with values reported in the literature [173]. The band gap energies decreased in the following order: 1 wt.% Cu-Ni/TiO_2 < 1 wt.% Ni/TiO_2.< 1 wt.% Cu/TiO_2 < TiO_2. This indicates that bimetallic co-catalysts (Cu-Ni) yielded the lowest band gap and enhanced visible light absorption compared to the monometallic co-catalysts (Cu , Ni). Additionally, it is noted that as Cu loading (wt.%) on TiO_2 increased, the band gap energy values decreased to 2.87 eV. These results are consistent with those reported by Kumar et al. [166], where the band gap values dropped to a minimum of 2.56 eV with an increased Cu loading. Hussein et al. [174] also reported similar observations for Ni modified TiO_2.

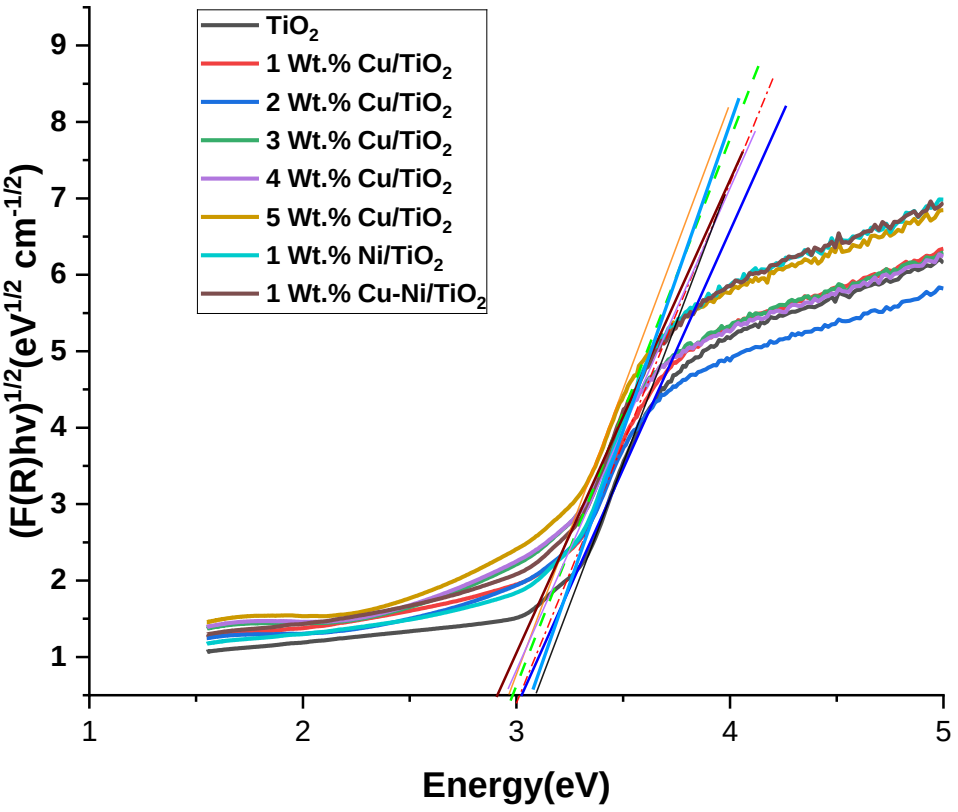

Figure 3.7: Tauc plots for various TiO_2 based catalysts.

Overall, the type of metal and its loading on TiO_2 significantly affected its bandgap energy. This agrees with the literature discussed in Chapter 2, which indicated that the reduction in bandgap due to metal modification may result from surface plasmon resonance effects or charge transfer between TiO_2 bands and the surface-deposited metal particles [175]. Metal modified TiO_2 resulted in a decreased bandgap energy and increased visible light absorption, indicating its potential for enhanced photocatalytic activity.

Table 3.1: Bandgap energy values of TiO_2 and metal- modified TiO_2 catalysts.

Catalyst	Bandgap energy (eV)
TiO_2	3.12
1 wt.% Cu/TiO_2	3.08
2 wt.% Cu/TiO_2	2.98
3 wt.% Cu/TiO_2	2.94
4 wt.% Cu/TiO_2	2.93
5 wt.% Cu/TiO_2	2.87
1 wt.% Ni/TiO_2	3.05
1 wt.% $Cu\text{-}Ni/TiO_2$	3.00

4.1.1.4 Summary of Characterisation Results

Three different catalysts- Cu/TiO_2, Ni/TiO_2 and $Cu\text{-}Ni/TiO_2$ were synthesized by modifying commercially available TiO_2 using wet-impregnation. Characterization techniques, including XRD, SEM, EDS, and UV-Vis spectroscopy, confirmed successful synthesis and metal incorporation. XRD analysis showed that metal modification increased the anatase content without altering TiO_2's structure, indicating good metal dispersion on the TiO_2 surface. SEM images revealed slightly spherical particles with homogenous size distribution, while EDS confirmed successful metal loading. UV-Vis spectroscopy indicated strong UV absorption for all samples, with metal-modified TiO_2 extending absorption into the visible region, showing that metal content influences the bandgap. Additionally, the synthesized Cu/TiO_2, Ni/TiO_2 $Cu\text{-}Ni/TiO_2$ exhibited distinct colours (light blue-green, light green, and light green-blue, respectively), confirming the presence of CuO, NiO and CuO-NiO on the surface of TiO_2 [173]. In summary, Cu/TiO_2, Ni/TiO_2 and $Cu\text{-}Ni/TiO_2$ catalysts were successfully synthesized with desirable properties for photocatalytic applications.

4.1.2 Evaluation of Photocatalytic Activity

The synthesized catalysts were evaluated for hydrogen production via a photocatalytic process, with experiments conducted under varied conditions as summarized in Table 4.2 . As outlined in Chapter 3, two different reactor setups were used for assessing photocatalytic hydrogen production. In the Type I Photo-reactor, the light source was positioned 7 cm away from the reactor. This configuration resulted in no detectable gas production, and no observable changes

occurred in the reaction solution containing the catalyst, water, and sacrificial reagent. The lack of hydrogen detection could be attributed to insufficient light absorption by the TiO_2 catalyst, which requires adequate energy and intensity to excite electrons from the valence band and generate electron-hole pairs (e^-/h^+) for initiating a water-splitting reaction.

The absence of hydrogen detection may have resulted from several factors related to reactor design and light source properties. Firstly, the distance between the light source and the reactor limited the light intensity reaching the catalyst, allowing light to penetrate only one side of the reactor. This setup likely prevented effective illumination of the entire reaction mixture, significantly reducing photon absorption by the catalyst. This aligns with the findings by Meinhardová et al.[176], who reported that the optimal positioning of the light source in a photocatalytic reactor is essential for maximising photocatalyst illumination and hydrogen production efficiency. Moreover, the illuminated surface area is a key parameter influencing the overall reactor design.

Secondly, the specific type of UV light source used may not have been suitable for this process. In this setup, purple UV bulbs were utilized, which may not have provided photons with an adequate energy for efficient TiO_2 activation. As Aldosari et al.[177] highlighted, successful photocatalyst excitation requires photons with sufficient energy levels. Thus, the limitations of the Type I reactor, particularly in the choice of light source, suggest that an inappropriate light source was used for this setup. This is consistent with findings in the literature, such as those in [176], which emphasize that that the properties of the irradiation source, including type, wavelength, intensity within the reaction volume, and distribution inside the reactor are critical factors in achieving effective photocatalytic hydrogen production. Overall, it can be concluded that the Type I photo reactor setup used was ineffective for photocatalytic hydrogen production.

Using the Type-II photoreactor for photocatalytic hydrogen production did not yield detectable gas. However, notable changes occurred in the reaction solutions under metal- modified TiO_2 catalysts, including 2 wt.%, 4 wt.%, 5 wt.% Cu/TiO_2, as well as 1%Cu-Ni/TiO_2, and unmodified TiO_2, following UV irradiation. For instance, the CuO/TiO_2 catalyst turned dark black when methanol was used as the sacrificial reagent (Figure 4.8 (b)), dark brown when ethanol was used (Figure 4.9(a)), and remained green in pure water (Figure 4.8(a)). This rapid colour change, occurring within just 20 minutes of irradiation, suggests that the sacrificial reagents (methanol and ethanol) facilitated the reduction of CuO particles to metallic Cu(Cu^0). This aligns with previous findings by Chen et al. [173], where similar colour changes were observed during photocatalytic hydrogen production in alcohol-water mixtures under UV light.

Chen et al. [173] explained that this reduction of CuO is influenced by the redox potential of the CuO/Cu^0 couple (-0.42 V), which is close to the conduction band potential of TiO_2 (-0.5V), providing a minimal driving force for electron transfer from TiO_2 to CuO in pure water. However, in the presence of sacrificial reagents, alcohols undergo photooxidation, forming alpha-hydroxy radicals ($^{\cdot}CH_2OH$) with a redox potential of -0.76 V. This potential is significantly more negative than both the CuO/Cu and TiO_2 conduction band potentials, driving the reduction of CuO to Cu on the TiO_2 surface and causing a shift in colour from light green to dark black. Once the CuO is fully reduced to Cu^0, these alpha-hydroxy radicals can continue to donate electrons to the conduction band of TiO_2, potentially enabling hydrogen production. According to Chen et al.[173], Cu^0 nanoparticles serve as an effective co-catalyst, enhancing the hydrogen generation efficiency.

Interestingly, a similar colour change was observed with unmodified TiO_2 when methanol was used as the sacrificial reagent. While the unmodified TiO_2 catalyst is originally white, it turned dark blue upon UV irradiation in the presence of methanol (Figure 4.9 (b) & Figure 4.10 (b)), whereas it remained pure white in the presence of only water (Figure 4.10 (a)). These findings align with previous observations in the literature, where it was noted that colour changes in TiO_2 under UV irradiation vary significantly depending on metal loading [178]. In this study, metal-loaded TiO_2 catalysts changed to dark grey or black, whereas unmodified TiO_2 turned dark or light blue, as shown in Figure 4.8-4.10. According to Bowker et al. [178], colour change of TiO_2 upon UV irradiation can be attributed to several factors: i) formation of photogenerated electron (e^-) and hole (h^+) pairs, and ii) methanol acting as a hole scavenger, which traps photogenerated electrons and reduces Ti^{4+} to Ti^{3+} in the absence of oxygen. The appearance of a blue colour indicates the anion/oxygen vacancies and Ti^{3+} centres. This is significant because, as Fajrina et al. [179] reports, the presence of oxygen or anion vacancies can extend charge carrier lifetimes and inhibits electron-hole recombination, potentially enhancing hydrogen production efficiency.

After exposure to air, all catalyst samples, both modified TiO_2 and unmodified TiO_2 returned to their original colours, as shown in Figure 4.11 (a-c). This reversion suggests that metals like Cu and Ni on the TiO_2 reoxidised to CuO and NiO, while Ti^{3+} centres in unmodified TiO_2 reverted to Ti^{4+}, restoring its white colour. This indicates that the synthesised catalysts facilitated photocatalytic reactions. The observed colour changes imply that the photocatalytic processes, such as electron-hole pair generation and alcohol oxidation, occurred during the testing. However, hydrogen gas production could not be quantified, as no hydrogen peaks were

detected in any gas analysis across experiments, even with different gas collection methods discussed in Chapter 3. Table 4.2 shows several parameters, including catalyst dosage, sacrificial reagent type and concentration, and irradiation time, which were varied, but none yielded detectable hydrogen.

Based on these findings and literature comparisons, the absence of hydrogen detection may result from several factors. Firstly, the literature suggests that photocatalytic hydrogen production rates are very low(e.g., 3-20 mmol/g.h for Cu/TiO_2), possibly falling below the detection limits of the gas chromatography used in this study. Additionally, while sacrificial reagent should minimize electron-hole recombination, rapid recombination may still have limited hydrogen generation. To further reduce recombination, a carrier gas was used to continuously flush the headspace and prevent hydrogen-oxygen recombination.

Overall, the observed colour changes and alignment with literature data suggest that electron transfer reactions and alcohol oxidation occurred, indicating that the photocatalyst was active under UV irradiation. While it is likely that trace amount of hydrogen was produced based on the observed catalyst changes, these amounts were either below detection limits or the photogenerated electron-holes pairs recombined, resulting in no net hydrogen production. The Type-II photoreactor proved to be more effective than the Type-I reactor due to its improved light distribution and proximity. With a view to adding value to knowledge, despite the non-detection of hydrogen, the process was simulated using Aspen plus to further evaluate potential hydrogen yield and identify factors affecting hydrogen production rates.

Table 3.2: Experimental details and observations.

Experiment	Catalyst	Sacrificial reagent (SR)	Reactor setup	Total Volume (Water + SR) (ml)	Sacrificial reagent (Vol%)	Catalyst dosage (mg/ml)	Time (h)	Observations
1	4%Cu/TiO_2	No SR	Type II	400	20	1.25	4	The solution remained green throughout the experiment, with no gas detected.
2	4%Cu/TiO_2	Methanol	Type II	400	20	1.25	4	After 10-20 minutes of UV light irradiation, the solution turned dark black, and the catalyst colour also changed to black but reverted to light green upon exposure to air.
3	5%Cu/ TiO_2	Methanol	Type II	400	20	1.25	4	In a similar observation, the solution turned dark brown/black after 20 minutes of UV light irradiation
4	1%Cu-Ni/TiO_2	Glycerol	Type II	400	20	1.00	6	Similar to experiment 2
5	2%Cu/ TiO_2	Ethanol	Type II	400	20	1.25	4	Similar to experiment 2
6	TiO_2 (A/R: 65/35)	Methanol	Type II	400	20	1.25	4	The solution turned light blue after UV irradiation, and no gas was produced or detected.
7	TiO_2	Methanol	Type II	400	20	1.00	4	Similar to experiment 6

	(A/R= 65/35)							
8	TiO_2 (A/R= 65/35)	No SR	Type II	400	0	1.00	4	The solution remained white after UV irradiation, no gas was produced or detected.
9	TiO_2 (100% Rutile)	No SR	Type II	400	0	1.00	4	Similar to experiment 8
10	TiO_2 (100% Rutile)	Methanol	Type II	400	20	1.00	4	Similar to experiment 8
10	TiO_2 (A/R= 65/35)	Methanol	Type II	400	50	1.00	4	Similar to experiment 6
11	TiO_2 (A/R= 65/35)	Methanol	Type II	400	70	1.00	4	Similar to experiment 6
12	1 wt.% Cu/TiO_2	Glycerol	Type I	100	20	1.25	4	Similar to experiment 1
13	TiO_2	Ethanol	Type I	150	20	1.25	4	Similar to experiment 8
14	TiO_2	No SR	Type I	100	0	1.25	4	Similar to experiment 8

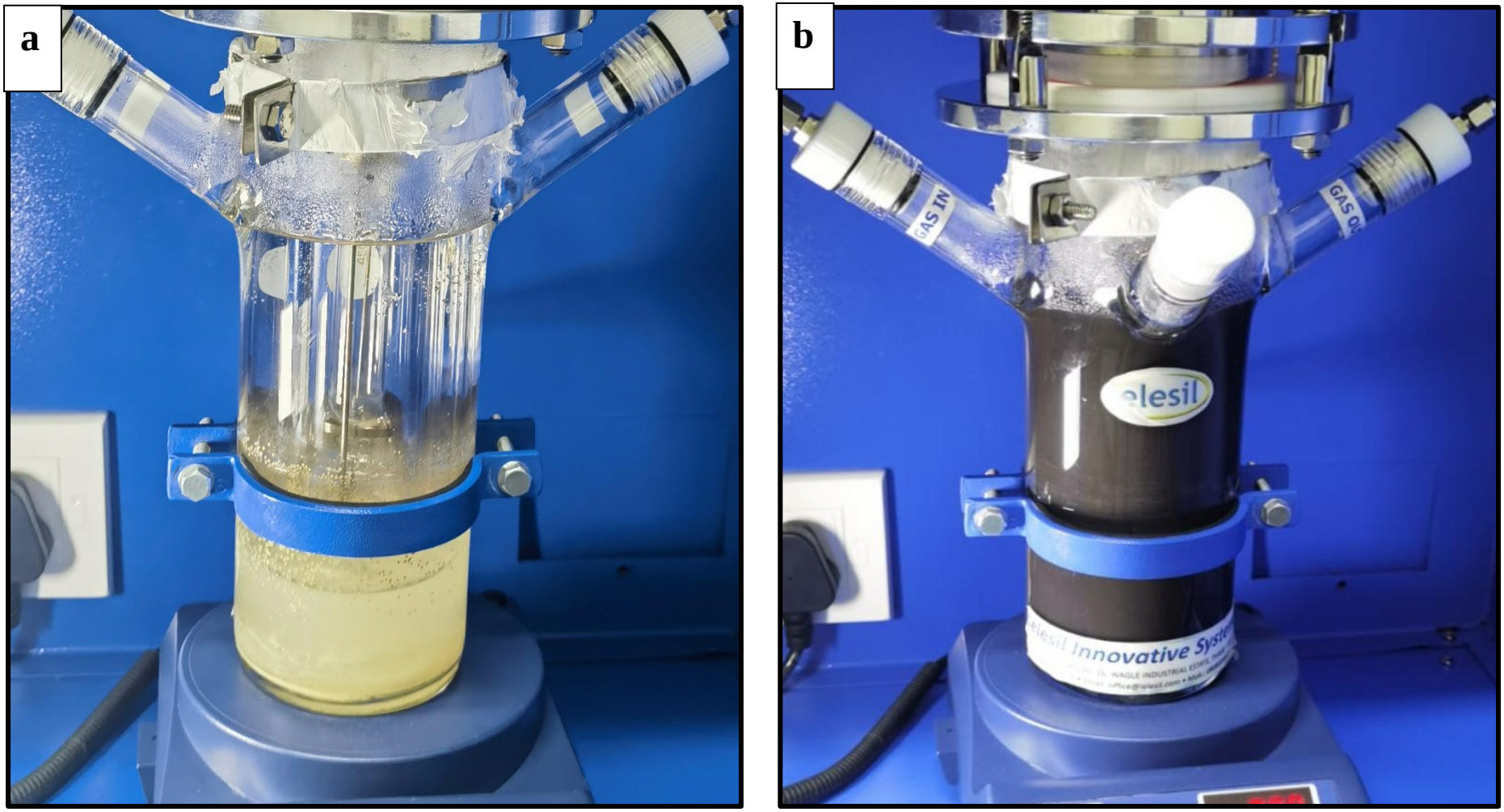

Figure 3.8: (a) Experiment 1: 4 wt.%Cu/TiO_2 without sacrificial reagent; (b) Experiment 3: 4 wt.%Cu/TiO_2 with methanol.

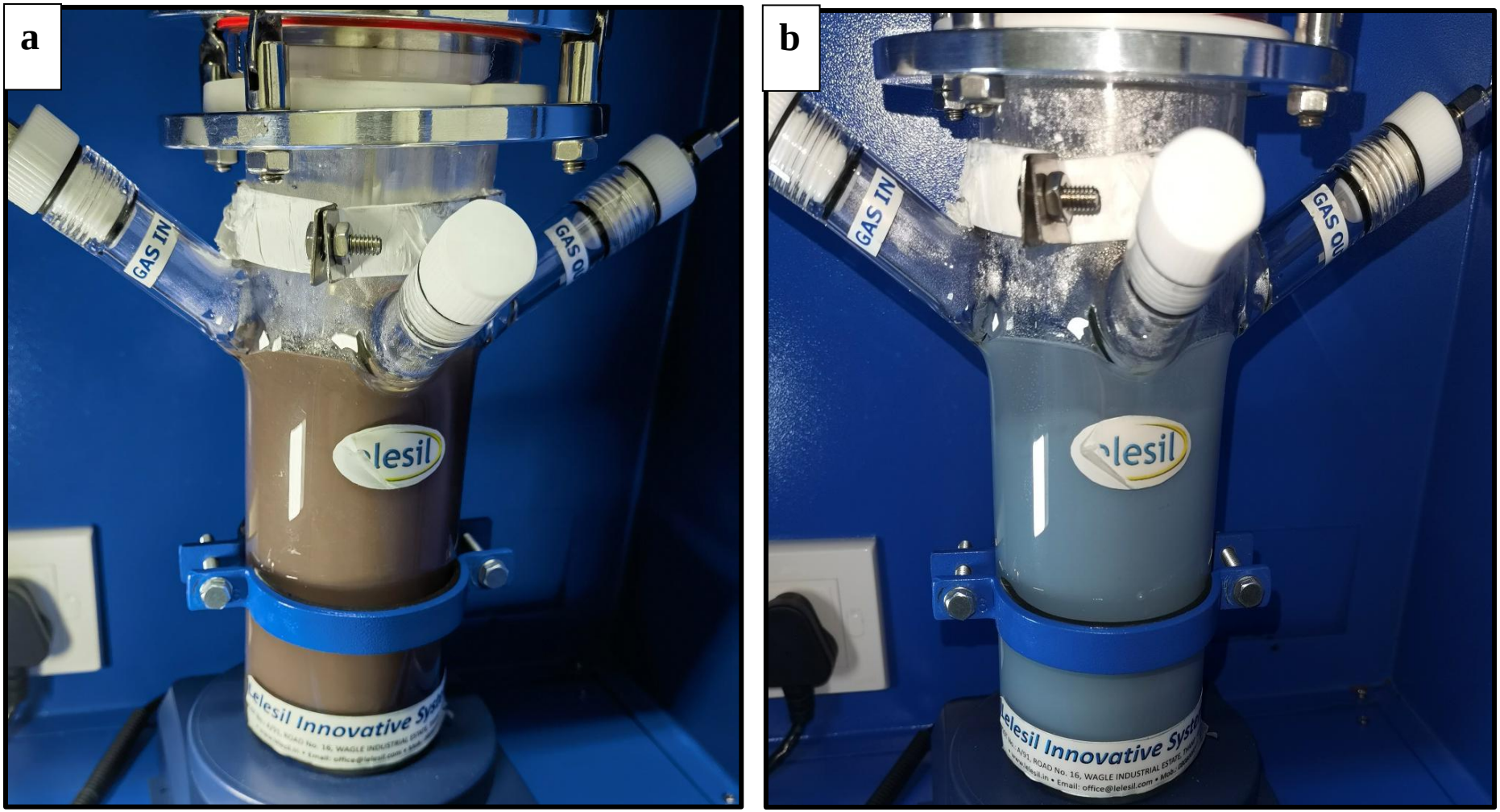

Figure 3.9: (a) Experiment 5: 2 wt.% Cu/TiO_2 with ethanol; (b) Experiment 6: TiO_2 with methanol.

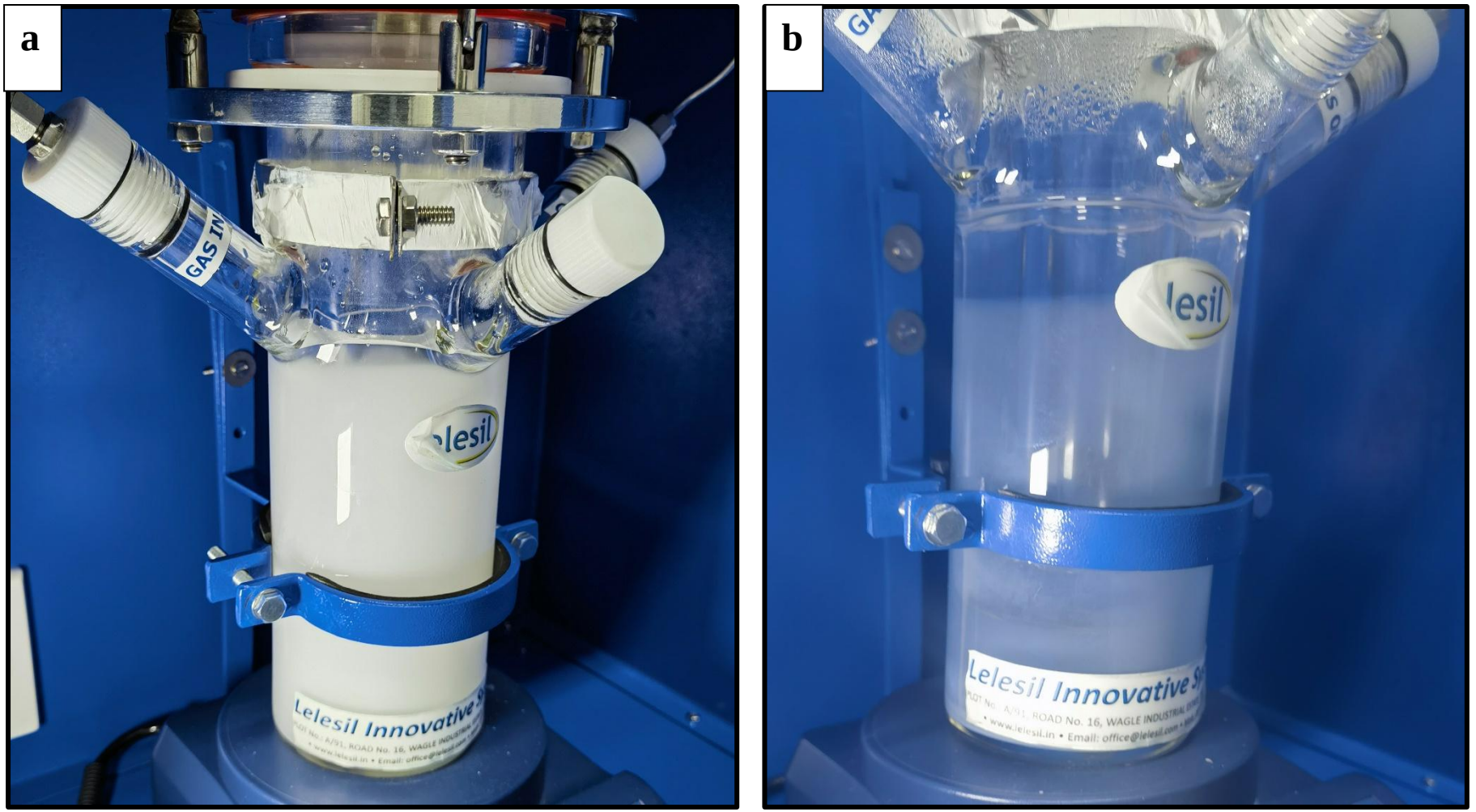

Figure 3.10 : (a) Experiment 8: TiO_2 with water only; (b) Experiment 11: TiO_2 with 70 vol% methanol.

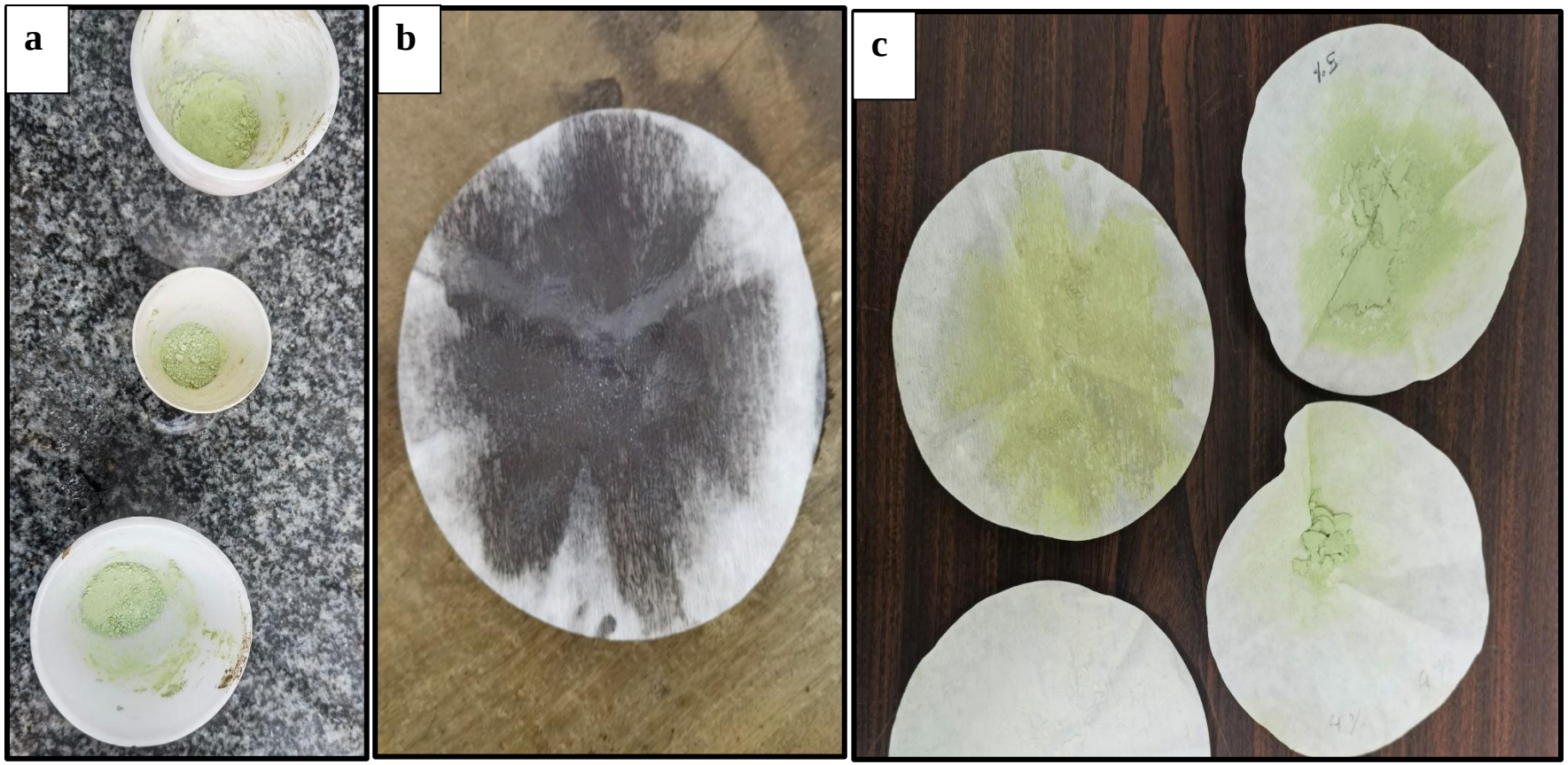

Figure 3.11: (a) Cu/TiO_2 before the experiment; (b) Cu/TiO_2 recovered after the experiment; (c) Cu/TiO_2 after exposure to air for a period of time.

4.2. Aspen Plus Modelling and Simulation of Photocatalytic Hydrogen Production

4.2.1 Modelling and Simulation

Modelling and simulation were conducted following a standard procedure that included: i) selection of chemical components, ii) selection of thermodynamic model , iii) creation of a flowsheet by choosing unit operations and defined feed stream properties, iv) specifying equipment parameters, and v) generating data output. The chemical components selected for this simulation included water, four different sacrificial reagents (Methanol, Ethanol, Ethylene glycol, Glycerol), hydrogen, and carbon dioxide. A flowsheet was developed using the batch reactor model available in Aspen plus. The batch reactor was assumed to operate as a continuously stirred system, treating the setup as a single well-mixed batch reactor. The kinetics of the reactions were modelled using the Langmuir-Hinshelwood-Hougen-Watson (LHHW) kinetic model, which is commonly employed to describe reactions by heterogeneous catalysts where both kinetics and adsorption phenomena are significant [180].

The overall chemical reaction for the different sacrificial reagents (Equation 4.3) were specified, assuming that intermediates and by-products are negligible, thereby focusing on the primary product, such as hydrogen. The effect of critical parameters such as the photocatalyst dosage and light intensity were integrated into the reaction rate constant.

$$\boldsymbol{C_X H_Y O_Z + (2X - Z) H_2 O \rightarrow X CO_2 + (2X - Z + \frac{1}{2} Z) H_2} \qquad \textit{Equation 4.3}$$

4.2.1.1 Kinetic Modelling

Photocatalytic hydrogen production is a heterogenous process, and its activity is commonly described using the Langmuir-Hinshelwood (L-H) model [181]. This model predicts based on the assumption that the reactants adsorb onto the catalyst surface, where reactions occur between adsorbed species, followed by the desorption of products from the catalyst surface [182]. As reported in the literature [182], for a chemical reaction represented as $\boldsymbol{A + B \rightarrow C + D}$, the rate of the reaction can be expressed by the following L-H kinetic model.

$$\mathbf{r = \frac{k K_A K_B C_A C_B}{(1 + K_A C_A)(1 + K_B C_B)}} \qquad \textit{Equation 4.4}$$

Where:

r = reaction rate

k = rate constant

K_A, K_B = Adsorption constant of A and B, respectively

C_A , C_B = Concentration in liquid phase, respectively

In scenarios where the concentration of reactant A is significantly higher than that of reactant B, the change in concentration of A becomes negligible, allowing for a simplified expression of the reaction rate:

$$\mathbf{r} = \frac{k' K_B C_B}{(1+K_B C_B)} \qquad \textit{Equation 4.5}$$

where k' represents the apparent rate constant. Studies by various researchers indicate that the hydrogen production rate at lower concentrations of sacrificial reagents follows the Langmuir-Hinshelwood-type kinetic model [183], [184], [185], [186], [187], confirming its applicability for modelling photocatalytic reactions in Aspen Plus. For instance, Alkaabi et al. [188] successfully modelled a photodegradation process in Aspen Plus using the Langmuir-Hinshelwood (LH) kinetic model to design a photoreactor.

The experimental results reported by Chen et al. [173], [189] for various metal-loaded TiO_2 catalysts and sacrificial reagents were utilized to derive the kinetic parameters for the simulation. The experimental data obtained were fitted to the following L-H model by plotting $1/RH_2$ against $1/ [SR]_0$.

$$R_{H_2} = k_{H_2}\left(\frac{K[SR]_0}{1+K[SR]_0}\right) \qquad \textit{Equation 4.6}$$

In Equation 4.6, $[SR]_0$ represents the initial concentration of the sacrificial reagent in the solution. The values for k_{H2} and K obtained for three different types of metal-loaded catalysts and four sacrificial reagents are summarised in Table 4.3.

Table 3.3: Kinetic parameters derived from the Langmuir-Hinshelwood model.

Catalyst	**1 wt.% Cu/TiO_2**		**2 wt.% Au/TiO_2**		**0.5 wt. %Ni/TiO_2**	
Sacrificial Reagent	**k_{H_2} (mmol/g.h)**	**K (L/mol)**	**k_{H_2} (mmol/g.h)**	**K (L/mol)**	**k_{H_2} (mmol/g.h)**	**K (L/mol)**
Methanol	14.51	1.19	21.55	2.04	24.21	1.33
Ethanol	13.12	1.70	16.92	1.15	13.50	3.58
Ethylene glycol	18.87	2.62	26.04	12.00	22.68	13.36
Glycerol	19.19	10.63	33.11	8.88	24.69	28.93

4.2.1.2 Simulation

To establish a photocatalytic hydrogen production simulation environment in Aspen plus, experimental conditions such as reactor and process parameters (temperature, pressure, volume, catalyst weight) specified by Chen et al. [173], [189] were used as input. The flowsheet was created based on these input conditions and kinetic data obtained, as detailed in Table 4.3. The flowsheet includes a batch reactor with an inlet stream containing water and sacrificial reagent and an outlet stream comprising hydrogen and carbon dioxide as the primary products (Figure 4.12).

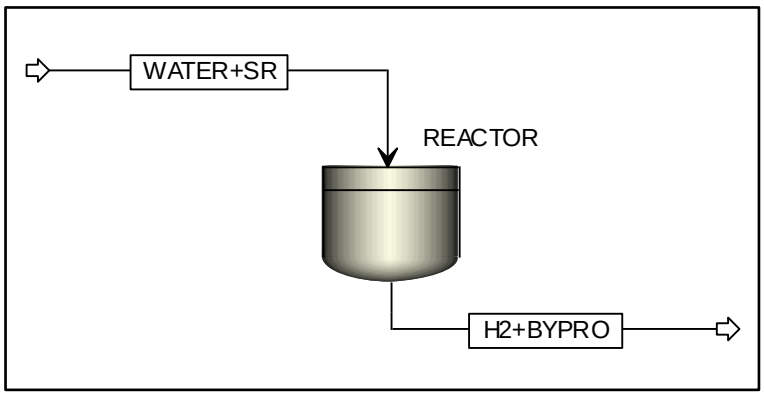

Figure 3.12: Aspen Plus flowsheet.

4.2.2 Model Validation

The simulation of photocatalytic hydrogen production was done, and the resulting data obtained were analysed. These data were validated against experimental results to ensure the accuracy of the model. The comparison between the simulated results from Aspen plus and the experimental data is illustrated in Figures 4.13 and 4.14. From these figures, it is evident that the Aspen Plus simulation results closely align with the experimental outcomes. This correspondence indicates that the input kinetic data have been accurately implemented in the model, and that the kinetic model used can reliably predict the behaviour of the photocatalytic reactions at lower concentrations. It also indicates that the assumptions and data used in the simulation are appropriate and valid. Overall, this validation confirms that the model and simulation setup are correctly established, capable of accurately reproducing known results, and effective in predicting outcomes under different conditions.

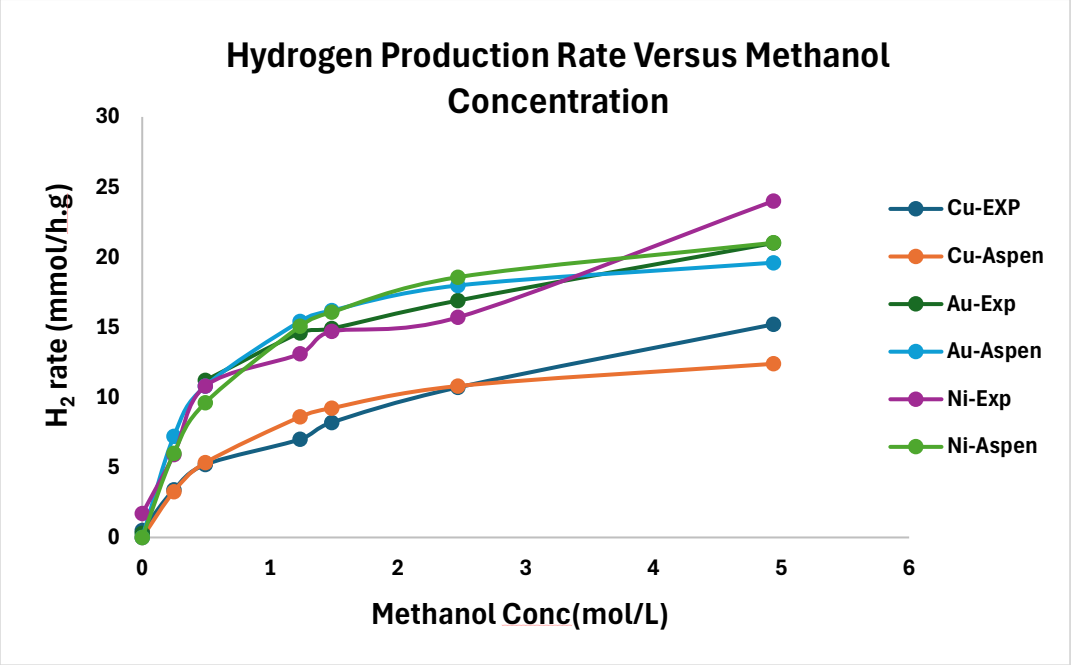

Figure 3.13: Comparison of experimental data with simulated results. [173], [189]

Figure 4.13 shows that the simulated results demonstrate different behaviour across the concentration range of methanol as a sacrificial reagent, depending on the catalyst used. At low methanol concentrations ([SR] <1), the rate of hydrogen production increased sharply for all catalyst systems, indicating a strong dependence on sacrificial reagent concentration. In contrast, at higher methanol concentrations ([SR] >1), the rate of hydrogen production remained relatively constant. This behaviour suggests a transition from first order kinetics, where the reaction rate is proportional to the concentration of methanol, to zero order kinetics, where the rate becomes independent of the sacrificial reagent concentration. This observation aligns with the findings reported by Gomathisankar et al. [184].

For Cu/TiO_2 and Ni/TiO_2 catalysts, minor deviations between simulated (Aspen) and experimental results (EXP) were noticed even at methanol concentrations below 2.5 mol/L. These deviations may have arisen from specific interactions between metals and the TiO_2 surface that were not fully captured by the Langmuir-Hinshelwood model. This variation became more pronounced at higher concentrations, where the experimental data showed a sharper increase in hydrogen production rate than the simulated results. In the case of Au/TiO_2 catalyst, the simulated and experimental results aligned well at lower concentrations, but deviations became apparent as the concentration exceeded 2.5 mol/L.

Across all catalysts systems, the most significant deviations between simulated and experimental results occurred at methanol concentrations above 2.5 mol/L. This observation is

consistent with findings reported by López et al. [187], who noted that the Langmuir-Hinshelwood model is typically most accurate within smaller concentrations ranges. The differences at higher concentrations may be due to additional factors such as catalyst surface saturation, competitive adsorption, or secondary reaction pathways, which are not accounted for in the model. Overall, the simulated results closely match with the experimental results at lower methanol concentrations indicating that a more comprehensive model may be necessary at higher concentration.

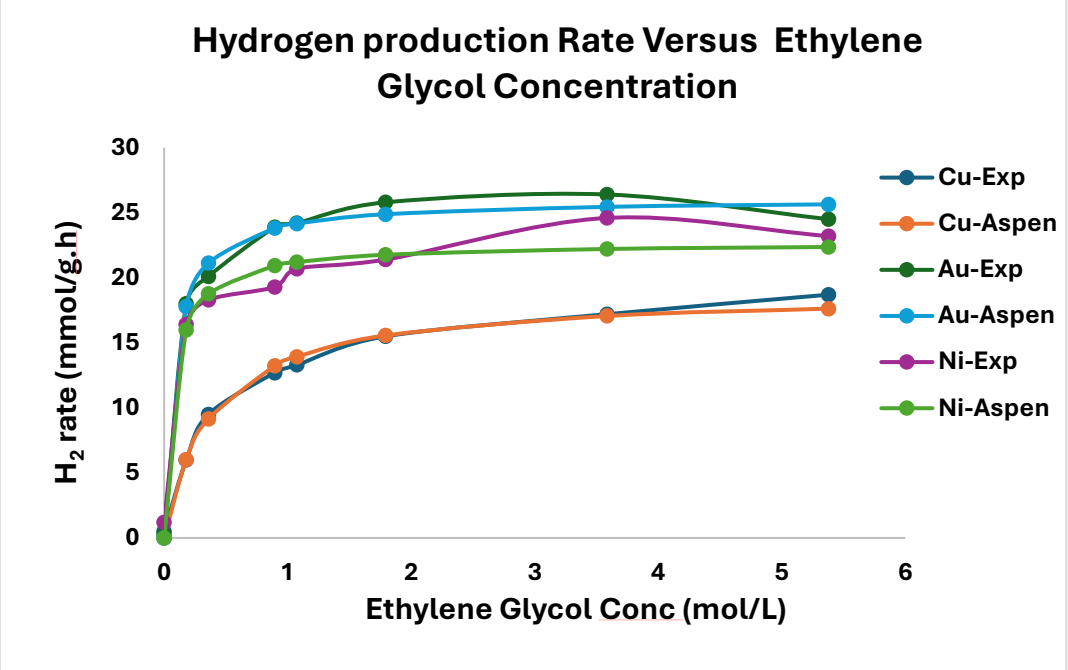

Figure 3.14: Comparison of simulated data and experimental results. [173], [189]

Figure 4.14 illustrates the hydrogen production rate for Cu-, Au- and Ni-loaded TiO_2 catalysts at varying ethylene glycol (EG) concentrations. The trends observed for each catalyst revealed different behaviours as the concentration of ethylene glycol changed. Similar to Figure 4.13, at lower concentrations, the hydrogen production rate increased for all three catalysts, indicating first order kinetics. As the concentration increased beyond 1 mol/L, the hydrogen production rate began to level off, eventually becoming relatively constant at higher concentrations. This plateau indicates a transition to zero order kinetics, where the reaction rate became independent of the ethylene glycol concentration. This suggests that at higher concentrations, the reaction rate becomes limited by other factors, such as catalyst surface saturation, rather than by the concentration of sacrificial reagent.

For the Cu/TiO_2 catalyst, the hydrogen production rate showed a moderate increase at lower ethylene glycol concentrations, but the rate began to plateau earlier compared to Au- and Ni

loaded TiO_2. This behaviour may be attributed to the specific surface activity of Cu and its interaction with the TiO_2 support, which limited further adsorption of ethylene glycol at higher concentrations. In contrast, Au and Ni loaded TiO_2 systems exhibited a relatively increased hydrogen production rate as the EG concentration increased.

The Cu/TiO_2 catalyst demonstrated excellent agreement between simulated and experimental results across the entire concentration range up to 4.5 mol/L, with minimal deviations observed even at higher concentrations. In contrast, for Au and Ni/TiO_2, the simulated results aligned well with experimental data at lower concentrations (<2 mol/L) but began to deviate slightly as the concentration increased. At higher concentrations (> 3 mol/L), the deviations became more pronounced, suggesting limitations in the kinetic model when describing the behaviour at elevated sacrificial reagent concentrations.

Overall, when comparing the simulated results with experimental data, it is clear that the Aspen Plus simulation accurately predicts the hydrogen production rate at lower sacrificial reagent concentration for Cu, Ni and Au/TiO_2 systems. This suggests that the model could be further refined to incorporate additional factors affecting the reaction at higher sacrificial reagent concentration. Despite these limitations, the simulation effectively predicts the key trends and behaviours of the photocatalytic hydrogen production process. Overall, the Aspen plus simulation was effectively implemented using the kinetic model, demonstrating its capability to predict photocatalytic hydrogen production rates at lower sacrificial reagent concentrations (0-5 mol/L, 0-30 Vol%). Consequently, the developed Aspen Plus simulation was further utilized to assess the effects of various process parameters.

4.2.3 Effect of Process Parameters on Photocatalytic Hydrogen Production

4.2.3.1 Effect of sacrificial reagent type on hydrogen production

This study considered four types of sacrificial reagents for photocatalytic hydrogen production. Figure 4.15 presents the hydrogen production rates obtained from Aspen Plus simulations based on the developed kinetic model. As shown in Figure 4.15, glycerol showed the highest hydrogen production rate for all metal-modified TiO_2 catalysts, followed by ethylene glycol, methanol, and ethanol. This result aligns with the literature findings and as discussed in Chapter 2, is likely due to glycerol's high number of alpha-H hydrogen atoms, which are readily liberated to form hydrogen molecules during the reaction. This observed trend at lower concentrations of sacrificial reagents is consistent across studies [190][191]. Additionally,

Chen et al. [189] attributed this trend to other properties of sacrificial reagents, such as the number of OH groups, polarity, and redox potential, which can significantly influence photocatalytic reactions. From Figure 4.15, it is clear that the type of sacrificial reagent plays a crucial role in determining the hydrogen production rate. Glycerol outperformed the other reagents across all catalyst systems, suggesting that its chemical structure and properties facilitate more efficient photocatalytic hydrogen production.

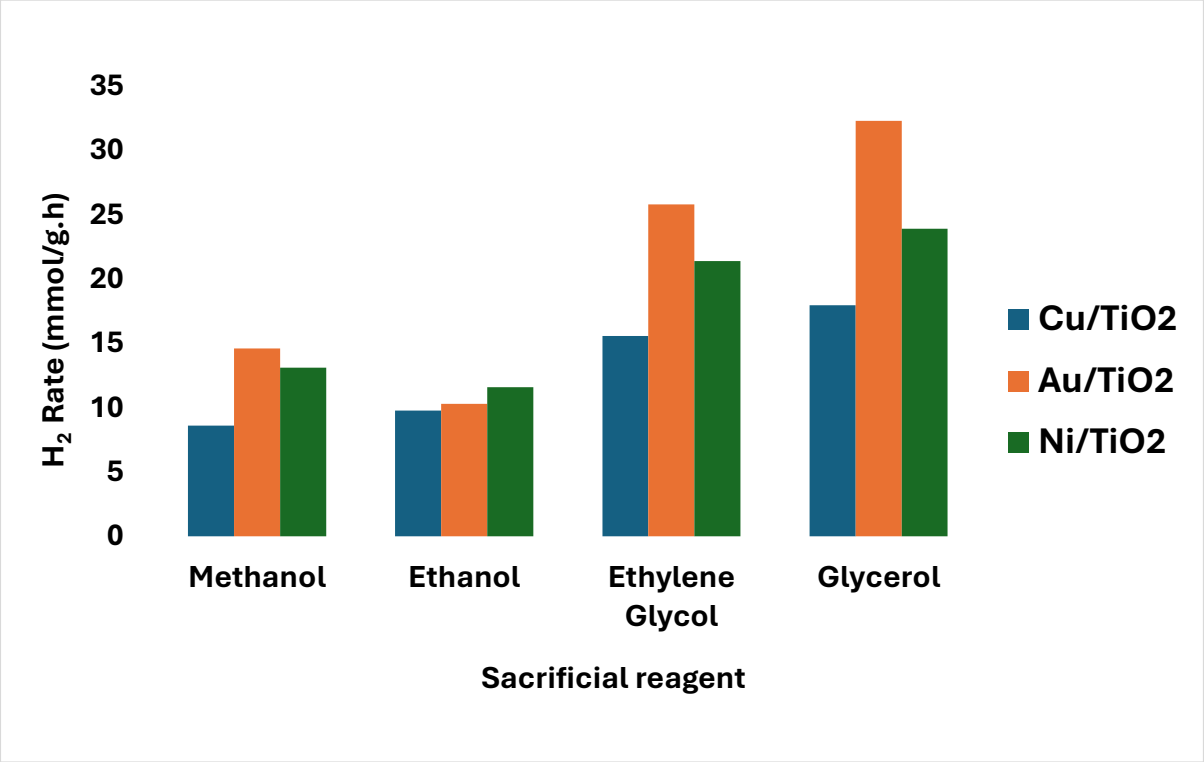

Figure 3.15: Effect of sacrificial reagent on hydrogen production rate for different catalysts.

Furthermore, the hydrogen production rate followed the catalyst order of Au/TiO_2>Ni/TiO_2> Cu/TiO_2. This result support our catalyst characterisation findings where the bandgap of Ni/TiO_2 was smaller than that of Cu/TiO_2, enabling Ni/TiO_2 to absorbs more light effectively and enhance hydrogen production. Interestingly, the hydrogen production rates for Cu- and Ni- modified TiO_2 are comparable to that of Au/TiO_2, suggesting that Ni and Cu/TiO_2 are effective photocatalysts and could serve as cost effective alternatives to more expensive metal-modified photocatalysts like Au- and Pt-TiO_2.

Despite these promising trends, the highest hydrogen production rate achieved with Ni/TiO_2 was 25 mmol/g.h when using glycerol as the sacrificial reagent, while the lowest was 12 mmol/g.h with ethanol. These values highlight that while the photocatalytic hydrogen production can be enhanced with the choice of sacrificial reagent and catalyst, the overall yield

remains relatively low. The production typically falls within the micromole to millimole range, which is consistent with values reported in the literature. This could be another possible reason why hydrogen production could not be quantified during the experimental work. This low yield is often attributed to challenges such as rapid electron-hole recombination, which can significantly limit the overall efficiency of the photocatalytic process. Moreover, even with the use of sacrificial reagents, the rate remains low, suggesting that additional factors such as optimizing the catalyst structure, improving light absorption, and reducing recombination losses should be explored to improve photocatalytic hydrogen production.

The prior studies by Chen et al. [173], [189] examined only the effects of the type and concentration of sacrificial reagents for different metal-loaded catalysts on hydrogen production rates, while keeping catalyst dosage and light intensity constant. However, photocatalytic hydrogen production is also influenced by additional factors, such as the catalyst dosage and light intensity. This motivated an analysis of these parameters' impact on hydrogen production rate, presented in section 4.2.3.2 and 4.2.3.3.

4.2.3.2 Effect of catalyst dosage on hydrogen production

The Aspen Plus model was further employed to examine the influence of catalyst dosage on hydrogen production rate. For this purpose, previously obtained kinetic data was used with empirical correlations from the literature. In the following Langmuir-Hinshelwood (L-H) kinetic model, K_{H_2} is an apparent kinetic constant that depends on the intrinsic constant k and catalyst dosage as shown in Equation 4.7 [192], [193].

$$\boldsymbol{K_{H_2} = k[Cat]^{\alpha}} \qquad \textit{Equation 4.7}$$

Here, $\propto$ is a constant (less than 1) to account for the undesirable effects of extensive catalyst dosage. The value of $\propto$ depends on the efficiency of electron-hole formation and recombination of photogenerated charges [192]. For this analysis, the value of $\propto$ was adopted from the work of Karimi Estahbanati et al. [193], who developed a kinetic model for liquid phase photocatalytic hydrogen production. In their study, $\propto$ was determined to be 0.4 for glycerol and this value was used as the basis for examining the effect of catalyst dosage on hydrogen production. Figure 4.16 illustrates the variation in hydrogen production rate with catalyst dosage, using glycerol as the sacrificial reagent, Cu/TiO_2 as the catalyst and a light intensity of 6.5 mW/cm^2.

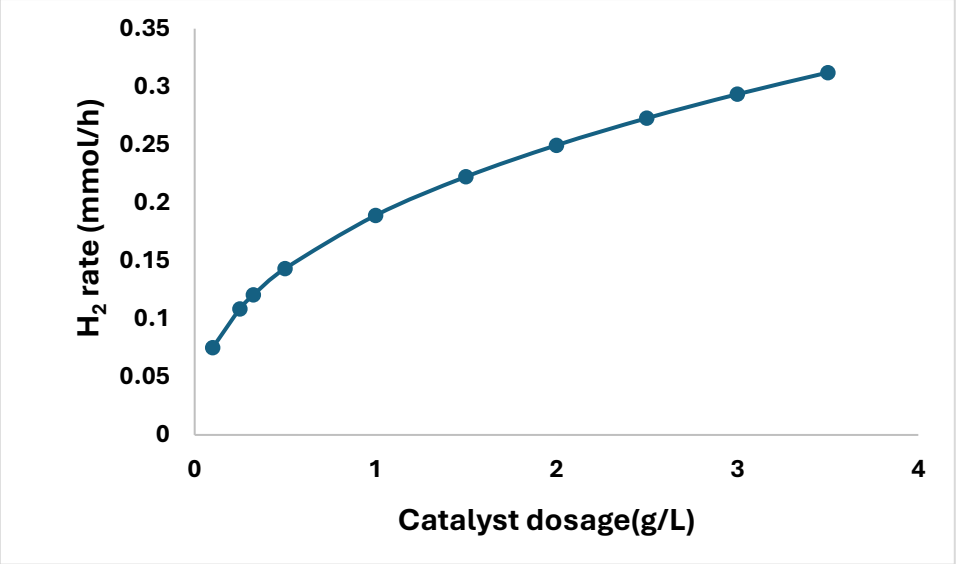

Figure 3.16: Rate of hydrogen production versus catalyst dosage.

From Figure 4.16, it can be seen that the hydrogen production rate increases with catalyst dosage but not linearly. Initially, the rate of hydrogen production increased sharply at lower catalyst dosage(g/L); however, as the dosage continued to increase, the rate of increment became more gradual. As shown in Figure 4.16, as catalyst dosage increases from 0.5 to 1.2 g/L the hydrogen production rate rises significantly, after which the rate increase slows. According to Zhou et al. [194], this relationship between hydrogen production rate and catalyst dosage can be divided into two regions. In the first region, the hydrogen production rate (mmol/h) is directly proportional to catalyst dosage, indicating a first-order reaction. The production rate reaches an equilibrium in the second region, increasing only slightly with additional catalysts, suggesting near zero-order kinetics.

Notably, the relative hydrogen production rate (mmol/h.g) decreased quickly with increased catalyst dosage and then gradually declined at higher catalyst dosage (Figure 4.17). This trend aligns with results reported by many researchers [193], [194], [195], [196], [197], [198]. This relationship may be explained by light absorption dynamics. At low catalyst dosage, all particles can absorb light without interference, resulting in an efficient rate increase. However, at higher dosages, the particles may shield one another, reducing light penetration. Excessive catalyst particles can also lead to particle aggregation, increased solution opacity, and light scattering , which limit light absorption and reduce photocatalytic activity [196]. This screening effect explains the observed reduction in hydrogen production rate per gram of catalyst (mmol/g.h) at high catalyst dosage.

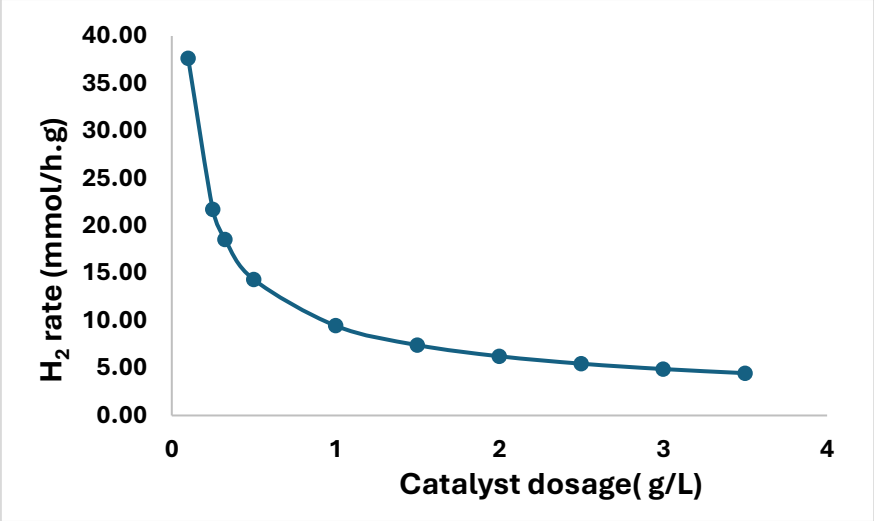

Figure 3.17: Relative rate of hydrogen production versus catalyst dosage.

4.2.3.3 Effect of light intensity on hydrogen production

Light intensity is another critical factor influencing photocatalytic activity. The effect of light intensity on hydrogen production rate was determined by incorporating kinetic data with empirical correlations in the Aspen plus model. This empirical corelation enabled the estimation of photocatalytic hydrogen production behaviour under varying light intensities and catalyst dosage. In the Langmuir-Hinshelwood kinetic model, K_{H_2} is an apparent kinetic constant dependent on the intrinsic rate constant k and light intensity, as shown in Equation 4.8 [199].

$$K_{H_2} = k[I]^{\gamma} \qquad \textit{Equation 4.8}$$

Here, γ is a constant (less than 1) to account for the diminishing effects at very high intensities. The value of γ reflects the rate of electron-hole pair generation [193]. The value of γ, equal to 0.265, was taken from work of Karimi et al. [193] and used as a baseline assumption to analyse the effect of light intensity on hydrogen production. To assess this effect, light intensity was varied between 5 to 50 mW/cm^2 while other parameters were kept constant (20 vol% Glycerol, 1 wt.% Cu/TiO_2, 0.325 g/L catalyst dosage).

Figure 4.18 presents the resulting hydrogen production rates, showing an inverse relationship compared to catalyst dosage and relative hydrogen production rates. At low light intensities, hydrogen production rate increased with light intensity as more photons are available to excite electrons and holes, initiating the photocatalytic reactions. However, at very high intensities, the rate reached a saturation point. This plateau likely resulted from increased electron-hole

recombination and limited photon absorption [193], [196]. According to Bloh [195], higher catalyst concentrations may be needed at higher light intensities to maintain efficiency and effectively absorb photons. However, it can be observed that as light intensity increased from 6 to 50 mW/cm^2, the relative hydrogen production rate increased from 20 to 30 mmol/h.g. This indicates that light intensity is a key parameter that can be optimized to enhance photocatalytic hydrogen production.

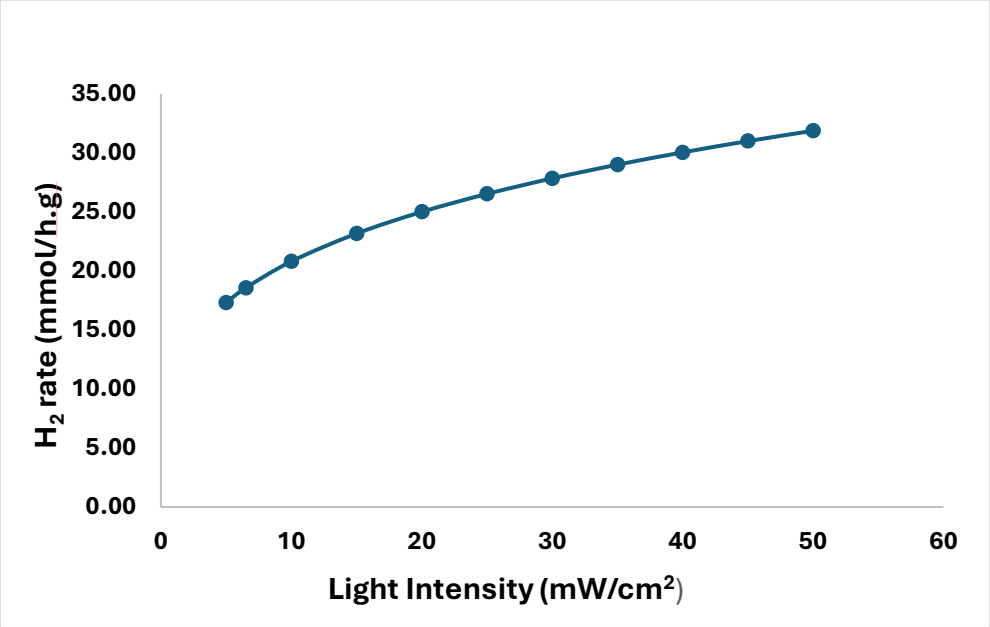

Figure 3.18: Relative rate of hydrogen production versus light intensity.

Overall, these findings indicate that factors such as the type and properties of the catalyst, the concentration and type of sacrificial reagents, catalyst dosage, and light intensity significantly influence hydrogen production rates. Optimizing these factors is essential for enhancing the efficiency of photocatalytic hydrogen production.

4.2.4 Limitations of the Aspen simulation model

The Aspen Plus simulation of photocatalytic hydrogen production was developed using the Langmuir-Hinshelwood (L-H) kinetic model based on experimental data available in the literature. This simulation serves as a foundation for analysing the effects of various parameters on the process, while there is a notable agreement between the simulated values and experimental data, confirming the model's ability to simulate the photocatalytic hydrogen production process, it is important to note that no such study has been reported in open literature. Due to the lack of experimental data and no prior studies in literature specifically

focusing on Aspen plus simulation of this process, the kinetic model relies on some assumptions. However, the simulation has limitations such as :

1. Simplistic kinetic Model: The Langmuir-Hinshelwood (L-H) model, while useful, is relatively simplistic and may not fully capture the complexities of photocatalytic reactions or the associated reaction pathways. As a result, it does not account for the formation of reaction intermediates. To address these limitations, more precise or user-defined kinetic models are needed to accurately represent the detailed chemistry of photocatalytic hydrogen production.
2. Variability in kinetic Parameters: The kinetic parameters derived from experimental data often vary due to differences in experimental conditions. These variations cause deviations in the model, highlighting the need for careful parameter estimation and standardization of experimental setups.
3. Concentration limitations: The L-H model is most effective at moderate reactant concentrations, but its accuracy diminishes at very high concentrations of sacrificial reagent, where additional factors such as surface saturation or secondary reaction pathways may become significant.
4. Stability and deactivation: The model does not account for the stability and potential deactivation of the photocatalyst over time, which could impact hydrogen production efficiency.

4.3 Techno-economic analysis photocatalytic hydrogen production

Techno-economic analysis (TEA) evaluates the technical and economic aspects of a process to assess its feasibility, competitiveness, and potential impact. Economic feasibility is a critical factor in the acceptance of new technologies [200]. Various researchers have conducted techno-economic analyses of the photocatalytic hydrogen production process. For instance, Pinaud et al. [201] found that using four different reactor types the cost of hydrogen from photocatalytic hydrogen production process varied between \$1.6-10.4 per Kg H_2. In another study, a Monte Carlo-based analysis revealed that the Levelized cost of Hydrogen (LCOH) for the base case scenario was \$100/Kg H_2, and the authors suggested that the solar-to-hydrogen (STH) efficiency must reach at least 6% to lower production cost significantly [202]. Both studies employed plastic bag reactors to assess the economic viability. Conversely, Maurya et al. [200] evaluated the economic potential of photocatalytic panel-based reactors and reported that LCOH ranges from \$4.9-7.8/Kg H_2. Meanwhile, Kuspanov et al.[203] emphasized that

suspension or slurry photoreactors hold advantages due to their simplicity and cost-effectiveness compared to panel (immobilized photocatalytic panels) systems. Toe et al. [204] concluded that the design of photocatalytic slurry systems is approximately 12% more cost-effective than panel photoreactor systems when producing 10 kg H_2 under base case conditions. The variations in predicted hydrogen cost across these studies can be attributed to differences in photocatalyst used, their efficiencies, reactor types, and the assumptions used to develop the TEA models.

4.3.1 Goal and Scope definition

This preliminary techno-economic analysis of photocatalytic hydrogen production aims to assess the economic feasibility of the process and identify areas for development, as well as the technological advancements required to achieve cost competitiveness. The analysis included stages such as feedstock supply, energy input, and hydrogen production. However, it does not include product separation, storage, or the transportation of hydrogen to distribution and end-use sites. Consequently, the current model focuses exclusively on the cost of production of photocatalytic hydrogen, excluding expenses related to downstream processes. This analysis is based on results from a pilot scale photocatalytic reactor (25 L), which represents a small-scale installation with a reported production capacity of 5.4 mmols/day .

4.3.2 Process Description

Photocatalytic hydrogen production consists of several key stages: catalyst synthesis, hydrogen generation using the catalyst, water and a sacrificial reagent, and product separation. To simplify the analysis, the catalyst synthesis units are excluded from the process design, and the cost of the modified catalyst is obtained from literature [204]. In the hydrogen generation stage, the photocatalyst is mixed with water and the sacrificial reagent in a mixing tank to form a homogenous mixture. The solution is then purged with nitrogen gas to remove oxygen and pumped into a photoreactor powered by natural sunlight. A block flow diagram illustrating the high-level description of the photocatalytic hydrogen production system is provided in Figure 4.19.

Laboratory scale reactors, such as batch reactor used in this study, are not suitable for large scale hydrogen production, as they are primarily designed for evaluating the photocatalyst. Therefore, more effective reactors are needed to achieve high photocatalytic efficiencies. Currently, there are no commercial-scale plants for photocatalytic hydrogen production, but researchers have developed various prototypes, including suspension/slurry and panel-type

photoreactors [204]. Various pilot programs have utilized parabolic photocatalytic concentrator (CPC) reactor, which optimize sunlight utilization by redirecting both direct and scattered rays into the reactor [203]. Detailed information about this reactor design can be found in the referenced literature [203], [204]. A schematic diagram of the CPC photoreactor is presented in Figure 4.20. Although, the design of the photoreactor is beyond the scope of this analysis; the cost estimation is based on the design parameters and cost data available in the literature.

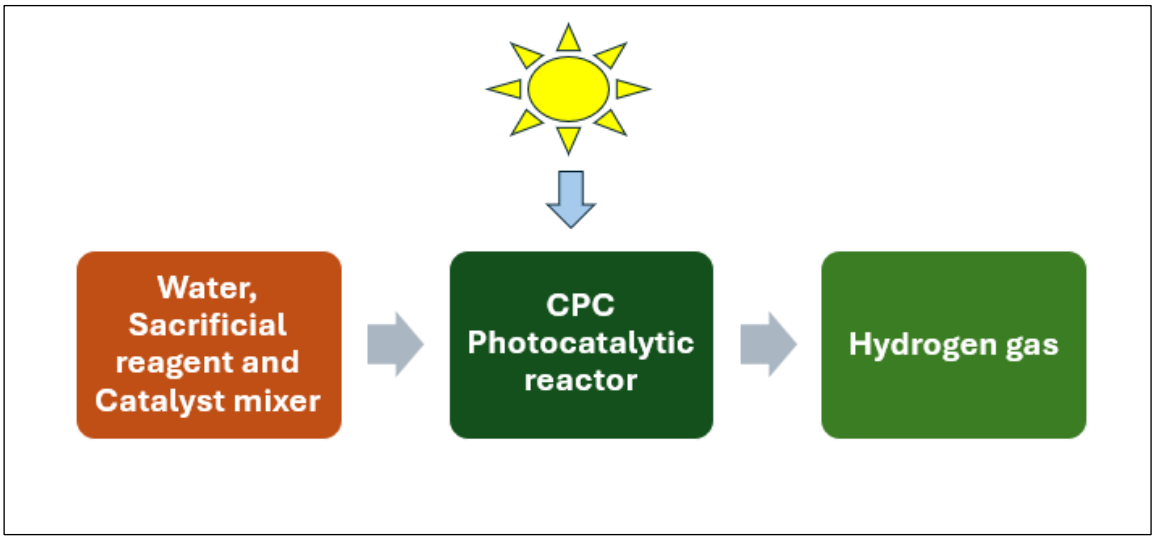

Figure 3.19: Block flow diagram illustrating the photocatalytic hydrogen production system.

4.3.3 Cost Analysis

This section presents a basic cost analysis of photocatalytic hydrogen production process, using data from the work done by Ruiz-Aguirre et al. [205], who conducted a pilot-plant scale assessment of solar photocatalytic hydrogen production using a CuO-TiO_2 photocatalyst, a CPC photoreactor, and glycerol as a sacrificial reagent. The pilot plant consisted of a 27 L tank connected to a 25 L CPC reactor with a surface area of 2 m^2. Nitrogen was used to displace oxygen and function as a carrier gas. The results indicated that hydrogen production, using 25 L of water, 0.075M glycerol, and 100 mg/L of CuO-TiO_2, yielded 90 mmol of hydrogen over a 10-hour illumination period (5 hours per day over 2 days), achieving a solar-to-hydrogen efficiency (STH) of 0.9%. The analysis hence estimates the cost per kg of hydrogen based on this small-scale setup that achieved STH efficiency of 0.9%. The analysis estimates the cost per kilogram of hydrogen based on the performance of this small-scale setup.

For the techno-economic analysis, a method described by Genç et al.[206] was applied. This approach involved evaluating both fixed and operating costs to estimate the cost per unit of hydrogen. The fixed cost or fixed capital investment (FCI) was determined by adding up the direct costs such as the purchased equipment (PE) cost, PE installation, instrumentation and controls, and land costs. Indirect costs and working capital were not included in this analysis, as it is based on a small-scale plant installation rather than a full industrial-scale plant.

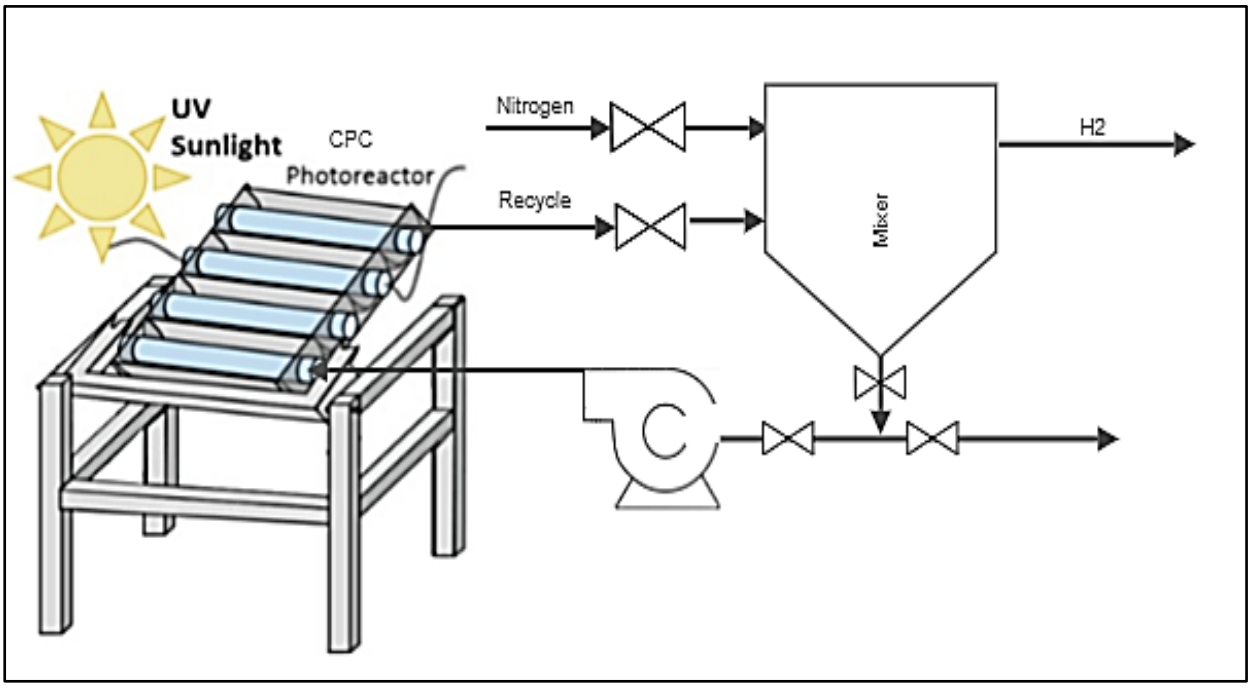

Figure 3.20: A flowsheet of photocatalytic hydrogen generation pilot plant [207], [208].

The cost of major equipment, such as the photoreactor, was obtained from [204], and the Chemical Engineering Plant Cost Index (CEPCI) of 2022 and 2024 were used to update these costs. The annual capital cost was then calculated by dividing the FCI by the assumed plant lifetime of 10 years. The setup for the photocatalytic hydrogen production reactor, including all components, is assumed to occupy 50 m^2 of land, with the land cost estimated based on the current land prices in South Africa.

The operating costs included various components such as the costs of chemicals including the photocatalyst (CuO/TiO_2), water, nitrogen (N_2) for purging and glycerol (sacrificial reagent), as well as the power cost required for operating the mixer and pump. Additionally, maintenance cost was considered, which included the expenses to keep the plant running, including labour, materials, and supervision. It was assumed that the catalyst is replaced

annually as a photocatalyst lifespan of at least one year is essential for practical application [204]. A detailed breakdown of the specific costs per component is outlined in Table 4.4.

To estimate the specific hydrogen cost, the annual capital cost and operating costs were divided by the hydrogen produced per hour and the total annual operating time of the plant. In the pilot plant, the hydrogen production rate was 9 mmols/hour. Given that the plant only operates during daylight hours, and with South Africa receiving an average of 2500 hours of sunlight per year, the annual operating time of the plant was estimated to be 2500 hours. The results of preliminary cost analysis are presented in Table 4.4.

Table 3.4: Cost breakdown of photocatalytic hydrogen production.

Component	Cost per unit(R)	Unit	Total cost (R)
Capital cost			**16565**
Annual capital cost (R/year)			**1656**
Total equipment cost			**5200**
Mixer	R2000/unit	1	2000
Photoreactor			2700
Tubes	R750/m^2	2.1 m^2	1575
Support frame	R560/m^2	2.1 m^2	1176
Pump	R500/unit	1	500
Control system and construction, installation	R650/m^2	2.1 m^2	**1365**
Land			**10000**
Operating cost (R/year)			**2271**
Cost of materials			1212
Photocatalyst	R2400/kg	0.0025 kg/year	6
Water	R20/L	25 L/year	500
Glycerol	R2000/L	0.137 L/year	274
Nitrogen for purging	R1/L	432 L/year	432
Power cost	R3.2 /kWh	300 kWh/year	960
Maintenance	R1656/yr	6% of annual capital cost	99
Total Cost (R/year) = Capital cost + Operating cost			**3928**
Specific hydrogen cost = Total cost/ (amount of H_2 per day *annual operating time)			**872849**

The specific cost of hydrogen, as calculated and shown in Table 4.4, is R872, 849.00 per kg of hydrogen based on the pilot plant specifications and a hydrogen production rate of 0.9 mmol/h. The calculated cost per kilogram of hydrogen is significantly high, primarily due to the very low solar-to-hydrogen (STH) efficiency (less than 1%) and the small production volumes associated with this scale. The limited amount of hydrogen produced per volume of water results in a disproportionately high cost per unit of hydrogen, as significant capital and operational costs are incurred relative to the minimal hydrogen output. This highlights the economic challenges of photocatalytic hydrogen production, especially considering the current STH efficiency of around 1%. The high costs are due to the inefficiencies of the process at this

scale, where the low hydrogen production rate makes it hard to achieve a reasonable cost per kilogram of hydrogen.

To assess the economic feasibility of the process, the Gross Economic Potential (GEP) (R/year) was calculated by determining the difference between the value of the products (hydrogen) and the value of the feeds (water, catalyst, glycerol). The GEP value was found to be negative, primarily due to the extremely low hydrogen productivity. This indicates that the process is not economically feasible due to high costs and very low yields. However, it is important to note that it is a preliminary cost analysis based on the data from a plot plant.

A key finding is that the process can only become economically viable if its efficiency exceeds 10%. Therefore, continued research for better catalysts is essential. To significantly reduce hydrogen production costs, improving solar-to-hydrogen (STH) efficiency and optimizing reactor design and operational parameters will be crucial. Further research should focus on scaling up hydrogen production and enhancing STH efficiency to improve the economic viability of photocatalytic hydrogen production.

CHAPTER 5
CONCLUSIONS AND RECOMMENDATIONS

This study explored the potential of photocatalytic hydrogen production using metal-modified TiO_2 catalysts. The metal-modified catalysts were synthesized using the incipient wetness impregnation method, with Cu, Ni, and Cu-Ni metals loaded onto TiO_2. Characterization techniques, including XRD, SEM, EDS, and UV-DRS, confirmed successful metal loading on the TiO_2 surface, with CuO, NiO, and CuO-NiO forming as the metal phases. The metal modification of TiO_2 reduced its band gap from 3.12 eV to 3.08eV and 3.05 eV when modified with 1 wt.% Cu and 1 wt.% Ni, respectively. The bimetallic catalysts exhibited even a lower bandgap (3.00 eV) compared to the monometallic catalysts. Furthermore, the band gap decreased steadily with increasing metal concentration, dropping from 3.08 eV to 2.87 eV.

Photocatalytic hydrogen production was assessed under varying conditions using two different photoreactors. The Type II photoreactor demonstrated better efficiency when compared to the Type I reactor, primarily due to improved light distribution and proximity. During the experiments, pure TiO_2 and the metal-loaded TiO_2 catalysts exhibited colour changes upon UV irradiation in the presence of sacrificial reagents, indicating the occurrence of photocatalytic reactions such as electron-hole generation and alcohol oxidation. However, hydrogen production could not be detected, likely due to the recombination of photogenerated charges or hydrogen levels being too low for detection.

An Aspen Plus model was developed using Langmuir-Hinshelwood kinetics to simulate the hydrogen production process. The model showed good agreement with experimental data, validating the use of the Langmuir-Hinshelwood model for predicting the behaviour of photocatalytic reactions at lower concentrations. The model also allowed for the investigation of process parameters, showing that the rate of hydrogen production followed first-order kinetics at lower sacrificial reagent concentrations and zero-order kinetics at higher concentrations. It was also found that the performance of the sacrificial reagent with respect to the hydrogen production was in this order: glycerol > ethylene glycol > methanol > ethanol. From the two catalysts Cu/TiO_2 and Ni/TiO_2, Ni/TiO_2 showed the highest hydrogen production rate, which aligned with the characterization results. Additionally, increasing catalyst dosage reduced the relative rate of hydrogen production due to screening effects at higher loadings,

while increasing light intensity initially boosted the production rate, but eventually reaching a saturation point due to limited photon absorption.

A preliminary techno-economic revealed that the photocatalytic hydrogen process using Cu/TiO_2 is currently not economically feasible due to high production costs and extremely low hydrogen yields, with a solar-to-hydrogen efficiency of less than 1%. These inefficiencies result in excessively high costs and a negative Gross Economic Potential (GEP), highlighting the challenges in scaling up the process.

The research indicates that bimetallic-modified TiO_2 catalyst has a reduced bandgap compared to both monometallic modified TiO_2 and unmodified TiO_2. Therefore, further research should focus on improving the properties of this catalyst to enhance its photocatalytic activity and stability. A detailed study of metal support interactions is essential to enhance charge separation and transfer. Additionally, investigating different nanoparticle shapes of TiO_2 could optimize its surface area and further improve photocatalytic performance.

The study also found that the Type II photoreactor exhibited better efficiency than the Type I reactor. Future research should focus on optimizing reactor designs to achieve more uniform light distribution and improved catalyst substrate interaction. Additionally, the experimental work highlighted challenges in detecting photocatalytic hydrogen, suggesting a need for more sensitive equipment for hydrogen detection. Furthermore, the study observed that glycerol was the most effective sacrificial reagent for hydrogen production. Investigating the use of renewable glycerol and exploring strategies for its recycling could enhance sustainability and reduce operating costs.

In conclusion, to improve the economic feasibility of the process, significant advancements are required in catalyst performance, photoreactor design, and solar-to-hydrogen (STH) efficiency. While photocatalytic hydrogen production shows promise as a sustainable technology, further research and developments are essential to enhance its efficiency and make it commercially viable.

REFERENCES

[1] A. Pareek, R. Dom, J. Gupta, J. Chandran, V. Adepu, and P. H. Borse, “Insights into renewable hydrogen energy: Recent advances and prospects,” *Mater Sci Energy Technol*, vol. 3, pp. 319–327, Jan. 2020, doi: 10.1016/j.mset.2019.12.002.

[2] I. Dincer and C. Acar, “Review and evaluation of hydrogen production methods for better sustainability,” *Int J Hydrogen Energy*, vol. 40, no. 34, pp. 11094–11111, Aug. 2014, doi: 10.1016/j.ijhydene.2014.12.035.

[3] O. M. Akinbami, S. R. Oke, and M. O. Bodunrin, “The state of renewable energy development in South Africa: An overview,” *Alexandria Engineering Journal*, vol. 60, no. 6, pp. 5077–5093, Dec. 2021, doi: 10.1016/j.aej.2021.03.065.

[4] C. H. Liao, C. W. Huang, and J. C. S. Wu, “Hydrogen production from semiconductor-based photocatalysis via water splitting,” Oct. 17, 2012, *Multidisciplinary Digital Publishing Institute (MDPI)*. doi: 10.3390/catal2040490.

[5] X. Liu, S. Gu, Y. Zhao, G. Zhou, and W. Li, “BiVO4, Bi2WO6 and Bi2MoO6 photocatalysis: A brief review,” Nov. 01, 2020, *Chinese Society of Metals*. doi: 10.1016/j.jmst.2020.04.023.

[6] Y. Dai *et al.*, “Fabrication of a novel double Z-scheme WO3/Cd0.97Zn0.03S/CoSx photocatalyst for facilitating photocatalytic hydrogen production,” *Mater Lett*, vol. 338, May 2023, doi: 10.1016/j.matlet.2023.134072.

[7] L. Zhang *et al.*, “A comprehensive review of the promising clean energy carrier: Hydrogen production, transportation, storage, and utilization (HPTSU) technologies,” *Fuel*, vol. 355, Jan. 2024, doi: 10.1016/j.fuel.2023.129455.

[8] P. J. Megia, A. J. Vizcaino, J. A. Calles, and A. Carrero, “Hydrogen Production Technologies: From Fossil Fuels toward Renewable Sources. A Mini Review,” Oct. 21, 2021, *American Chemical Society*. doi: 10.1021/acs.energyfuels.1c02501.

[9] H. Eidsvåg, S. Bentouba, P. Vajeeston, S. Yohi, and D. Velauthapillai, “TiO2 as a Photocatalyst for Water Splitting—An Experimental and Theoretical Review,” *Molecules*, vol. 26, no. 6, p. 1687, Mar. 2021, doi: 10.3390/molecules26061687.

[10] D. ’Fitzgerald, M. ’Le Roux, B. ’Bekker, W. ’Pierce, S. ’Morison, and L. ’Snyman, “Visualisation of South African Energy Data,” Oct. 2024, *Centre for renewable & sustainable energy studies*.

[11] V. Kumaravel *et al.*, “Photocatalytic hydrogen production: Role of sacrificial reagents on the activity of oxide, carbon, and sulfide catalysts,” *Catalysts*, vol. 9, no. 3, Mar. 2019, doi: 10.3390/catal9030276.

[12] Giorgio Simbolotti and Giancarlo Tosato, “Hydrogen Production & Distribution,” 2014.

[13] N. Ain, A. M. Amin, H. Fatimah, and M. Zaid, “A Review of Photocatalytic Water Splitting for Hydrogen Production Using Tandem Solar Cell,” 2023, doi: 10.20944/preprints202309.2044.v1.

[14] E. Nurlaela, F. K. Chong, B. K. Dutta, and N. Riaz, “Bimetallic Cu-Ni/TiO 2 as photocatalyst for hydrogen production from water.”

[15] M. Saleh, H. N. Abdelhamid, D. M. Fouad, and H. M. El-Bery, “Enhancing photocatalytic water splitting: Comparative study of TiO2 decorated nanocrystals (Pt and Cu) using different synthesis methods,” *Fuel*, vol. 354, Dec. 2023, doi: 10.1016/j.fuel.2023.129248.

[16] S. Pokrant, S. Dilger, S. Landsmann, and M. Trottmann, “Size effects of cocatalysts in photoelectrochemical and photocatalytic water splitting,” *Mater Today Energy*, vol. 5, pp. 158–163, Sep. 2017, doi: 10.1016/j.mtener.2017.06.005.

[17] M. Ji and J. Wang, “Review and comparison of various hydrogen production methods based on costs and life cycle impact assessment indicators,” Nov. 11, 2021, *Elsevier Ltd*. doi: 10.1016/j.ijhydene.2021.09.142.

[18] M. Amin *et al.*, “Hydrogen production through renewable and non-renewable energy processes and their impact on climate change,” Sep. 08, 2022, *Elsevier Ltd*. doi: 10.1016/j.ijhydene.2022.07.172.

[19] Z. Saddique *et al.*, “Bismuth-based nanomaterials-assisted photocatalytic water splitting for sustainable hydrogen production,” *Int J Hydrogen Energy*, vol. 52, pp. 594–611, Jan. 2024, doi: 10.1016/j.ijhydene.2023.05.047.

[20] A. Albahnasawi and M. Eyvaz, “Introductory Chapter: Hydrogen Energy,” in *Clean Energy Technologies - Hydrogen and Gasification Processes*, IntechOpen, 2022. doi: 10.5772/intechopen.108635.

[21] M. S. Herdem *et al.*, “A brief overview of solar and wind-based green hydrogen production systems: Trends and standardization,” *Int J Hydrogen Energy*, vol. 51, pp. 340–353, Jan. 2024, doi: 10.1016/j.ijhydene.2023.05.172.

[22] N. Fajrina and M. Tahir, “A critical review in strategies to improve photocatalytic water splitting towards hydrogen production,” Jan. 08, 2019, *Elsevier Ltd*. doi: 10.1016/j.ijhydene.2018.10.200.

[23] P. Shandilya, R. Sharma, R. K. Arya, A. Kumar, D.-V. N. Vo, and G. Sharma, “Recent progress and challenges in photocatalytic water splitting using layered double hydroxides (LDH) based nanocomposites,” *Int J Hydrogen Energy*, vol. 47, no. 88, pp. 37438–37475, Oct. 2022, doi: 10.1016/j.ijhydene.2021.08.190.

[24] H. Ahmad, S. K. Kamarudin, L. J. Minggu, and M. Kassim, “Hydrogen from photo-catalytic water splitting process: A review,” *Renewable and Sustainable Energy Reviews*, vol. 43, pp. 599–610, Mar. 2015, doi: 10.1016/j.rser.2014.10.101.

[25] S. N. A. Sulaiman, M. Zaky Noh, N. Nadia Adnan, N. Bidin, and S. N. Ab Razak, “Effects of photocatalytic activity of metal and non-metal doped Tio $_2$ for Hydrogen production enhancement - A Review,” *J Phys Conf Ser*, vol. 1027, p. 012006, May 2018, doi: 10.1088/1742-6596/1027/1/012006.

[26] C. H. Liao, C. W. Huang, and J. C. S. Wu, “Hydrogen production from semiconductor-based photocatalysis via water splitting,” Oct. 17, 2012, *MDPI AG*. doi: 10.3390/catal2040490.

[27] M. Yu *et al.*, “Highly efficient visible-light photocatalytic hydrogen production using ZIF-derived Co9S8/N, S-CNTs-ZnIn2S4 composite,” *Chem Phys Lett*, vol. 821, p. 140470, Jun. 2023, doi: 10.1016/j.cplett.2023.140470.

[28] P. J. Megia, A. J. Vizcaino, J. A. Calles, and A. Carrero, “Hydrogen Production Technologies: From Fossil Fuels toward Renewable Sources. A Mini Review,” Oct. 21, 2021, *American Chemical Society*. doi: 10.1021/acs.energyfuels.1c02501.

[29] B. Rusinque, S. Escobedo, and H. de Lasa, “Hydrogen production via pd-TiO2 photocatalytic water splitting under near-uv and visible light: Analysis of the reaction mechanism,” *Catalysts*, vol. 11, no. 3, Mar. 2021, doi: 10.3390/catal11030405.

[30] C. H. Liao, C. W. Huang, and J. C. S. Wu, “Hydrogen production from semiconductor-based photocatalysis via water splitting,” Oct. 17, 2012, *Multidisciplinary Digital Publishing Institute (MDPI)*. doi: 10.3390/catal2040490.

[31] M. Amin *et al.*, “Hydrogen production through renewable and non-renewable energy processes and their impact on climate change,” Sep. 08, 2022, *Elsevier Ltd*. doi: 10.1016/j.ijhydene.2022.07.172.

[32] L. Zhang *et al.*, “A comprehensive review of the promising clean energy carrier: Hydrogen production, transportation, storage, and utilization (HPTSU) technologies,” *Fuel*, vol. 355, Jan. 2024, doi: 10.1016/j.fuel.2023.129455.

[33] P. Nikolaidis and A. Poullikkas, “A comparative overview of hydrogen production processes,” Jan. 01, 2017, *Elsevier Ltd*. doi: 10.1016/j.rser.2016.09.044.

[34] L. M. Gandía, G. Arzamendi, and P. M. Diéguez, “Renewable Hydrogen Energy: An Overview,” in *Renewable Hydrogen Technologies: Production, Purification, Storage, Applications and Safety*, Elsevier B.V., 2013, pp. 1–17. doi: 10.1016/B978-0-444-56352-1.00001-5.

[35] C. Acar and I. Dincer, “Comparative assessment of hydrogen production methods from renewable and non-renewable sources,” Jan. 02, 2014. doi: 10.1016/j.ijhydene.2013.10.060.

[36] A. Pareek, R. Dom, J. Gupta, J. Chandran, V. Adepu, and P. H. Borse, “Insights into renewable hydrogen energy: Recent advances and prospects,” *Mater Sci Energy Technol*, vol. 3, pp. 319–327, Jan. 2020, doi: 10.1016/j.mset.2019.12.002.

[37] M. Ji and J. Wang, “Review and comparison of various hydrogen production methods based on costs and life cycle impact assessment indicators,” Nov. 11, 2021, *Elsevier Ltd*. doi: 10.1016/j.ijhydene.2021.09.142.

[38] I. Dincer and C. Acar, “Review and evaluation of hydrogen production methods for better sustainability,” *Int J Hydrogen Energy*, vol. 40, no. 34, pp. 11094–11111, Aug. 2014, doi: 10.1016/j.ijhydene.2014.12.035.

[39] S. Z. Baykara, “Hydrogen production by direct solar thermal decomposition of water, possibilities for improvement of process efficiency,” *Int J Hydrogen Energy*, vol. 29, no. 14, pp. 1451–1458, Nov. 2004, doi: 10.1016/j.ijhydene.2004.02.014.

[40] S.-E. Lindquist and C. Fell, “FUELS – HYDROGEN PRODUCTION | Photoelectrolysis,” in *Encyclopedia of Electrochemical Power Sources*, Elsevier, 2009, pp. 369–383. doi: 10.1016/B978-044452745-5.00319-1.

[41] Z. Saddique *et al.*, “Bismuth-based nanomaterials-assisted photocatalytic water splitting for sustainable hydrogen production,” *Int J Hydrogen Energy*, vol. 52, pp. 594–611, Jan. 2024, doi: 10.1016/j.ijhydene.2023.05.047.

[42] A. Pareek, R. Dom, J. Gupta, J. Chandran, V. Adepu, and P. H. Borse, “Insights into renewable hydrogen energy: Recent advances and prospects,” *Mater Sci Energy Technol*, vol. 3, pp. 319–327, Jan. 2020, doi: 10.1016/j.mset.2019.12.002.

[43] R. Ameta, M. S. Solanki, S. Benjamin, and S. C. Ameta, “Photocatalysis,” in *Advanced Oxidation Processes for Waste Water Treatment*, Elsevier, 2018, pp. 135–175. doi: 10.1016/B978-0-12-810499-6.00006-1.

[44] L. M. Gandía, G. Arzamendi, and P. M. Diéguez, “Renewable Hydrogen Energy: An Overview,” in *Renewable Hydrogen Technologies: Production, Purification, Storage, Applications and Safety*, Elsevier B.V., 2013, pp. 1–17. doi: 10.1016/B978-0-444-56352-1.00001-5.

[45] N. Fajrina and M. Tahir, “A critical review in strategies to improve photocatalytic water splitting towards hydrogen production,” Jan. 08, 2019, *Elsevier Ltd*. doi: 10.1016/j.ijhydene.2018.10.200.

[46] K. Qanugo, D. Bose, and K. K. Thakur, “A Review on Photocatalytic Water Splitting”, doi: 10.1051/e3sconf/202130.

[47] H. Eidsvåg, S. Bentouba, P. Vajeeston, S. Yohi, and D. Velauthapillai, “Tio2 as a photocatalyst for water splitting—an experimental and theoretical review,” 2021, *MDPI AG*. doi: 10.3390/molecules26061687.

[48] C. H. Liao, C. W. Huang, and J. C. S. Wu, “Hydrogen production from semiconductor-based photocatalysis via water splitting,” Oct. 17, 2012, *Multidisciplinary Digital Publishing Institute (MDPI)*. doi: 10.3390/catal2040490.

[49] M. Archer, “Solar energy conversion: a photoelectrochemical approach,” *J Photochem Photobiol A Chem*, vol. 60, no. 1, pp. 129–130, Aug. 1991, doi: 10.1016/1010-6030(91)90012-I.

[50] R. Li and C. Li, “Scalable solar water splitting using particulate photocatalysts,” Feb. 01, 2022, *Elsevier B.V.* doi: 10.1016/j.cogsc.2021.100577.

[51] V. Kumaravel *et al.*, “Photocatalytic hydrogen production: Role of sacrificial reagents on the activity of oxide, carbon, and sulfide catalysts,” *Catalysts*, vol. 9, no. 3, Mar. 2019, doi: 10.3390/catal9030276.

[52] H. Ahmad, S. K. Kamarudin, L. J. Minggu, and M. Kassim, “Hydrogen from photo-catalytic water splitting process: A review,” 2015, *Elsevier Ltd*. doi: 10.1016/j.rser.2014.10.101.

[53] D. Jiang, H. Zhao, Z. Jia, J. Cao, and R. John, “Photoelectrochemical behaviour of methanol oxidation at nanoporous TiO2 film electrodes,” *J Photochem Photobiol A Chem*, vol. 144, no. 2–3, pp. 197–204, Nov. 2001, doi: 10.1016/S1010-6030(01)00527-5.

[54] A. Sudhir, K. Sinha, U. Ojha, Z. Alam, and A. A. Tripathi, “Production of Hydrogen via Water Splitting Using Photocatalytic and Photoelectrocatalytic Route.” [Online]. Available: www.intechopen.com

[55] Ali Ghasemi, “Nanoferrite photocatalysts,” *Magnetic Ferrites and Related Nanocomposites*, 2022.

[56] V. Kumaravel, S. Mathew, J. Bartlett, and S. C. Pillai, “Photocatalytic hydrogen production using metal doped TiO2: A review of recent advances,” May 05, 2019, *Elsevier B.V.* doi: 10.1016/j.apcatb.2018.11.080.

[57] A. Adamu, M. Isaacs, K. Boodhoo, and F. R. Abegão, “Investigation of Cu/TiO2 synthesis methods and conditions for CO2 photocatalytic reduction via conversion of bicarbonate/carbonate to formate,” *Journal of CO2 Utilization*, vol. 70, Apr. 2023, doi: 10.1016/j.jcou.2023.102428.

[58] X. Liu, S. Gu, Y. Zhao, G. Zhou, and W. Li, “BiVO4, Bi2WO6 and Bi2MoO6 photocatalysis: A brief review,” Nov. 01, 2020, *Chinese Society of Metals*. doi: 10.1016/j.jmst.2020.04.023.

[59] D. R. Eddy *et al.*, “Heterophase Polymorph of TiO2 (Anatase, Rutile, Brookite, TiO2 (B)) for Efficient Photocatalyst: Fabrication and Activity,” Feb. 01, 2023, *MDPI*. doi: 10.3390/nano13040704.

[60] D. D. Anggoro, W. Udaibah, and A. Prasetyaningrum, “Modification of morphology and optic properties of TiO2 as photoreforming catalyst for H2 production from biomass derivatives: a review,” *IOP Conf Ser Mater Sci Eng*, vol. 1053, no. 1, p. 012055, Feb. 2021, doi: 10.1088/1757-899x/1053/1/012055.

[61] K. Villa, J. R. Galán-Mascarós, N. López, and E. Palomares, “Photocatalytic water splitting: advantages and challenges,” Sep. 21, 2021, *Royal Society of Chemistry*. doi: 10.1039/d1se00808k.

[62] N. A. A. Mohd Amin and H. F. Mohd Zaid, “A Review of Photocatalytic Water Splitting for Hydrogen Production Using Tandem Solar Cell,” *Preprints (Basel)*, 2023.

[63] H. Yang, B. Yang, W. Chen, and J. Yang, “Preparation and Photocatalytic Activities of TiO2-Based Composite Catalysts,” Oct. 01, 2022, *MDPI*. doi: 10.3390/catal12101263.

[64] N. S. Ibrahim, W. L. Leaw, D. Mohamad, S. H. Alias, and H. Nur, “A critical review of metal-doped TiO2 and its structure–physical properties–photocatalytic activity relationship in hydrogen production,” Oct. 30, 2020, *Elsevier Ltd*. doi: 10.1016/j.ijhydene.2020.07.233.

[65] L. Díaz *et al.*, “M/tio2(m = fe, co, ni, cu, zn) catalysts for photocatalytic hydrogen production under uv and visible light irradiation,” *Inorg Chem Front*, vol. 8, no. 14, pp. 3491–3500, Jul. 2021, doi: 10.1039/d0qi01311k.

[66] B. Rusinque, S. Escobedo, and H. de Lasa, “Hydrogen production via pd-TiO2 photocatalytic water splitting under near-uv and visible light: Analysis of the reaction mechanism,” *Catalysts*, vol. 11, no. 3, Mar. 2021, doi: 10.3390/catal11030405.

[67] E. Nurlaela, F. K. Chong, B. K. Dutta, and N. Riaz, “Bimetallic Cu-Ni/TiO 2 as photocatalyst for hydrogen production from water.”

[68] D. Gogoi, A. Namdeo, A. K. Golder, and N. R. Peela, “Ag-doped TiO2 photocatalysts with effective charge transfer for highly efficient hydrogen production through water splitting,” *Int J Hydrogen Energy*, vol. 45, no. 4, pp. 2729–2744, Jan. 2020, doi: 10.1016/j.ijhydene.2019.11.127.

[69] M. A. Aziz Aljar, M. Zulqarnain, A. Shah, M. S. Akhter, and F. J. Iftikhar, “A review of renewable energy generation using modified titania for photocatalytic water splitting,” Jul. 01, 2020, *American Institute of Physics Inc*. doi: 10.1063/5.0006196.

[70] I. Majeed *et al.*, “Understanding the role of metal supported on TiO2in photoreforming of oxygenates,” Nov. 01, 2022, *Royal Society of Chemistry*. doi: 10.1039/d2ya00110a.

[71] P. Sangpour, F. Hashemi, and A. Z. Moshfegh, “Photoenhanced Degradation of Methylene Blue on Cosputtered M:TiO_2 (M = Au, Ag, Cu) Nanocomposite Systems: A Comparative Study,” *The Journal of Physical Chemistry C*, vol. 114, no. 33, pp. 13955–13961, Aug. 2010, doi: 10.1021/jp910454r.

[72] W. Chen *et al.*, “Non-noble metal Cu as a cocatalyst on TiO 2 nanorod for highly efficient photocatalytic hydrogen production.”

[73] M. Hussein, N. Assadi, and D. A. H. Hanaor, “The effects of copper doping on photocatalytic activity at (101) planes of anatase TiO2: A theoretical study,” *Appl Surf Sci*, vol. 387, 2016, doi: 10.1016/j.apsusc.2016.06.178ï.

[74] M. Hinojosa-Reyes, R. Camposeco-Solís, R. Zanella, and V. Rodríguez González, “Hydrogen production by tailoring the brookite and Cu2O ratio of sol-gel Cu-TiO2 photocatalysts,” *Chemosphere*, vol. 184, pp. 992–1002, Oct. 2017, doi: 10.1016/j.chemosphere.2017.06.066.

[75] V. Thi Quyen *et al.*, “Copper doped titanium dioxide as a low-cost visible light photocatalyst for water splitting,” *Solar Energy*, vol. 218, pp. 150–156, Apr. 2021, doi: 10.1016/j.solener.2021.02.036.

[76] M. Kotesh Kumar, G. Naresh, V. , Vijay Kumar, B. Sai Vasista, B. Sasikumar, and A. Venugopal, “Improved H2 yields over Cu-Ni-TiO2 under solar light irradiation: Behaviour of alloy nano particles on photocatalytic H2O splitting,” *Appl Catal B*, vol. 299, Dec. 2021, doi: 10.1016/j.apcatb.2021.120654.

[77] X. Chen, J. Xiong, J. Shi, S. Xia, S. Gui, and W. Shangguan, “Roles of various Ni species on TiO2 in enhancing photocatalytic H2 evolution,” *Frontiers in Energy*, vol. 13, no. 4, pp. 684–690, Dec. 2019, doi: 10.1007/s11708-018-0585-8.

[78] W. T. Chen, A. Chan, D. Sun-Waterhouse, T. Moriga, H. Idriss, and G. I. N. Waterhouse, “Ni/TiO2: A promising low-cost photocatalytic system for solar H2 production from ethanol-water mixtures,” *J Catal*, vol. 326, pp. 43–53, Jun. 2015, doi: 10.1016/j.jcat.2015.03.008.

[79] A. T. Montoya and E. G. Gillan, “Enhanced Photocatalytic Hydrogen Evolution from Transition-Metal Surface-Modified TiO2,” *ACS Omega*, vol. 3, no. 3, pp. 2947–2955, Mar. 2018, doi: 10.1021/acsomega.7b02021.

[80] N. Naseri, P. Sangpour, and S. H. Mousavi, “Applying alloyed metal nanoparticles to enhance solar assisted water splitting,” *RSC Adv.*, vol. 4, no. 87, pp. 46697–46703, Sep. 2014, doi: 10.1039/C4RA08216H.

[81] H. Tian, S. Z. Kang, X. Li, L. Qin, M. Ji, and J. Mu, “Fabrication of an efficient noble metal-free TiO2-based photocatalytic system using Cu-Ni bimetallic deposit as an active center of H2 evolution from water,” *Solar Energy Materials and Solar Cells*, vol. 134, pp. 309–317, 2015, doi: 10.1016/j.solmat.2014.12.016.

[82] R. E. Fuentes, J. Farell, and J. W. Weidner, “Multimetallic Electrocatalysts of Pt, Ru, and Ir Supported on Anatase and Rutile TiO[sub 2] for Oxygen Evolution in an Acid Environment,” *Electrochemical and Solid-State Letters*, vol. 14, no. 3, p. E5, 2011, doi: 10.1149/1.3528163.

[83] N. Riaz, F. K. Chong, Z. B. Man, M. S. Khan, and B. K. Dutta, “Photodegradation of orange II under visible light using Cu-Ni/TiO 2: Influence of Cu: Ni mass composition, preparation, and calcination temperature,” *Ind Eng Chem Res*, vol. 52, no. 12, pp. 4491–4503, Mar. 2013, doi: 10.1021/ie303255v.

[84] S. Ibrahim *et al.*, “Novel hetero-bimetallic coordination polymer as a single source of highly dispersed Cu/Ni nanoparticles for efficient photocatalytic water splitting,” *Inorg Chem Front*, vol. 5, no. 8, pp. 1816–1827, Aug. 2018, doi: 10.1039/c8qi00355f.

[85] I. Majeed *et al.*, “Controlled Synthesis of TiO2 Nanostructures: Exceptional Hydrogen Production in Alcohol-Water Mixtures over Cu(OH)2–Ni(OH)2/TiO2 Nanorods,” *ChemistrySelect*, vol. 2, no. 25, pp. 7497–7507, Aug. 2017, doi: 10.1002/slct.201701080.

[86] D. Hanaor, C. C. Sorrell, and D. A. H. Hanaor, “Review of the anatase to rutile phase transformation,” *J Mater Sci*, vol. 46, no. 4, 2011, doi: 10.1007/s10853-010-5113-0ï.

[87] S. N. A. Sulaiman, M. Zaky Noh, N. Nadia Adnan, N. Bidin, and S. N. Ab Razak, “Effects of photocatalytic activity of metal and non-metal doped Tio2 for Hydrogen production enhancement - A Review,” in *Journal of Physics: Conference Series*, Institute of Physics Publishing, May 2018. doi: 10.1088/1742-6596/1027/1/012006.

[88] C. Wang *et al.*, “Efficient hydrogen production by photocatalytic water splitting using N-doped TiO 2 film,” *Appl Surf Sci*, vol. 283, pp. 188–192, Oct. 2013, doi: 10.1016/j.apsusc.2013.06.080.

[89] C. Wang *et al.*, “Effective water splitting using N-doped TiO2 films: Role of preferred orientation on hydrogen production,” *Int J Hydrogen Energy*, vol. 39, no. 5, pp. 1967–1971, Feb. 2014, doi: 10.1016/j.ijhydene.2013.11.097.

[90] M. J. Molaei, “Recent advances in hydrogen production through photocatalytic water splitting: A review,” Jun. 01, 2024, *Elsevier Ltd*. doi: 10.1016/j.fuel.2024.131159.

[91] K. Qi, C. Imparato, O. Almjasheva, A. Khataee, and W. Zheng, “TiO2-based photocatalysts from type-II to S-scheme heterojunction and their applications,” *J Colloid Interface Sci*, vol. 675, pp. 150–191, Dec. 2024, doi: 10.1016/j.jcis.2024.06.204.

[92] M. Ni, M. K. H. Leung, D. Y. C. Leung, and K. Sumathy, “A review and recent developments in photocatalytic water-splitting using TiO2 for hydrogen production,” Apr. 2007. doi: 10.1016/j.rser.2005.01.009.

[93] C. W. Lai and S. Sreekantan, “Preparation of hybrid WO3–TiO2 nanotube photoelectrodes using anodization and wet impregnation: Improved water-splitting hydrogen generation performance,” *Int J Hydrogen Energy*, vol. 38, no. 5, pp. 2156–2166, Feb. 2013, doi: 10.1016/j.ijhydene.2012.12.025.

[94] J. Georgieva, E. Valova, S. Armyanov, N. Philippidis, I. Poulios, and S. Sotiropoulos, “Bi-component semiconductor oxide photoanodes for the photoelectrocatalytic oxidation of organic solutes and vapours: A short review with emphasis to TiO2–WO3 photoanodes,” *J Hazard Mater*, vol. 211–212, pp. 30–46, Apr. 2012, doi: 10.1016/j.jhazmat.2011.11.069.

[95] R. Del Angel, J. C. Durán-Álvarez, and R. Zanella, “TiO2-Low Band Gap Semiconductor Heterostructures for Water Treatment Using Sunlight-Driven Photocatalysis,” in *Titanium Dioxide - Material for a Sustainable Environment*, InTech, 2018. doi: 10.5772/intechopen.76501.

[96] Y. Zhao *et al.*, “Classification and catalytic mechanisms of heterojunction photocatalysts and the application of titanium dioxide (TiO2)-based heterojunctions in environmental remediation,” *J Environ Chem Eng*, vol. 10, no. 3, Jun. 2022, doi: 10.1016/j.jece.2022.108077.

[97] K. Qi, C. Imparato, O. Almjasheva, A. Khataee, and W. Zheng, “TiO2-based photocatalysts from type-II to S-scheme heterojunction and their applications,” *J Colloid Interface Sci*, vol. 675, pp. 150–191, Dec. 2024, doi: 10.1016/j.jcis.2024.06.204.

[98] M. Y. Xie, K. Y. Su, X. Y. Peng, R. J. Wu, M. Chavali, and W. C. Chang, “Hydrogen production by photocatalytic water-splitting on Pt-doped TiO2–ZnO under visible

light," *J Taiwan Inst Chem Eng*, vol. 70, pp. 161–167, Jan. 2017, doi: 10.1016/j.jtice.2016.10.034.

[99] D. Spanu, S. Recchia, S. Mohajernia, P. Schmuki, and M. Altomare, "Site-selective Pt dewetting on WO3-coated TiO2 nanotube arrays: An electron transfer cascade-based H2 evolution photocatalyst," *Appl Catal B*, vol. 237, pp. 198–205, Dec. 2018, doi: 10.1016/j.apcatb.2018.05.061.

[100] S. Y. Toledo Camacho, A. Rey, M. D. Hernández-Alonso, J. Llorca, F. Medina, and S. Contreras, "Pd/TiO2-WO3 photocatalysts for hydrogen generation from water-methanol mixtures," *Appl Surf Sci*, vol. 455, pp. 570–580, Oct. 2018, doi: 10.1016/j.apsusc.2018.05.122.

[101] L. Tian, X. Guan, S. Zong, A. Dai, and J. Qu, "Cocatalysts for Photocatalytic Overall Water Splitting: A Mini Review," Feb. 01, 2023, *MDPI*. doi: 10.3390/catal13020355.

[102] M. Saleh, H. N. Abdelhamid, D. M. Fouad, and H. M. El-Bery, "Enhancing photocatalytic water splitting: Comparative study of TiO2 decorated nanocrystals (Pt and Cu) using different synthesis methods," *Fuel*, vol. 354, Dec. 2023, doi: 10.1016/j.fuel.2023.129248.

[103] Z. H. N. Al-Azri *et al.*, "The roles of metal co-catalysts and reaction media in photocatalytic hydrogen production: Performance evaluation of M/TiO2 photocatalysts (M = Pd, Pt, Au) in different alcohol-water mixtures," *J Catal*, vol. 329, pp. 355–367, Jun. 2015, doi: 10.1016/j.jcat.2015.06.005.

[104] W. T. Chen, A. Chan, D. Sun-Waterhouse, J. Llorca, H. Idriss, and G. I. N. Waterhouse, "Performance comparison of Ni/TiO2 and Au/TiO2 photocatalysts for H2 production in different alcohol-water mixtures," *J Catal*, vol. 367, pp. 27–42, Nov. 2018, doi: 10.1016/j.jcat.2018.08.015.

[105] C. Wang *et al.*, "Effective water splitting using N-doped TiO2 films: Role of preferred orientation on hydrogen production," *Int J Hydrogen Energy*, vol. 39, no. 5, pp. 1967–1971, Feb. 2014, doi: 10.1016/j.ijhydene.2013.11.097.

[106] U. Caudillo-Flores, M. J. Muñoz-Batista, M. Fernández-García, and A. Kubacka, "Bimetallic Pt-Pd co-catalyst Nb-doped TiO2 materials for H2 photo-production under UV and Visible light illumination," *Appl Catal B*, vol. 238, pp. 533–545, Dec. 2018, doi: 10.1016/j.apcatb.2018.07.047.

[107] T. Sun *et al.*, "Fe and Ni co-doped TiO 2 nanoparticles prepared by alcohol-thermal method: Application in hydrogen evolution by water splitting under visible light irradiation," *Powder Technol*, vol. 228, pp. 210–218, Sep. 2012, doi: 10.1016/j.powtec.2012.05.018.

[108] Slamet, D. A. Agriyfani, T. Elysabeth, M. Ibadurrohman, and M. Nurdin, “Synthesis of Ni-and N-doped titania nanotube arrays for photocatalytic hydrogen production from glycerol–water solutions,” *Catalysts*, vol. 10, no. 11, pp. 1–17, Nov. 2020, doi: 10.3390/catal10111234.

[109] H. Drobná *et al.*, “Partially Reduced Ni-NiO-TiO2 Photocatalysts for Hydrogen Production from Methanol–Water Solution,” *Catalysts*, vol. 13, no. 2, Feb. 2023, doi: 10.3390/catal13020293.

[110] N. A. M. Barakat, E. Ahmed, M. T. Amen, M. A. Abdelkareem, and A. A. Farghali, “N-doped Ni/C/TiO2 nanocomposite as effective photocatalyst for water splitting,” *Mater Lett*, vol. 210, pp. 317–320, Jan. 2018, doi: 10.1016/j.matlet.2017.09.009.

[111] A. L. Luna *et al.*, “Photocatalytic Hydrogen Evolution Using Ni-Pd/TiO2: Correlation of Light Absorption, Charge-Carrier Dynamics, and Quantum Efficiency,” *Journal of Physical Chemistry C*, vol. 121, no. 26, pp. 14302–14311, Jul. 2017, doi: 10.1021/acs.jpcc.7b01167.

[112] Y. Li, L. Wang, J. Liang, F. Gao, K. Yin, and P. Dai, “Hierarchical Heterostructure of ZnO@TiO2 Hollow Spheres for Highly Efficient Photocatalytic Hydrogen Evolution,” *Nanoscale Res Lett*, vol. 12, 2017, doi: 10.1186/s11671-017-2304-5.

[113] X. Guo, X. Liu, J. Shan, G. Zhao, and S. Liu, “Heterojunction Design between WSe2 Nanosheets and TiO2 for Efficient Photocatalytic Hydrogen Generation,” *Catalysts*, vol. 12, no. 12, Dec. 2022, doi: 10.3390/catal12121668.

[114] H. Wang *et al.*, “Engineering of SnO2/TiO2 heterojunction compact interface with efficient charge transfer pathway for photocatalytic hydrogen evolution,” *Chinese Chemical Letters*, vol. 34, no. 1, Jan. 2023, doi: 10.1016/j.cclet.2022.01.018.

[115] X. Han, B. Yao, K. Li, W. Zhu, and X. Zhang, “Preparation and Photocatalytic Performances of WO3/TiO2Composite Nanofibers,” *J Chem*, vol. 2020, 2020, doi: 10.1155/2020/2390486.

[116] V. Q. Hieu *et al.*, “TiO2/Ti3C2/g-C3N4 ternary heterojunction for photocatalytic hydrogen evolution,” *Chemosphere*, vol. 285, Dec. 2021, doi: 10.1016/j.chemosphere.2021.131429.

[117] V. H. Nguyen and J. C. S. Wu, “Recent developments in the design of photoreactors for solar energy conversion from water splitting and CO2 reduction,” *Appl Catal A Gen*, vol. 550, pp. 122–141, Jan. 2018, doi: 10.1016/j.apcata.2017.11.002.

[118] L. K. Tinoco Navarro and C. Jaroslav, “Enhancing Photocatalytic Properties of TiO2 Photocatalyst and Heterojunctions: A Comprehensive Review of the Impact of Biphasic Systems in Aerogels and Xerogels Synthesis, Methods, and Mechanisms for Environmental Applications,” Dec. 01, 2023, *Multidisciplinary Digital Publishing Institute (MDPI)*. doi: 10.3390/gels9120976.

[119] C. B. Anucha, I. Altin, E. Bacaksiz, and V. N. Stathopoulos, “Titanium dioxide (TiO_2)-based photocatalyst materials activity enhancement for contaminants of emerging concern (CECs) degradation: In the light of modification strategies,” *Chemical Engineering Journal Advances*, vol. 10, May 2022, doi: 10.1016/j.ceja.2022.100262.

[120] S. Al Jitan, G. Palmisano, and C. Garlisi, “Synthesis and surface modification of TiO2-based photocatalysts for the conversion of CO2,” Feb. 01, 2020, *MDPI*. doi: 10.3390/catal10020227.

[121] H. Park, Y. Park, W. Kim, and W. Choi, “Surface modification of TiO2 photocatalyst for environmental applications,” *Journal of Photochemistry and Photobiology C: Photochemistry Reviews*, vol. 15, pp. 1–20, Jun. 2013, doi: 10.1016/j.jphotochemrev.2012.10.001.

[122] N. Liu, S. P. Albu, K. Lee, S. So, and P. Schmuki, “Water annealing and other low temperature treatments of anodic TiO2 nanotubes: A comparison of properties and efficiencies in dye sensitized solar cells and for water splitting,” *Electrochim Acta*, vol. 82, pp. 98–102, Nov. 2012, doi: 10.1016/j.electacta.2012.06.006.

[123] V. Jagadeesh Babu, S. Vempati, and S. Ramakrishna, “A review on 1D and 2D nanostructured materials for hydrogen generation,” *Phys.Chem.Chem.Phys*, 2014, doi: 10.1039/c0xx00000x.

[124] H. Wang, H. Jiang, P. Huo, M. Filip Edelmannová, L. Čapek, and K. Kočí, “Hydrogen production from methanol-water mixture over NiO/TiO2 nanorods structure photocatalysts,” *J Environ Chem Eng*, vol. 10, no. 1, Feb. 2022, doi: 10.1016/j.jece.2021.106908.

[125] F. Li, Y. Huang, H. Peng, Y. Cao, and Y. Niu, “Preparation and Photocatalytic Water Splitting Hydrogen Production of Titanium Dioxide Nanosheets,” *International Journal of Photoenergy*, vol. 2020, 2020, doi: 10.1155/2020/3617312.

[126] J. Wu, S. Lu, D. Ge, L. Zhang, W. Chen, and H. Gu, “Photocatalytic properties of Pd/TiO2 nanosheets for hydrogen evolution from water splitting,” *RSC Adv*, vol. 6, no. 72, pp. 67502–67508, 2016, doi: 10.1039/c6ra10408h.

[127] A. G. M. da Silva *et al.*, “PdPt-TiO2 nanowires: correlating composition, electronic effects and O-vacancies with activities towards water splitting and oxygen

reduction," *Appl Catal B*, vol. 277, Nov. 2020, doi: 10.1016/j.apcatb.2020.119177.

[128] Q. Liu *et al.*, "CoNi bimetallic alloy cocatalyst-modified TiO2 nanoflowers with enhanced photocatalytic hydrogen evolution," *Int J Hydrogen Energy*, vol. 48, no. 14, pp. 5529–5540, Feb. 2023, doi: 10.1016/j.ijhydene.2022.11.037.

[129] W. Buraso, V. Lachom, P. Siriya, and P. Laokul, "Synthesis of TiO2 nanoparticles via a simple precipitation method and photocatalytic performance," *Mater Res Express*, vol. 5, no. 11, Nov. 2018, doi: 10.1088/2053-1591/aadbf0.

[130] S. P. Ramírez, J. A. Wang, M. A. Valenzuela, L. F. Chen, and A. Dalai, "CuO@TiO2 and NiO@TiO2 core-shell catalysts for hydrogen production from the photocatalytic reforming of glycerol aqueous solution," *Journal of Applied Research and Technology*, vol. 18, no. 6, pp. 390–409, Dec. 2020, doi: 10.22201/icat.24486736e.2020.18.6.1365.

[131] W.-T. Chen *et al.*, "Effect of TiO2 polymorph and alcohol sacrificial agent on the activity of Au/TiO2 photocatalysts for H2 production in alcohol–water mixtures," *J Catal*, vol. 329, pp. 499–513, Sep. 2015, doi: 10.1016/j.jcat.2015.06.014.

[132] C. R. López, E. P. Melián, J. A. Ortega Méndez, D. E. Santiago, J. M. Doña Rodríguez, and O. González Díaz, "Comparative study of alcohols as sacrificial agents in H2 production by heterogeneous photocatalysis using Pt/TiO2 catalysts," *J Photochem Photobiol A Chem*, vol. 312, pp. 45–54, Nov. 2015, doi: 10.1016/j.jphotochem.2015.07.005.

[133] K. Lalitha, J. K. Reddy, M. V. Phanikrishna Sharma, V. D. Kumari, and M. Subrahmanyam, "Continuous hydrogen production activity over finely dispersed Ag2O/TiO2 catalysts from methanol:water mixtures under solar irradiation: A structure–activity correlation," *Int J Hydrogen Energy*, vol. 35, no. 9, pp. 3991–4001, May 2010, doi: 10.1016/j.ijhydene.2010.01.106.

[134] Y. Jiang, L. Mao, J. Shi, B. Zheng, X. Guan, and F. Liu, "Effects of mixed sacrificial reagents on hydrogen evolution over typical photocatalysts," *J Photonics Energy*, vol. 10, no. 02, p. 1, Dec. 2019, doi: 10.1117/1.jpe.10.023503.

[135] I. Reim, B. Wriedt, Ü. Tastan, D. Ziegenbalg, and M. Karnahl, "Impact of the Type of Reactor and the Catalytic Conditions on the Photocatalytic Production of Hydrogen Using a Fully Noble-Metal-Free System," *ChemistrySelect*, vol. 3, no. 11, pp. 2905–2911, Mar. 2018, doi: 10.1002/slct.201800289.

[136] V. Meinhardová, L. Dubnová, H. Drobná, L. Matějová, K. Kočí, and L. Čapek, "Role of lamp type in conventional batch and micro-photoreactor for photocatalytic hydrogen production," *Front Chem*, vol. 11, 2023, doi: 10.3389/fchem.2023.1271410.

[137] B. Bakbolat *et al.*, “Recent developments of TiO2-based photocatalysis in the hydrogen evolution and photodegradation: A review,” Sep. 01, 2020, *MDPI AG*. doi: 10.3390/nano10091790.

[138] Z. Zhang and P. A. Maggard, “Investigation of photocatalytically-active hydrated forms of amorphous titania, TiO2·nH2O,” *J Photochem Photobiol A Chem*, vol. 186, no. 1, pp. 8–13, Feb. 2007, doi: 10.1016/j.jphotochem.2006.07.004.

[139] A. Boudjemaa *et al.*, “Fe2O3/carbon spheres for efficient photo-catalytic hydrogen production from water and under visible light irradiation,” *Solar Energy Materials and Solar Cells*, vol. 140, pp. 405–411, Sep. 2015, doi: 10.1016/j.solmat.2015.04.036.

[140] M. Muscetta, L. Clarizia, M. Race, R. Andreozzi, R. Marotta, and I. Di Somma, “Visible—Light Driven Systems: Effect of the Parameters Affecting Hydrogen Production through Photoreforming of Organics in Presence of Cu2O/TiO2 Nanocomposite Photocatalyst,” *Applied Sciences (Switzerland)*, vol. 13, no. 4, Feb. 2023, doi: 10.3390/app13042337.

[141] J. J. Velázquez, R. Fernández-González, L. Díaz, E. Pulido Melián, V. D. Rodríguez, and P. Núñez, “Effect of reaction temperature and sacrificial agent on the photocatalytic H2-production of Pt-TiO2,” *J Alloys Compd*, vol. 721, pp. 405–410, 2017, doi: 10.1016/j.jallcom.2017.05.314.

[142] S. K. Lakhera, A. Rajan, R. T.P., and N. Bernaurdshaw, “A review on particulate photocatalytic hydrogen production system: Progress made in achieving high energy conversion efficiency and key challenges ahead,” Dec. 01, 2021, *Elsevier Ltd*. doi: 10.1016/j.rser.2021.111694.

[143] Y. Wu, G. Lu, and S. Li, “The Role of Cu(I) Species for Photocatalytic Hydrogen Generation Over CuO x /TiO2,” *Catal Letters*, vol. 133, no. 1–2, pp. 97–105, Nov. 2009, doi: 10.1007/s10562-009-0165-y.

[144] A. NADA, H. HAMED, M. BARAKAT, N. MOHAMED, and T. VEZIROGLU, “Enhancement of photocatalytic hydrogen production rate using photosensitized TiO2/RuO2-MV2+,” *Int J Hydrogen Energy*, vol. 33, no. 13, pp. 3264–3269, Jul. 2008, doi: 10.1016/j.ijhydene.2008.04.027.

[145] Z. Zhang and P. A. Maggard, “Investigation of photocatalytically-active hydrated forms of amorphous titania, TiO2·nH2O,” *J Photochem Photobiol A Chem*, vol. 186, no. 1, pp. 8–13, Feb. 2007, doi: 10.1016/j.jphotochem.2006.07.004.

[146] M. R. Karimi Estahbanati, N. Mahinpey, M. Feilizadeh, F. Attar, and M. C. Iliuta, “Kinetic study of the effects of pH on the photocatalytic hydrogen production from alcohols,” *Int J Hydrogen Energy*, vol. 44, no. 60, pp. 32030–32041, Dec. 2019, doi: 10.1016/j.ijhydene.2019.10.114.

[147] H. Chakhtouna, H. Benzeid, N. Zari, A. El Kacem Qaiss, and R. Bouhfid, “Recent progress on Ag/TiO 2 photocatalysts: photocatalytic and bactericidal behaviors”, doi: 10.1007/s11356-021-14996-y/Published.

[148] A. Haruna, F. K. Chong, Y. C. Ho, and Z. M. A. Merican, “Preparation and modification methods of defective titanium dioxide-based nanoparticles for photocatalytic wastewater treatment—a comprehensive review,” Oct. 01, 2022, *Springer Science and Business Media Deutschland GmbH*. doi: 10.1007/s11356-022-22749-8.

[149] T. M. Roldán, “PHOTOCATALYTIC MICROREACTOR FOR THE PRODUCTION OF HYDROGEN Report and annexes,” 2021.

[150] C. C. Lo, C. W. Huang, C. H. Liao, and J. C. S. Wu, “Novel twin reactor for separate evolution of hydrogen and oxygen in photocatalytic water splitting,” *Int J Hydrogen Energy*, vol. 35, no. 4, pp. 1523–1529, Feb. 2010, doi: 10.1016/j.ijhydene.2009.12.032.

[151] A. Haruna, F. K. Chong, Y. C. Ho, and Z. M. A. Merican, “Preparation and modification methods of defective titanium dioxide-based nanoparticles for photocatalytic wastewater treatment—a comprehensive review,” Oct. 01, 2022, *Springer Science and Business Media Deutschland GmbH*. doi: 10.1007/s11356-022-22749-8.

[152] M. Matsuoka, M. Kitano, M. Takeuchi, K. Tsujimaru, M. Anpo, and J. M. Thomas, “Photocatalysis for new energy production. Recent advances in photocatalytic water splitting reactions for hydrogen production,” *Catal Today*, vol. 122, no. 1–2, pp. 51–61, Apr. 2007, doi: 10.1016/j.cattod.2007.01.042.

[153] C. Acar, I. Dincer, and G. F. Naterer, “Review of photocatalytic water-splitting methods for sustainable hydrogen production,” Sep. 01, 2016, *John Wiley and Sons Ltd*. doi: 10.1002/er.3549.

[154] S. Escobedo Salas, B. Serrano Rosales, and H. De Lasa, “Quantum yield with platinum modified TiO2 photocatalyst for hydrogen production,” *Appl Catal B*, vol. 140–141, pp. 523–536, Aug. 2013, doi: 10.1016/j.apcatb.2013.04.016.

[155] B. Rusinque, S. Escobedo, and H. de Lasa, “Kinetic Modeling and Quantum Yields: Hydrogen Production via Pd-TiO2 Photocatalytic Water Splitting under Near-UV and Visible Light,” *Catalysts*, vol. 12, no. 2, Feb. 2022, doi: 10.3390/catal12020113.

[156] B. Rusinque, “Hydrogen Production by Photocatalytic Water Splitting Under Hydrogen Production by Photocatalytic Water Splitting Under Near-UV and Visible Light Using Doped Pt and Pd TiO2 Near-UV and Visible Light Using Doped Pt and Pd TiO2,” 2018. [Online]. Available: https://ir.lib.uwo.ca/etd

[157] Y. Zhang *et al.*, “Single-atom Cu anchored catalysts for photocatalytic renewable H2 production with a quantum efficiency of 56%,” *Nat Commun*, vol. 13, no. 1, Dec. 2022, doi: 10.1038/s41467-021-27698-3.

[158] A. Albahnasawi and M. Eyvaz, “Introductory Chapter: Hydrogen Energy,” in *Clean Energy Technologies - Hydrogen and Gasification Processes*, IntechOpen, 2022. doi: 10.5772/intechopen.108635.

[159] Giorgio, “IEA-ETSAP© Technology Brief P12-February 2014-www.etsap.org ENERGY TECHNOLOGY SYSTEM ANALYSIS PROGRAMME Hydrogen Production & Distribution.” [Online]. Available: www.etsap.org

[160] M. Kanoglu, A. Bolatturk, and C. Yilmaz, “Thermodynamic analysis of models used in hydrogen production by geothermal energy,” *Int J Hydrogen Energy*, vol. 35, no. 16, pp. 8783–8791, Aug. 2010, doi: 10.1016/j.ijhydene.2010.05.128.

[161] A. M. Abdalla, S. Hossain, O. B. Nisfindy, A. T. Azad, M. Dawood, and A. K. Azad, “Hydrogen production, storage, transportation and key challenges with applications: A review,” Jun. 01, 2018, *Elsevier Ltd*. doi: 10.1016/j.enconman.2018.03.088.

[162] M. G. Rasul, M. A. Hazrat, M. A. Sattar, M. I. Jahirul, and M. J. Shearer, “The future of hydrogen: Challenges on production, storage and applications,” Nov. 15, 2022, *Elsevier Ltd*. doi: 10.1016/j.enconman.2022.116326.

[163] S. A. Althabaiti *et al.*, “One-Pot Facile Synthesis of CuO–CdWO4 Nanocomposite for Photocatalytic Hydrogen Production,” *Nanomaterials*, vol. 12, no. 24, Dec. 2022, doi: 10.3390/nano12244472.

[164] M. Saleh, H. N. Abdelhamid, D. M. Fouad, and H. M. El-Bery, “Enhancing photocatalytic water splitting: Comparative study of TiO2 decorated nanocrystals (Pt and Cu) using different synthesis methods,” *Fuel*, vol. 354, Dec. 2023, doi: 10.1016/j.fuel.2023.129248.

[165] H. Tian, S. Z. Kang, X. Li, L. Qin, M. Ji, and J. Mu, “Fabrication of an efficient noble metal-free TiO2-based photocatalytic system using Cu-Ni bimetallic deposit as an active center of H2 evolution from water,” *Solar Energy Materials and Solar Cells*, vol. 134, pp. 309–317, 2015, doi: 10.1016/j.solmat.2014.12.016.

[166] M. Kotesh Kumar, G. Naresh, V. Vijay Kumar, B. Sai Vasista, B. Sasikumar, and A. Venugopal, “Improved H2 yields over Cu-Ni-TiO2 under solar light irradiation: Behaviour of alloy nano particles on photocatalytic H2O splitting,” *Appl Catal B*, vol. 299, Dec. 2021, doi: 10.1016/j.apcatb.2021.120654.

[167] K. A. Jacob, P. M. Peter, P. E. Jose, C. J. Balakrishnan, and V. J. Thomas, “A simple method for the synthesis of anatase-rutile mixed phase TiO2 using a convenient

precursor and higher visible-light photocatalytic activity of Co-doped TiO2," in *Materials Today: Proceedings*, Elsevier Ltd, 2021, pp. 1408–1417. doi: 10.1016/j.matpr.2021.07.104.

[168] A. Adamu, M. Isaacs, K. Boodhoo, and F. R. Abegão, "Investigation of Cu/TiO2 synthesis methods and conditions for CO2 photocatalytic reduction via conversion of bicarbonate/carbonate to formate," *Journal of CO2 Utilization*, vol. 70, Apr. 2023, doi: 10.1016/j.jcou.2023.102428.

[169] M. Salazar-Villanueva, L. R. Morales-Juárez, O. Flores Sánchez, A. Cruz-López, A. Tovar-Corona, and O. Vázquez-Cuchillo, "Enhanced photocatalytic water splitting hydrogen production on TiO2 nanospheres: A theoretical- experimental approach," *J Photochem Photobiol A Chem*, vol. 434, Jan. 2023, doi: 10.1016/j.jphotochem.2022.114212.

[170] V. Thi Quyen *et al.*, "Copper doped titanium dioxide as a low-cost visible light photocatalyst for water splitting," *Solar Energy*, vol. 218, pp. 150–156, Apr. 2021, doi: 10.1016/j.solener.2021.02.036.

[171] N. Riaz, F. K. Chong, Z. B. Man, M. S. Khan, and B. K. Dutta, "Photodegradation of orange II under visible light using Cu-Ni/TiO 2: Influence of Cu: Ni mass composition, preparation, and calcination temperature," *Ind Eng Chem Res*, vol. 52, no. 12, pp. 4491–4503, Mar. 2013, doi: 10.1021/ie303255v.

[172] E. Nurlaela, F. K. Chong, B. K. Dutta, and N. Riaz, "Bimetallic Cu-Ni/TiO 2 as photocatalyst for hydrogen production from water."

[173] W. T. Chen, Y. Dong, P. Yadav, R. D. Aughterson, D. Sun-Waterhouse, and G. I. N. Waterhouse, "Effect of alcohol sacrificial agent on the performance of Cu/TiO2 photocatalysts for UV-driven hydrogen production," *Appl Catal A Gen*, vol. 602, Jul. 2020, doi: 10.1016/j.apcata.2020.117703.

[174] M. Hussein, N. Assadi, and D. A. H. Hanaor, "The effects of copper doping on photocatalytic activity at (101) planes of anatase TiO2: A theoretical study," *Appl Surf Sci*, vol. 387, 2016, doi: 10.1016/j.apsusc.2016.06.178ï.

[175] A. T. Montoya and E. G. Gillan, "Enhanced Photocatalytic Hydrogen Evolution from Transition-Metal Surface-Modified TiO2," *ACS Omega*, vol. 3, no. 3, pp. 2947–2955, Mar. 2018, doi: 10.1021/acsomega.7b02021.

[176] V. Meinhardová, L. Dubnová, H. Drobná, L. Matějová, K. Kočí, and L. Čapek, "Role of lamp type in conventional batch and micro-photoreactor for photocatalytic hydrogen production," *Front Chem*, vol. 11, 2023, doi: 10.3389/fchem.2023.1271410.

[177] O. F. Aldosari and I. Hussain, “Unlocking the potential of TiO2-based photocatalysts for green hydrogen energy through water-splitting: Recent advances, future perspectives and techno feasibility assessment,” *Int J Hydrogen Energy*, vol. 59, pp. 958–981, Mar. 2024, doi: 10.1016/j.ijhydene.2024.01.306.

[178] M. Bowker and W. Jones, “Methanol photo-reforming with water on pure titania for hydrogen production: Methanol photo-reforming,” in *Philosophical Transactions of the Royal Society A: Mathematical, Physical and Engineering Sciences*, Royal Society Publishing, Jul. 2020. doi: 10.1098/rsta.2020.0058.

[179] N. Fajrina and M. Tahir, “A critical review in strategies to improve photocatalytic water splitting towards hydrogen production,” Jan. 08, 2019, *Elsevier Ltd*. doi: 10.1016/j.ijhydene.2018.10.200.

[180] B. Wiederkehr, D. A. Mitchell, L. F. de Lima Luz, and N. Krieger, “Use of the Langmuir-Hinshelwood-Hougen-Watson equation to describe the ethyl esterification of fatty acids catalyzed by a fermented solid with lipase activity,” *Biochem Eng J*, vol. 168, Apr. 2021, doi: 10.1016/j.bej.2021.107936.

[181] S. Escobedo and H. de Lasa, “Synthesis and performance of photocatalysts for photocatalytic hydrogen production: Future perspectives,” Dec. 01, 2021, *MDPI*. doi: 10.3390/catal11121505.

[182] P. Ganguly, C. Byrne, A. Breen, and S. C. Pillai, “Antimicrobial activity of photocatalysts: Fundamentals, mechanisms, kinetics and recent advances,” Jun. 05, 2018, *Elsevier B.V.* doi: 10.1016/j.apcatb.2017.11.018.

[183] X. Fu *et al.*, “Photocatalytic reforming of biomass: A systematic study of hydrogen evolution from glucose solution,” *Int J Hydrogen Energy*, vol. 33, no. 22, pp. 6484–6491, 2008, doi: 10.1016/j.ijhydene.2008.07.068.

[184] P. Gomathisankar, D. Yamamoto, H. Katsumata, T. Suzuki, and S. Kaneco, “Photocatalytic hydrogen production with aid of simultaneous metal deposition using titanium dioxide from aqueous glucose solution,” *Int J Hydrogen Energy*, vol. 38, no. 14, pp. 5517–5524, May 2013, doi: 10.1016/j.ijhydene.2013.03.014.

[185] P. Chowdhury, G. Malekshoar, M. B. Ray, J. Zhu, and A. K. Ray, “Sacrificial hydrogen generation from formaldehyde with Pt/TiO2 photocatalyst in solar radiation,” *Ind Eng Chem Res*, vol. 52, no. 14, pp. 5023–5029, Apr. 2013, doi: 10.1021/ie3029976.

[186] C. Wang *et al.*, “Improved hydrogen production from glycerol photoreforming over sol-gel derived TiO2 coupled with metal oxides,” *Chemical Engineering Journal*, vol. 317, pp. 522–532, 2017, doi: 10.1016/j.cej.2017.02.033.

[187] C. R. López, E. P. Melián, J. A. Ortega Méndez, D. E. Santiago, J. M. Doña Rodríguez, and O. González Díaz, "Comparative study of alcohols as sacrificial agents in H2 production by heterogeneous photocatalysis using Pt/TiO2 catalysts," *J Photochem Photobiol A Chem*, vol. 312, pp. 45–54, Nov. 2015, doi: 10.1016/j.jphotochem.2015.07.005.

[188] M. Alkaabi *et al.*, "Design of a Microfluidic Photocatalytic Reactor for Removal of Volatile Organic Components: Process Simulation and Techno-Economic Assessment," *ACS Omega*, vol. 7, no. 10, pp. 8306–8313, Mar. 2022, doi: 10.1021/acsomega.1c05431.

[189] W. T. Chen, A. Chan, D. Sun-Waterhouse, J. Llorca, H. Idriss, and G. I. N. Waterhouse, "Performance comparison of Ni/TiO2 and Au/TiO2 photocatalysts for H2 production in different alcohol-water mixtures," *J Catal*, vol. 367, pp. 27–42, Nov. 2018, doi: 10.1016/j.jcat.2018.08.015.

[190] S. K. Lakhera, A. Rajan, R. T.P., and N. Bernaurdshaw, "A review on particulate photocatalytic hydrogen production system: Progress made in achieving high energy conversion efficiency and key challenges ahead," Dec. 01, 2021, *Elsevier Ltd*. doi: 10.1016/j.rser.2021.111694.

[191] V. Kumaravel *et al.*, "Photocatalytic hydrogen production: Role of sacrificial reagents on the activity of oxide, carbon, and sulfide catalysts," *Catalysts*, vol. 9, no. 3, Mar. 2019, doi: 10.3390/catal9030276.

[192] A. Castedo, I. Uriz, L. Soler, L. M. Gandía, and J. Llorca, "Kinetic analysis and CFD simulations of the photocatalytic production of hydrogen in silicone microreactors from water-ethanol mixtures," *Appl Catal B*, vol. 203, pp. 210–217, Apr. 2017, doi: 10.1016/j.apcatb.2016.10.022.

[193] M. R. Karimi Estahbanati, M. Feilizadeh, and M. C. Iliuta, "An intrinsic kinetic model for liquid-phase photocatalytic hydrogen production," *AIChE Journal*, vol. 65, no. 11, Nov. 2019, doi: 10.1002/aic.16724.

[194] L. Zhou, C. Rao, Y. Pang, D. Yang, H. Lou, and X. Qiu, "More Accurate Method for Evaluating the Activity of Photocatalytic Hydrogen Evolution and Its Reaction Kinetics Equation," *Langmuir*, vol. 39, no. 9, pp. 3431–3438, Mar. 2023, doi: 10.1021/acs.langmuir.2c03371.

[195] J. Z. Bloh, "A holistic approach to model the kinetics of photocatalytic reactions," *Front Chem*, vol. 7, no. MAR, 2019, doi: 10.3389/fchem.2019.00128.

[196] H. C. Yatmaz, A. Akyol, and M. Bayramoglu, "Kinetics of the photocatalytic decolorization of an azo reactive dye in aqueous ZnO suspensions," *Ind Eng Chem Res*, vol. 43, no. 19, pp. 6035–6039, 2004, doi: 10.1021/ie049921z.

[197] L. Clarizia *et al.*, “Effect of Synthesis Method on Reaction Mechanism for Hydrogen Evolution over CuxOy/TiO2 Photocatalysts: A Kinetic Analysis,” *Int J Mol Sci*, vol. 24, no. 3, Feb. 2023, doi: 10.3390/ijms24032004.

[198] M. R. Karimi Estahbanati, A. Babin, M. Feilizadeh, Z. Nayernia, N. Mahinpey, and M. C. Iliuta, “Photocatalytic conversion of alcohols to hydrogen and carbon-containing products: A cleaner alcohol valorization approach,” *J Clean Prod*, vol. 318, Oct. 2021, doi: 10.1016/j.jclepro.2021.128546.

[199] A. Castedo, A. Casanovas, I. Angurell, L. Soler, and J. Llorca, “Effect of temperature on the gas-phase photocatalytic H2 generation using microreactors under UVA and sunlight irradiation,” *Fuel*, vol. 222, pp. 327–333, Jun. 2018, doi: 10.1016/j.fuel.2018.02.128.

[200] J. Maurya, E. Gemechu, and A. Kumar, “The development of techno-economic assessment models for hydrogen production via photocatalytic water splitting,” *Energy Convers Manag*, vol. 279, Mar. 2023, doi: 10.1016/j.enconman.2023.116750.

[201] B. A. Pinaud *et al.*, “Technical and economic feasibility of centralized facilities for solar hydrogen production via photocatalysis and photoelectrochemistry,” *Energy Environ Sci*, vol. 6, no. 7, pp. 1983–2002, Jul. 2013, doi: 10.1039/c3ee40831k.

[202] J. Schneidewind, “How Much Technological Progress is Needed to Make Solar Hydrogen Cost-Competitive?,” *Adv Energy Mater*, vol. 12, no. 18, May 2022, doi: 10.1002/aenm.202200342.

[203] Z. Kuspanov, B. Bakbolat, A. Baimenov, A. Issadykov, M. Yeleuov, and C. Daulbayev, “Photocatalysts for a sustainable future: Innovations in large-scale environmental and energy applications,” Aug. 10, 2023, *Elsevier B.V.* doi: 10.1016/j.scitotenv.2023.163914.

[204] C. Y. Toe, J. Pan, J. Scott, and R. Amal, “Identifying Key Design Criteria for Large-Scale Photocatalytic Hydrogen Generation from Engineering and Economic Perspectives,” Jun. 10, 2022, *American Chemical Society*. doi: 10.1021/acsestengg.2c00030.

[205] A. Ruiz-Aguirre *et al.*, “Assessment of pilot-plant scale solar photocatalytic hydrogen generation with multiple approaches: Valorization, water decontamination and disinfection,” *Energy*, vol. 260, Dec. 2022, doi: 10.1016/j.energy.2022.125199.

[206] S. Genç and H. Koku, “A preliminary techno-economic analysis of photofermentative hydrogen production,” *Int J Hydrogen Energy*, vol. 52, pp. 212–222, Jan. 2024, doi: 10.1016/j.ijhydene.2023.03.475.

[207] J. Moreno-SanSegundo, C. Casado, and J. Marugán, “Enhanced numerical simulation of photocatalytic reactors with an improved solver for the radiative transfer equation,” *Chemical Engineering Journal*, vol. 388, May 2020, doi: 10.1016/j.cej.2020.124183.

[208] S. Y. Toledo-Camacho, A. Rey, M. I. Maldonado, J. Llorca, S. Contreras, and F. Medina, “Photocatalytic hydrogen production from water-methanol and -glycerol mixtures using Pd/TiO2(-WO3) catalysts and validation in a solar pilot plant,” *Int J Hydrogen Energy*, vol. 46, no. 73, pp. 36152–36166, Oct. 2021, doi: 10.1016/j.ijhydene.2021.08.141.